CLUSTER BOOTSTRAP IN $\mathcal{N} = 4$ SUPER-YANG-MILLS SCATTERING AMPLITUDES

by

Thomas M. Harrington

M.Sc. in Physics, Brown University, 2014

M.Sc. in Physics, University of Massachusetts Lowell, 2012

B.S. in Physics & Mathematics, University of Massachusetts Lowell, 2011

A DISSERTATION SUBMITTED IN PARTIAL FULFILLMENT OF THE REQUIREMENTS FOR

THE DEGREE OF DOCTOR OF PHILOSOPHY

IN THE DEPARTMENT OF PHYSICS AT BROWN UNIVERSITY

Providence, Rhode Island

May 2017

This dissertation by Thomas M. Harrington is accepted in its present form by
the Department of Physics as satisfying the
dissertation requirement for the degree of
Doctor of Philosophy

Date ....
Marcus Spradlin, Advisor

Recommended to the Graduate Council

Date ....
Stephon Alexander, Reader

Date ....
Jiji Fan, Reader

Approved by the Graduate Council

Date ....
Andrew G. Campbell
Dean of the Graduate School

Thomas M. Harrington
Curriculum Vitae

Physics Department
Barus and Holley Building
Brown University
182 Hope Street
Providence, RI 02906

thomas_harrington@brown.edu

Home Address:
44 Carrington Ave, Apt. 3
Providence, RI 02906
781-439-0702 (cell)

Education

- **Brown University**, Graduate Studies in Physics, Providence, RI
  - Candidate for Doctor of Philosophy in Physics, May 2017
    - Thesis: " ..." In preparation
    - Advisor: Prof. Marcus Spradlin
  - Master of Science in Physics, May 2014
- **University of Massachusetts Lowell**, College of Arts and Sciences, Lowell, MA
  - Master of Science in Physics, May 2012
  - Bachelor of Science in Physics and Mathematics, Commonwealth Honors Program, *summa cum laude*, May 2011

Experience

Research

- **Physics Research Assistantship**, Brown U., June 2014 – present
  - **High Energy Theory, Advisor: Marcus Spradlin**
    - Scattering amplitudes in $\mathcal{N} = 4$ supersymmetric Yang-Mills theory.
- **Private Contractor/Researcher**, Brandeis U., June 2012 –August 2012
  - **Experimental Nuclear Physics, Supervisor: Hermann Wellenstein**
    - Tested prototype neutron detector.
- **Undergraduate Physics Researcher**, U. of Massachusetts Lowell, June 2009 – May 2012
  - **Experimental Nuclear Physics, Advisor: Partha Chowdhury**

* Measured energy and time resolution of emerging scintillator crystals, developed digital signal processing techniques with 1 GHz storage oscilloscope, designed C++ programs to perform neutron-gamma discrimination, designed C++ programs to digitally determine the time resolution of planar high purity germanium detector.

– **Photonics, Advisor: William Goodhue**

* Assisted in maintaining molecular beam epitaxy (MBE) system, performed photo- and nano-lithography, performed Hall measurements to determine the doping/charge carrier concentrations of MBE grown samples.

– **Radiation Safety, Advisors: Steven Snay and Dr. David Medich**

* Performed laboratory surveys, calibrated radiation detectors, measured neutron flux to characterize UML neutron radiography beam.

Teaching

- **Physics Teaching Assistantship**, Brown U., September 2012 – May 2014, Spring 2016
  - PHYS 0040 Basic Physics (Spring 2016)
  - PHYS 1560 Modern Physics Laboratory (Spring 2014)
  - PHYS 2010 Techniques in Experimental Physics (September 2012 – May 2014)

List of Publications

- "Heptagons from the Steinmann Cluster Bootstrap", L. J. Dixon (Stanford U.), J. Drummond (U. of Southampton), T. Harrington (Brown U.), A. McLeod (Stanford U.), G. Papathanasiou (Standford U.), M. Spradlin (Brown U.), JHEP 1702 (2017) 137, arXiv:1612.08976.
- "Cluster Functions and Scattering Amplitudes for Six and Seven Points", T. Harrington (Brown U.), M. Spradlin (Brown U.) arXiv:1512.07910.
- "$N = 151$ Pu, Cm and Cf Nuclei Under Rotational Stress: Role of Higher-Order Deformations", S. S. Hota, P. Chowdhury, T. L. Khoo, M. P. Carpenter, R. V. F. Janssens, Y. Qiu, I. Ahmad, J. P. Greene, S. K. Tandel, D. Seweryniak, S. Zhu, P. F. Bertone, C. J. Chiara, A. Y. Deo, N. D'Olympia, S. Gros, C. J. Guess, T. Harrington, D. J. Hartley, G. Henning, C. R. Hoffman, E. G. Jackson, F. G. Kondev, S. Lakshmi, T. Lauritsen, C. J. Lister, E. A. McCutchan, K. Moran, C. Nair, D. Peterson, U. Shirwadkar, and I. Stefanescu, Phys. Lett. **B739**, 13-18 (2014)
- "Optimizing Cs_2LiYCl_6 for fast neutron spectroscopy", N. D'Olympia, P. Chowdhury, C.J. Guess, T. Harrington, E.G. Jackson, S. Lakshmi, C.J. Lister, J. Glodo, R. Hawrami, K. Shah, U. Shirwadkar, Nuclear Instruments and Methods in Physics Research Section A: Accelerators, Spectrometers, Detectors and Associated Equipment **694**, 140-146 (2012)

Notable Awards

- 1^{st} Place 2017 Brown University Datathon
- Award of Excellence as a Graduate Teaching Assistant, Brown U. (2014)
- Charles R. Mingins Scholarship Award to the Outstanding Senior Physics Major, Physics Department, U. of Massachusetts Lowell (2011)

- Department of Energy Nuclear Energy University Programs (NEUP) Scholarship, U. of Massachusetts Lowell, Awarded two consecutive years (2009, 2010)
- Daniel C. Cole Research Award- 1^{st} Prize, Physics Department, U. of Massachusetts Lowell (2010)
- Daniel C. Cole Scholarship Award to the Outstanding Junior Physics Major, Physics Department, U. of Massachusetts Lowell, (2010)
- Barry M. Goldwater Scholarship Honorable Mention, U. of Massachusetts Lowell, (2010)
- Ye-Yung Teng Scholarship Award to the Outstanding Sophomore Physics Major, Physics Department, U. of Massachusetts Lowell, (2009)
- Arthur S. Zamanakos Endowed Scholarship, Mathematics Department, U. of Massachusetts Lowell, (2010)
- Hoff Family Scholarship, U. of Massachusetts Lowell (2008, 2009, 2010)
- LaTorre Family Scholarship, U. of Massachusetts Lowell (2008, 2009, 2010)
- Dean's Scholarship, U. of Massachusetts Lowell (2007-2011)

Memberships/Professional Associations

- Alpha Lambda Delta
- American Physical Society (APS)
- National Honor Society
- Omicron Delta Kappa
- Pi Mu Epsilon
- Sigma Pi Sigma
- Sigma Xi
- Society of Physics Students (SPS)

Conferences Attended

- "Seventh New England String Meeting" Brown University, Providence RI (November 2015)
- "Sixth New England String Meeting" Brown University, Providence RI (October 2014)
- "Humboldt/Brown Mini-Conference" Brown University, Providence RI (October 2014)
- "American Physical Society (APS) Division of Nuclear Physics (DNP) Annual Meeting", East Lansing MI (Nov 2011)
- "American Physical Society (APS) Division of Nuclear Physics (DNP) Annual Meeting", Albuquerque NM (Nov 2010)
- "Annual Conference for Honor Societies", Boston MA (February 2009)

Conference Presentations

- American Physical Society (APS) Division of Nuclear Physics (DNP) Annual Meeting, Talk: "Depth of Gamma Ray Interaction in a Planar Ge Double-sided Strip Detector via Digital Signal Processing" (October 2011)
- Conference Experience for Undergraduates (CEU) Poster Titled: "Neutron-Gamma Discrimination in Emerging Scintillators Via Digital Signal Processing", American Physical Society (APS) Division of Nuclear Physics (DNP) Annual Meeting (Nov 2010)
- Undergraduate Research Symposium, Poster Titled: "Emerging Scintillation Detectors and Digital Signal Processing in Radiation Detection", University of Massachusetts Lowell (April 2010)
- Association of College Honor Societies (ACHS), Annual Conference for Honor Societies, Participated in Panel on the Importance of Undergraduate Research (February 2009)

Conference Proceedings

- P. Chowdhury, S. Hota, S. Lakshmi, S.K. Tandel, T. Harrington, E. Jackson, K. Moran, U. Shirwadkar, I. Ahmad, M.P. Carpenter, J. Greene, C.R. Hoffman, R.V.F. Janssens, T.L. Khoo, F.G. Kondev, T. Lauritsen, C.J. Lister, E.A. McCutchan, D. Seweryniak, I. Stefanescu, "Spectroscopy of neutron-rich Pu nuclei", AIP Conference Proceedings (2011)
- N. D'Olympia, P. Chowdhury, C. Guess, T. Harrington, E. Jackson, S. Lakshmi, C.J. Lister, J. Glodo, R. Hawrami, K. Shah, U. Shirwadkar, "Fast Neutron Spectroscopy with Cs2LiYCl6", APS New England Section Spring Meeting Abstracts (2012)
- S. Hota, P. Chowdhury, S. Lakshmi, S.K. Tandel, T. Harrington, E.G. Jackson, K. Moran, U. Shirwadkar, I. Ahmad, M.P. Carpenter, C.J. Chiara, J. Greene, C.R. Hoffman, R.V.F. Janssens, T.L. Khoo, FG Kondev, T Lauritsen, CJ Lister, EA McCutchan, D Seweryniak, I Stefanescu, S Zhu, "Spectroscopy of 244, 245, 246Pu", APS New England Section Spring Meeting Abstracts (2011)
- CJ Guess, P Chowdhury, N Borges, N D'Olympia, AY Deo, T Harrington, S Hota, EG Jackson, G Kegel, S Lakshmi, G Parker, VS Prasher, K Recca, T Regan, J Thomas, Q Yuan, "Nuclear Science with Thermal and Fast Neutrons at UMass Lowell", APS New England Section Spring Meeting Abstracts (2011)
- S. Hota, P Chowdhury, S Lakshmi, SK Tandel, T Harrington, E Jackson, K Moran, U Shirwadkar, I Ahmad, MP Carpenter, CJ Chiara, J Greene, CR Hoffman, RVF Janssens, TL Khoo, FG Kondev, T Lauritsen, CJ Lister, EA McCutchan, D Seweryniak, I Stefanescu, S Zhu, "Heavy Element Spectroscopy:^{244,245,246}Pu (Z= 94)", APS New England Section Spring Meeting Abstracts (2011)
- T. Harrington, S. Lakshmi, P. Chowdhury, "Neutron-Gamma Discrimination in Emerging Scintillators via Digital Signal Processing," Bull. Am. Phys. Soc. 55, No. 14 (2010).
- S. Hota, P. Chowdhury, S. Lakshmi, S.K. Tandel, E. Jackson, T. Harrington, K. Moran, U. Shirwadkar, I. Ahmad, M.P. Carpenter, C.J. Chiara, J. Greene, C.R. Hoffman, R.V.F. Janssens, T.L. Khoo, S. Zhu, F.G. Kon-Dev, T. Lauritsen, C.J. Lister, E.A. Mccutchan, D. Seweryniak, I. Stefanescu, "High-K Isomers and Band Structures in 244;245Pu," Bull. Am. Phys. Soc. 55, No. 14 (2010).
- P. Chowdhury, S. Hota, S. Lakshmi, S.K. Tandel, T. Harrington, E. Jackson, K. Moran, U. Shirwadkar, I. Ahmad, M.P. Carpenter, C.J. Chiara, J. Greene, C.R. Hoffman, R.V.F.

Janssens, T.L. Khoo, F.G. Kondev, T. Lauritsen, C.J. Lister, E.A. McCutchan, D. Seweryniak, I. Stefanescu, and S.Zhu, "Spectroscopy of Neutron-rich Pu Nuclei", Proceedings of the 3rd International Conference on Frontiers in Nuclear Structure, Astrophysics, and Reactions (2010).

Preface and Acknowledgments

I would like to start off by thanking my advisor, Marcus Spradlin, for all his guidance throughout my graduate career. I would also like to thank the entire Brown High Energy Theory faculty- Stephon Alexander, Jiji Fan, Antal Jevicki, David Lowe, Marcus Spradlin, Chung-I Tan, and Anastasia Volovich. Special thanks to Stephon Alexander and Jiji Fan for agreeing to read my thesis and serve on my PhD committee. Also I would like to thank Chung-I Tan and David Lowe for serving on my preliminary exam committee. None of this would have been possible without the efforts of my collaborators, Lance Dixon, James Drummond, Andrew McLeod, and Georgios Papathanasiou.

I am extremely grateful to the entire Brown Physics Department for being helpful throughout my time here with everything from academic guidance to career development. I would also like to acknowledge all of my office mates- Rohitvarma Basavaraju, Atreya Chatterjee, Igor Prlina, Stefan Stanojevic, Kenta Suzuki, Peter Tsang, and Michael Zlotnikov for the stimulating conversations. I would like to thank all my friends at Brown- Altan Allawala, Andrew Balchunas, Robert Bretz, Ansel Blumers, Kara Ford, Joshua Kerrigan, Daniel Kim, Shayan Lamé, Adam Lanman, Shing Chau John Leung, William Maulbetch, Declan Oller, Anders Schreiber, Robert Sims, Joseph Skitka, Rizki Syarif, Benjamin Wiener, Christos Zambas, Philip Zucker, and the others that I may have forgotten to list here.

Finally, I would like to thank my family for all their support- my father Kevin, mother Diane, my brothers: Kevin, Hank, Patrick, Eddie and my sister Catherine.

Contents

List of Figures

List of Tables

Chapter 1

Introduction

The nature of theoretical physics is to formulate theories that describe the physical world. Precisely explaining elementary particles, their properties, and their interactions is the focus of fundamental physics, specifically high energy theory. A deep understanding of quantum field theory (QFT), the union of quantum mechanics and special relativity, has led to the most accurate description of the microscopic world, the Standard Model of particle physics. The Standard Model correctly predicted the existence of multiple particles including gluons, W and Z bosons, and the Higgs boson before they were experimentally observed. Standard Model predictions for the fine structure constant have been experimentally confirmed to eight decimal points of precision by measuring the electron Landé g factor [1]!

The scattering amplitude is arguably the most important quantity that sheds light on understanding the quantum field theories used to describe nature. The interactions between elementary particles are described using scattering amplitudes calculations. The study of scattering amplitudes has revolutionized our understanding of elementary particles and their interactions. Beyond aiding in the development of our current theoretical models, scattering amplitude calculations are crucial to explain the background processes that occur in high-energy collider physics experiments. Modern scattering amplitude research seeks to further identify the mathematical structure of scattering amplitudes, simplify calculations with the aid of new mathematical tools, extend our knowledge through new calculations, and steer the direction of experimental collider experiments via predictions.

In this thesis, the focus will be scattering amplitudes in $\mathcal{N} = 4$ supersymmetric Yang-Mills (SYM) theory, which will be frequently abbreviated as $\mathcal{N} = 4$ SYM [2]. $\mathcal{N} = 4$ SYM is a supersymmetric theory of massless particles. In four dimensions, $\mathcal{N} = 4$ SYM is maximally supersymmetric. As

of this writing, supersymmetry has not been experimentally confirmed, but there are many Large Hadron Collider searches for some forms of supersymmetry. Unlike the standard model of particle physics, $\mathcal{N} = 4$ SYM is not a theory of physically observable particles. However, $\mathcal{N} = 4$ SYM is one of the most important theories in the field of scattering amplitudes nevertheless.

It is a natural question to ask why $\mathcal{N} = 4$ SYM is studied if the particles it describes are not experimentally observed (and not expected to be). The study of $\mathcal{N} = 4$ SYM is motivated by its surprising simplicity. As we will see in this work, advances in the study of scattering amplitudes have been accelerated by an increased understanding of $\mathcal{N} = 4$ SYM . $\mathcal{N} = 4$ SYM theory can arise in the study of string theories via the AdS/CFT correspondence, which relates a string theory living in the bulk of an anti-de Sitter (AdS) space to a CFT living on the boundary of that space. Research in $\mathcal{N} = 8$ supergravity has also benefited from $\mathcal{N} = 4$ SYM results by expressing supergravity as a double copy of SYM. $\mathcal{N} = 4$ SYM has found uses it in unexpected places.

In the work to be presented, the most relevant connection to physics is the appearance of $\mathcal{N} = 4$ SYM in relation to quantum chromodynamics (QCD) scattering amplitudes. QCD is the physical theory of quarks and gluons describing the strong interaction. $\mathcal{N} = 4$ SYM is commonly referred to as the cousin of QCD. QCD calculations are significantly harder than $\mathcal{N} = 4$ SYM calculations. In fact much of the progress in QCD computations arise from advancements on the $\mathcal{N} = 4$ SYM side [3]. At tree level, QCD and $\mathcal{N} = 4$ SYM pure gluon scattering amplitudes yield the same results![1] The tree level component is often considered the most important component because it provides valuable insight into the leading order behavior. The relationship between $\mathcal{N} = 4$ SYM and QCD amplitudes beyond tree level has been studied in the literature [4]. This work will not detail the applicability of $\mathcal{N} = 4$ SYM theory to QCD scattering amplitudes. The direct equivalence is lost at loop level calculations, which is the focus of this work.

In addition to being extremely useful to describe real physical theories, the true value of $\mathcal{N} = 4$ SYM lies in its computational power. Some of the most precise experiments to date match loop order quantum field theory calculations. The mathematical properties of $\mathcal{N} = 4$ SYM greatly simplify scattering amplitude calculations in the theory allowing analytic results to be obtained for multiple loop gluon scattering processes. To date, up to five loop calculations have been performed in $\mathcal{N} = 4$ SYM [5]. $\mathcal{N} = 4$ SYM is a conformal field theory (CFT). As with all conformal theories, $\mathcal{N} = 4$ SYM is invariant under rescalings and all of the particles in the theory are massless. A conformal theory does not depend on the choice of scale, allowing the most convenient scale for the given

[1] Note: To define asymptotic states and scattering amplitudes in $\mathcal{N} = 4$ SYM , $(4-2\epsilon)$-dimensional regularization is used to slightly break the conformal invariance.

problem to be selected. The ability to rescale variables in a given problem without changing the physics is a useful property.

It is believed that $\mathcal{N} = 4$ SYM in the planar limit (large number of colors) is exactly solvable. The relative simplicity has led to $\mathcal{N} = 4$ SYM being one of the most commonly used theories in scattering amplitudes. The beauty of $\mathcal{N} = 4$ SYM is realized through an understanding of symmetries arising from the mathematical structure of scattering amplitudes. The traditional Feynman diagram approach to scattering amplitudes obscures the mathematical structure possessed by these amplitudes. Much of the recent progress has been supercharged through a deeper knowledge of the symmetries possessed by $\mathcal{N} = 4$ SYM .

Overview of Thesis

There are many approaches leading from a standard physics graduate curriculum to modern scattering amplitude research in $\mathcal{N} = 4$ SYM theory. However, a complete understanding is not required to extract value from the results that are presented. In this thesis, I attempt to follow a pedestrian path leading from a standard graduate physics curriculum to the main results of this work. Of course, I strive to maintain coherency for the average reader as long as possible without sacrificing mathematical rigor. A technically well-versed reader should find the later chapters self contained.

The focus of this work will be $\mathcal{N} = 4$ SYM scattering amplitudes that are relevant to QCD, gluon scattering amplitudes in the planar limit. Specifically, recent seven point four-loop maximally helicity violating and three-loop next-to-maximally helicity violating will be presented. Chapter 2 reviews the field of scattering amplitudes leading to modern research. It includes a review of the spinor helicity formalism, QCD, $\mathcal{N} = 4$ SYM theory, twistor space, and modern loop amplitudes. Chapter 3 reviews the mathematical tools and terminology necessary to understand the main results presented. In Chapter 4 the recent results of seven- point gluon scattering amplitudes obtained through collaboration with Lance Dixon, James Drummond, Andrew McLeod, Georgios Papathanasiou, and Marcus Spradlin are presented. An investigation with Marcus Spradlin into the cluster algebra structure of six- and seven- point gluon scattering amplitudes is detailed in Chapter 5. Finally, the last chapter concludes this thesis by presenting possible directions of future work.

Chapter 2

Scattering Amplitudes

In a standard quantum mechanics course, a scattering amplitude is introduced as the amplitude of an outgoing wave relative to an incoming plane wave in a stationary-state scattering process. In quantum field theory, the scattering amplitude is the quantum mechanical amplitude for a process to occur. The differential cross section for a scattering process is proportional to the square of its scattering amplitude. A majority of a standard quantum field theory course is concerned with how to calculate scattering amplitudes for various physical processes. In general, scattering amplitudes cannot be calculated exactly so physicists resort to perturbatively expanding the scattering amplitude.

In 1948, Richard Feynman introduced a beautiful method that uses diagrams to compute scattering amplitudes [6]. In the Feynman diagram approach, each diagram represents a specific process and contribution to the scattering amplitude. The *tree-level* diagrams, those with no loops, determine the first term in the perturbative expansion of the scattering amplitude. The remaining contributions to the perturbative expansion of the coupling constant can be identified by diagrams with loops. As one would expect, the higher loop terms provide higher-order corrections to the *tree-level* result. The Feynman rules for evaluating the diagrams are determined by the theory that dictates the physical processes. Typically, the rules are derived from the Lagrangian of the theory. The Feynman diagram approach has been the canonical way to calculate scattering amplitudes for the past 50 years.

While it has proven indispensable to calculate the scattering amplitudes of countless physical scattering processes, the Feynman diagram approach becomes intractable for processes with a large number of external particles. Using the standard Feynman diagram approach, a $g+g \to g+g+g+g$ gluon

scattering amplitude at *tree-level* would require computing 220 diagrams. A $g+g \to g+g+g+g$ requires 2485 diagrams and a $g+g \to g+g+g+g+g+g$ would require 10525900 diagrams[7]! The number of diagrams grows quickly with the number of external legs. Surprisingly, the *tree-level* n-gluon maximally helicity violating amplitude can be expressed in a single line using the Parke-Taylor formula [8]. It is believed that such a simple form for the *tree-level* n-gluon amplitude is not accidental and there must be a way to construct the theory so the answer is easily obtained. This hope initiated research into the underlying mathematical structure of amplitudes.

The field of scattering amplitudes has transformed drastically over the past twenty years. Modern research is heavily focused on discovering and exploiting the mathematical structure of amplitudes in $\mathcal{N} = 4$ SYM theory. Many of the greatest advancements have been driven by a deeper understanding of the underlying mathematical structure. Additionally, the introduction of new mathematical tools, such as the symbol, has revolutionized how modern amplitudes are computed. In this thesis, we will focus on advancements in planar $\mathcal{N} = 4$ SYM scattering amplitudes.

The scattering amplitude essentials are presented and recent achievements relevant to gluon scattering amplitudes in $\mathcal{N} = 4$ SYM theory will be outlined. The chapter starts off with a kinematics section reviewing the spinor helicity formalism. Helicity classification of amplitudes is explained in Section 2.2. Then, a slight detour in Section 2.3 is taken to provide a lightning review of the essentials needed from quantum chromodynamics. $\mathcal{N} = 4$ SYM superamplitudes are covered in Section 2.4. Section 2.5 reviews twistor space and the twistor variables. Loop amplitudes are reviewed in Section 2.6, concluding the chapter.

2.1 Kinematics

External momenta of the scattering particles are the main input variables into scattering amplitudes in any physical theory. While the complexities of amplitudes vary immensely with the theory, the complexity of the form of a scattering amplitude is strongly dependent on the choice of variables used to encode the external momenta information. Amplitudeologists learned early on in history of the field of scattering amplitudes that enormous simplifications are obtainable through a change of momenta variables. As a result, modern scattering amplitudes are expressed in a plethora of different momenta variables. In this section, I hope to shed some light into how to relate these unusual (to the inexperienced amplitudeologist) variables to the more familiar Lorentz four-momenta.

In the standard Feynman diagram approach to amplitudes, scattering amplitudes are expressed as functions of the external particle kinematic data. Some kinematic variables of high importance

are: spin, mass, polarization, and four-momenta p_i^μ. For a given scattering amplitude, the physical diagrams are drawn and the Feynman rules for external lines, propagators, and vertex rules depend on the kinematic data. By using a spinor representation for the external momenta, many simplifications can be made leading to significant advancement in our ability to calculate scattering processes. Let's investigate how we can convert from the traditional momenta four-vectors to spinors.

From group theory we know that the Lorentz group transforms under a smaller spinor representation. The conversion of Lorentz vectors to spinors is simply a mapping of the Lorentz vectors in the SO(3, 1) representation to Weyl spinors in the $\left(\frac{1}{2}, \frac{1}{2}\right)$ spinor representation. We start off by introducing the spinor helicity formalism for spin-1/2 particles and then introduce spinor helicity for massless vectors by showing how polarizations are handled.

In this section, the transition from the traditional Feynman diagram approach to helicity amplitudes will be motivated and explained. The recipe for constructing spinors from Lorentz four-vector momenta, known as spinor helicity formalism, will be reviewed. The extension to massless vectors will be shown by expressing polarization vectors in the spinor language. Finally, the conventional amplitude helicity classification scheme will be explained and the difficulty of calculating an amplitude will be classified by how helicity violating the process is.

2.1.1 Spinor Helicity Introduction

We begin by discussing how the traditional momenta four-vectors for massless particles are encoded in modern scattering amplitude calculations. Throughout this chapter we adopt the conventions used in Srednicki's Quantum Field Theory textbook [9] and use the $\eta_{\mu\nu} = diag(-1, +1, +1, +1)$ metric. As we will show, the typical momenta four vectors used to describe the momenta of external particles can be replaced with more a favorable spinor representation using a formalism known as Spinor Helicity Formalism. We begin by quickly bridging the gap between a four-vector representation and spinor representation of momenta.

For a given particle with momenta p, the components of the momenta are packaged into the four-vector $p^\mu = (p^0, p^1, p^2, p^3)$ which satisfies $p^\mu p_\mu = -m^2$. If the momenta-four vector p_μ is contracted with the gamma matrices γ^μ, then the resulting matrix $\not{p} = p_\mu \gamma^\mu$ contains all of the components of the momenta four-vector. The $\not{p}$ matrix turns out to be extremely important since it appears frequently in scattering amplitude computations. Additionally, it appears in the Dirac equation and

Weyl equation. We will use the standard definition for the γ^μ matrices

$$\gamma^\mu = \begin{pmatrix} 0 & \sigma^\mu \\ \bar{\sigma}^\mu & 0 \end{pmatrix} \tag{2.1.1}$$

where $(\sigma^\mu) = (\mathbb{1}, \vec{\sigma}^i)$ and $(\bar{\sigma}^\mu) = (\mathbb{1}, -\vec{\sigma}^i)$ for $\mu = 0, \ldots, 3$. The σ^i are the standard Pauli spin matrices where

$$\sigma^1 = \begin{pmatrix} 0 & 1 \\ 1 & 0 \end{pmatrix} \qquad \sigma^2 = \begin{pmatrix} 0 & -i \\ i & 0 \end{pmatrix} \qquad \sigma^3 = \begin{pmatrix} 1 & 0 \\ 0 & -1 \end{pmatrix} \tag{2.1.2}$$

Contracting p_μ with γ^μ, we get

$$\not{p} = \begin{pmatrix} 0 & p_u\sigma^\mu \\ p_u\overline{\sigma}^\mu & 0 \end{pmatrix} \tag{2.1.3}$$

The resulting matrix is block-diagonal consisting of following 2×2 matrices

$$p_u\sigma^\mu = \begin{pmatrix} -p^0 + p^3 & p^1 - ip^2 \\ p^1 + ip^2 & -p^0 - p^3 \end{pmatrix} \tag{2.1.4}$$

and

$$p_u\overline{\sigma}^\mu = \begin{pmatrix} -p^0 - p^3 & -p^1 + ip^2 \\ -p^1 - ip^2 & -p^0 + p^3 \end{pmatrix} \tag{2.1.5}$$

The determinant of each of these matrices gives the square of the mass

$$\det(p_u\sigma^\mu) = \det(p_u\overline{\sigma}^\mu) = m^2 \tag{2.1.6}$$

For massless particles, the determinants of both of $p_u\sigma^\mu$ and $p_u\overline{\sigma}^\mu$ vanish

$$\det(p_u\sigma^\mu) = \det(p_u\overline{\sigma}^\mu) = 0 \tag{2.1.7}$$

and both $p_u\sigma^\mu$ and $p_u\overline{\sigma}^\mu$ are rank-one matrices. From linear algebra, we know that a 2×2 matrix with rank one can be formed by the outer (also known as dyadic) product of two spinors. Such matrices are commonly referred to as bispinors.

In order to understand how spinors will be used to represent the momenta bispinors appearing in the $\not{p}$ matrix, we begin by reviewing how Dirac spinors can be composed of Weyl spinors. We start with the general case of a massive particle and then restrict to massless particles. Relativistic

spin-1/2 particles are described by the Dirac equation (with $\hbar = 1$):

$$(-i\partial\!\!\!/ + m)\psi = 0 \tag{2.1.8}$$

where $\partial\!\!\!/ = \gamma^\mu \partial_\mu$. If we multiply the Dirac equation by $(i\partial\!\!\!/ + m)$, we see that a Dirac spinor ψ satisfying the Dirac equation also satisfies the Klein-Gordon equation:

$$(-\partial^2 + m^2)\psi = 0 \tag{2.1.9}$$

In order to solve for the Dirac spinor, we follow the traditional approach to solving the Klein-Gordon equation and consider a plane wave solution of the form:

$$\psi(x) = u(p)e^{ipx} + v(p)e^{-ipx} \tag{2.1.10}$$

Using the plane wave solution above, the Dirac spinors $u(p)$ and $v(p)$ must satisfy the following equations:

$$(p\!\!\!/ + m)u(p) = 0 \tag{2.1.11}$$

$$(-p\!\!\!/ + m)v(p) = 0 \tag{2.1.12}$$

Since we will be interested in forming spinor quantities that are invariant under Lorentz transformations, we would like to be able to form Lorentz invariants from Dirac spinors. Multiplying the Hermitian conjugate of a Dirac spinor and Dirac spinor does not produce a Lorentz invariant quantity. Instead, we introduce the barred Dirac spinors known as the Dirac adjoint such that the product of a Dirac adjoint and a Dirac spinor produce a Lorentz invariant quantity. The adjoint is defined in the following way with:

$$\overline{u}(p) \equiv u^\dagger \gamma^0 \tag{2.1.13}$$

$$\overline{v}(p) \equiv v^\dagger \gamma^0 \tag{2.1.14}$$

where

$$\gamma^0 = \begin{pmatrix} 0 & I \\ I & 0 \end{pmatrix} \tag{2.1.15}$$

The Dirac adjoints satisfy the following equations:

$$\overline{u}(p)(\not{p} + m) = 0 \tag{2.1.16}$$

$$\overline{v}(p)(-\not{p} + m) = 0 \tag{2.1.17}$$

At this point, we will restrict our story to massless particles. The equations for the Dirac spinors u, v, $\overline{u}$, and $\overline{v}$ become

$$\not{p}u(p) = \not{p}v(p) = \overline{u}(p)\not{p} = \overline{v}(p)\not{p} = 0 \text{ and } p^2 = 0 \tag{2.1.18}$$

From the form of the plane wave, eq. (2.1.10), we can see that term involving v is the outgoing Dirac spinor for an anti-fermion and the term involving u is for an incoming fermion. Similarly, $\overline{v}$ corresponds to an incoming anti-fermion and $\overline{u}$ corresponds to an outgoing fermion. In scattering amplitudes, we will often assume that all particles in a scattering event are outgoing and focus on v and $\overline{u}$.

When solving for the Dirac spinors $\overline{u}$ and v, each Dirac spinor can be expressed as two Weyl spinors of opposite handedness (one left-handed and one right-handed). Following standard practices, we label an outgoing particle with momentum p by its helicity. A positive helicity is represented using a square bracket $|p]_a$ and a negative helicity is represented using an angle bracket $|p\rangle^{\dot{a}}$. The indices on the angle and square brackets are written to express that these are spinor objects. Note that the indices for angle brackets are written with a dot over them in order to distinguish from indices belonging to a square bracket spinor. With this choice of angle and square bracket labeling,

$$v_+(p) = \begin{pmatrix} |p]_a \\ 0 \end{pmatrix} \qquad v_-(p) = \begin{pmatrix} 0 \\ |p\rangle^{\dot{a}} \end{pmatrix} \tag{2.1.19}$$

$$\overline{u}_+(p) = \begin{pmatrix} [p|^a & 0 \end{pmatrix} \qquad \overline{u}_-(p) = \begin{pmatrix} 0 & \langle p|_{\dot{a}} \end{pmatrix} \tag{2.1.20}$$

where $|p]_a$, $[p|^a$, $|p\rangle^{\dot{a}}$, and $\langle p|_{\dot{a}}$ are two component Weyl spinors. The Weyl equations that each of these spinors satisfies can be obtained by replacing v or $\overline{u}$ in eq. (2.1.18) with one of the spinors above.

Under charge conjugation, fermions become anti-fermions and vise-versa. Therefore there is a connection between the spinor of the same helicity with upper and lower indices. Expressed in terms of the Dirac spinors,

$$C\overline{u}_\pm(p)^T = v_\pm(p) \tag{2.1.21}$$

where C is the charge conjugation matrix. In the language of the angle and bracket spinors, the spinors with upper indices can be found from the spinors with lower indices using the 2×2 antisymmetric tensor ϵ^{ab} where

$$\epsilon^{ab} = \epsilon^{\dot{a}\dot{b}} = -\epsilon_{ab} = -\epsilon_{\dot{a}\dot{b}} = \begin{pmatrix} 0 & -1 \\ 1 & 0 \end{pmatrix} \tag{2.1.22}$$

Expressed in the angle/square bracket language, the relationships between the spinors are shown below

$$|p\rangle^{\dot{a}} = \epsilon^{\dot{a}\dot{b}}\langle p|_{\dot{b}} \tag{2.1.23}$$

$$|p]_a = \epsilon_{ab}[p|^b \tag{2.1.24}$$

$$\langle p|_{\dot{a}} = \epsilon_{\dot{a}\dot{b}}|p\rangle^{\dot{b}} \tag{2.1.25}$$

$$[p|^a = \epsilon^{ab}|p]_b \tag{2.1.26}$$

Now we are interested in how we can construct the $\not{p}$ matrix from the angle/square spinors. Specific products of (massless) Weyl spinors can be related to the $\not{p}$ matrix in the following way

$$u_\pm(p)\overline{u}_\pm(p) = \frac{1}{2}(1 \pm \gamma_5)(-\not{p}) \tag{2.1.27}$$

$$v_\pm(p)\overline{v}_\pm(p) = \frac{1}{2}(1 \mp \gamma_5)(-\not{p}) \tag{2.1.28}$$

where γ_5 is

$$\gamma_5 = \begin{pmatrix} -\mathbb{1} & 0 \\ 0 & \mathbb{1} \end{pmatrix} \tag{2.1.29}$$

The $\not{p}$ matrix may be expressed in terms of the Weyl spinors as

$$-\not{p} = u_\pm(p)\overline{u}_\pm(p) + v_\pm(p)\overline{v}_\pm(p) \tag{2.1.30}$$

Using the typical phase convention, the two types of particles can be related using

$$u_\mp(p) = v_\pm(p) \qquad \overline{v}_\pm(p) = \overline{u}_\mp(p) \tag{2.1.31}$$

In terms of the Weyl spinors defined in eqs. 2.1.19 and 2.1.20, $\not{p}$ can be expressed as

$$\not{p} = \begin{pmatrix} 0 & -|p]_a \langle p|_{\dot{a}} \\ -|p\rangle^{\dot{a}} [p|^a & 0 \end{pmatrix} \tag{2.1.32}$$

The two non-zero component objects are know as momentum bispinors. We define variables $p_{a\dot{a}}$ and $p^{\dot{a}a}$ for the two momentum bispinors in the following way

$$p_{a\dot{a}} = -|p]_a \langle p|_{\dot{a}} \qquad p^{\dot{a}a} = -|p\rangle^{\dot{a}} [p|^a \tag{2.1.33}$$

Now, we have arrived at an expression for the $\not{p}$ matrix using Weyl spinors and using the components of momenta four-vectors. The last step is to establish how the momenta can be expressed in terms of Weyl spinors. We originally wanted to formulate a representation of the momenta four-vectors in terms of Weyl spinors. If we look at the explicit form of $\not{p}$ in eq. 2.1.3, we notice that the two nonzero terms can be explicitly written as products of two spinors.

$$p_u \sigma^\mu = \begin{pmatrix} -p^0 + p^3 & p^1 - ip^2 \\ p^1 + ip^2 & -p^0 - p^3 \end{pmatrix} = \frac{t}{\sqrt{-p^0 + p^3}} \begin{pmatrix} -p^0 + p^3 \\ p^1 + ip^2 \end{pmatrix} \frac{t^{-1}}{\sqrt{-p^0 + p^3}} \begin{pmatrix} -p^0 + p^3 & p^1 - ip^2 \end{pmatrix} \tag{2.1.34}$$

and

$$p_u \overline{\sigma}^\mu = \begin{pmatrix} -p^0 - p^3 & -p^1 + ip^2 \\ -p^1 - ip^2 & -p^0 + p^3 \end{pmatrix} = \frac{t^{-1}}{\sqrt{-p^0 + p^3}} \begin{pmatrix} -p^1 + ip^2 \\ -p^0 + p^3 \end{pmatrix} \frac{t}{\sqrt{-p^0 + p^3}} \begin{pmatrix} -p^1 - ip^2 & -p^0 + p^3 \end{pmatrix} \tag{2.1.35}$$

Now, we can eqs. 2.1.32-2.1.35 to express the angle and square spinors in terms of the components of the momenta four-vector

$$|p]_a = \frac{t}{\sqrt{-p^0 + p^3}} \begin{pmatrix} -p^0 + p^3 \\ p^1 + ip^2 \end{pmatrix} \qquad \langle p|_{\dot{a}} = \frac{t^{-1}}{\sqrt{-p^0 + p^3}} \begin{pmatrix} -p^0 + p^3 & p^1 - ip^2 \end{pmatrix} \tag{2.1.36}$$

$$|p\rangle^{\dot{a}} = \frac{t^{-1}}{\sqrt{-p^0 + p^3}} \begin{pmatrix} -p^1 + ip^2 \\ -p^0 + p^3 \end{pmatrix} \qquad [p|^a = \frac{t}{\sqrt{-p^0 + p^3}} \begin{pmatrix} -p^1 - ip^2 & -p^0 + p^3 \end{pmatrix} \tag{2.1.37}$$

Looking at the form of the spinors, we see that they satisfy the expected relations, eq. (2.1.23), for raising/lowering spinor indices. As a result, the $\not{p}$ matrix can be parameterized with only $|p\rangle^{\dot{a}}$ and $|p]_a$.

Finally, we have arrived at expressions for the momenta four-vector in terms of Weyl spinors. Before we finish our review of Weyl spinors, it is important to express how the Lorentz-invariant quantities can be expressed using the square and angle bracket spinors. Lorentz invariant quantities are formed using

$$\overline{u}_-(p)v_-(q) = \langle p|_{\dot{a}}|q\rangle^{\dot{a}} \equiv \langle pq\rangle \tag{2.1.38}$$

$$\overline{u}_+(p)v_+(q) = [p|^a|q]_a \equiv [pq] \tag{2.1.39}$$

We skip a review of all of the various properties obeyed by these spinors. For a thorough review of spinor helicity formalism refer to [10].

2.1.2 Massless Vectors in Spinor Helicity

Now that we have discussed how to represent massless momenta four-vectors in the new spinor language, we are interested in extending this language to describe spin. Amplitudes for particles with spin are functions of the external momenta p_i and polarization vectors ϵ_i^μ. When moving from traditional momenta vectors to the momenta spinors, it is more convenient to express an amplitude in terms of the helicities, eliminating the polarization vector dependence. In order to move to an entirely spinor representation, the polarization vector must be written in the spinor language. Here, the polarization vectors in the spinor language will be stated without proof. The polarization vectors are given by

$$\epsilon_+^\mu = -\frac{\langle q|\gamma^\mu|p]}{\sqrt{2}\langle qp\rangle} \qquad \epsilon_-^\mu = -\frac{\langle p|\gamma^\mu|q]}{\sqrt{2}[qp]} \tag{2.1.40}$$

where q is a reference spinor. Note: we have dropped the indices on the spinors. For each external spin-one particle, a reference spinor q must be chosen so that $q \neq p$. The polarization vectors contracted with γ_μ take the form

$$\not{\epsilon}_+^\mu = -\frac{\sqrt{2}}{\langle qp\rangle}\left(|p]\langle q| + |q\rangle p|\right) \qquad \not{\epsilon}_-^\mu = -\frac{\sqrt{2}}{[qp]}\left(|p\rangle[q| + |q]\langle p|\right) \tag{2.1.41}$$

As discussed by Witten in [11], there is no natural way to pick a polarization vector associated with a given particle momentum and helicity. However, given a spinor decomposition and a helicity, a polarization vector up to a gauge transformation can be determined. More details associated with picking negative/positive helicity polarization vectors can be found in [12, 7].

Equipped with a representation of the momenta and polarization vector in terms of Weyl spinors, we can express scattering amplitudes of massless gauge bosons as a function of the spinors $|p\rangle$ and

$|p]$ and helicities $h_i = \pm 1$ of the external particles. A general scattering amplitude will be written as $\mathcal{A}(|i\rangle, |i], h_i)$ where i represents the momentum of the ith particle.

2.2 Helicity Classification

In the scattering of n gluons, it is common to assume that all of the gluons are outgoing for simplicity. Crossing symmetry, flipping the helicity of the particles when they are switched from outgoing to incoming, can be used to yield the remaining amplitudes of interest from amplitudes where all particles are outgoing. We will assume that all of the gluons are outgoing unless otherwise stated. Classifying scattering amplitudes based on the helicity structure of the external particles proves to be extremely useful for determining underlying mathematical structure since amplitudes belonging to the same helicity classification share many similarities.

It is a well known result that the scattering amplitude of n outgoing gluons with the same helicity vanishes. Additionally, the amplitude where one gluon helicity is different from all others is also zero for $n > 3$.

$$\mathcal{A}_n^{\text{tree}}(1^+2^+3^+\cdots n^+) = \mathcal{A}_n^{\text{tree}}(1^-2^+3^+\cdots n^+) = 0 \tag{2.2.1}$$

These results can be explained at tree level by looking at the general form of a gluon tree amplitude in the spinor representation and counting the powers of momenta [10]. The first non-zero tree amplitude, $\mathcal{A}_n(1^-2^-3^+\cdots n^+)$, has $n-2$ positive helicity gluons and 2 negative helicity gluons. This amplitude is known as the "maximally helicity violating" amplitude, or MHV. As we will see, this MHV amplitude is also the simplest tree level amplitude in $\mathcal{N} = 4$ SYM.

For this discussion we will relax the assumption that all particles are outgoing. The notion of "helicity violating" processes comes from considering $2 \to n-2$ scattering processes. If the helicities of the outgoing particles are identical to the helicities of the incoming particles, we say that there is no helicity violation. Maximum helicity violation occurs when the maximum number of outgoing particles have the opposite helicity as the helicity of the incoming particles. If all of the outgoing particles have the opposite helicity as the incoming particles, crossing symmetry would bring the amplitude to zero since it's an n outgoing gluon amplitude where all the particles have the same helicity. Similarly, an amplitude with only one outgoing particle helicity identical to the incoming helicity would vanish as well.

The MHV process is the process where two of the outgoing particles have the same negative helicity as the incoming particles and the remaining $(n-4)$ outgoing particles have the opposite

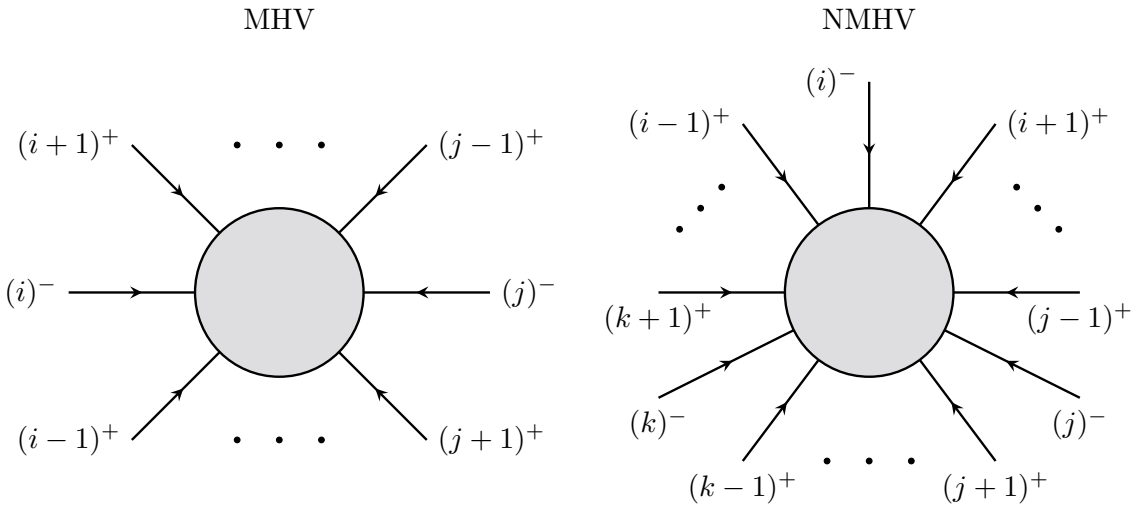

Figure 2.2.1: Helicity Specification

positive helicity. Using crossing symmetry this is an n outgoing gluon amplitude where only two of the particles have negative helicity and the remaining $(n-2)$ particles have positive helicity. We could have equivalently chosen to define MHV processes where the helicity violation we are referring to is helicity violation with respect to positive incoming particles, but those scattering amplitudes are known in the literature as anti-MHV or $\overline{\text{MHV}}$. Anti-MHV processes are those with n outgoing particles with $n-2$ negative helicity gluons and 2 positive helicity gluons. The $\overline{\text{MHV}}$ can be obtained from the MHV amplitude by flipping all the helicities. In explicit expressions consisting of angle and square brackets, this is accomplished by exchanging the two spinors.

As soon as we flip at least one of the outgoing positive helicity gluon to a negative helicity gluons in an MHV process (when considering $2 \to n-2$ scattering), we arrive at more complicated amplitudes known as next-to-maximally helicity violating (NMHV) amplitudes. Explicitly NMHV is the process of n outgoing gluons with three negative helicity gluons and $(n-3)$ positive helicity gluons. We can keep flipping positive helicities to negative helicities until we have only 2 outgoing positive helicity gluons left (where we have arrived at the $\overline{\text{MHV}}$ amplitude. Each successive flip of a positive helicity gluon to a negative helicity gluon in an MHV amplitude adds a "next-" to the name of the resulting process. For simplicity, we express these names with powers of N. For example N^2MHV refers to the amplitude for n outgoing gluons with four negative helicity gluons and $(n-4)$ positive helicity gluons. Generalizing further, a N^kMHV amplitude has $k+2$ negative helicity gluons and $n-k-2$ positive helicity gluons.

Before moving on we now take a short detour and review quantum chromodynamics and detail what an amplitude in the planar limit means.

2.3 Lightning QCD Review

Using the spinor helicity formalism and the Feynman rules, multi-gluon scattering amplitudes can be computed perturbatively in QCD. Perturbative computations are extremely challenging because the number of diagrams grows very quickly with the number of external gluons. In this section, the basics of quantum chromodynamics will be reviewed. We will briefly review how amplitudes can be constructed from *color-ordered* partial amplitudes. The Feynman rules for QCD will not be given here since we will not compute QCD scattering amplitudes. The Feynman rules for QCD can be found in [9]. The all n-gluon tree amplitude will be presented. After discussing extensions to loop amplitudes, we motivate the study of planar amplitudes and transition to $\mathcal{N} = 4$ SYM .

Let's start by off with a description of gluons in QCD. Gluons, in the absence of quarks, are described with an $SU(3)$ Yang-Mills theory. Full QCD results from coupling the gluons to quarks (represented by fermionic fields). While the gauge group of the gluons is SU(3), it can be generalized to $SU(N_c)$ for N_c colors. Gluons in an $SU(N_c)$ gauge theory have adjoint color indices $a = 1, 2, \ldots, N_C^2 - 1$. Quarks and antiquarks have indices i and $\bar{j}$ respectively where $i, \bar{j} = 1, 2, \ldots, N_C$. In the fundamental representation of QCD, the $SU(N_C)$ generators T^a are traceless hermitian $N_C \times N_C$ matrices. The commutation relations of these generators define the structure constants f^{abc} as

$$\left[T^a, T^b\right] = i\sqrt{2} f^{abc} T^c \tag{2.3.1}$$

Using the standard quantum field approach, the Feynman rules for a Yang-Mills theory can be derived from the Lagrangian

$$\mathcal{L}_{\text{YM}} = -\frac{1}{4}\text{Tr}\left(F^{\mu\nu}F_{\mu\nu}\right) \tag{2.3.2}$$

Looking at the Feynman rules, we can see that the group theory structure constants f^{abc} appear for pure gluon three-point vertices, products of the structure constants appear for pure gluon four-point vertices, and factors of the generators appear for gluon-quark-antiquark vertices. Since the structure constants are defined by the algebra, the structure constants that appear can be replaced with traces of the generators using the following relation

$$i\sqrt{2} f^{abc} = \text{Tr}(T^a T^b T^c) - \text{Tr}(T^a T^c T^b) \tag{2.3.3}$$

After using the Feynman rules to compute an amplitude and replacing the structure constants with the generators using the substitution above, a multi-gluon amplitude becomes a product of traces of

some combination of the generators. Additionally, products of the generators arising from external quarks can be reduced using the $SU(N_C)$ Fierz identity.

Tree level gluon amplitudes can then be reduced to a sum of single trace terms. An n-gluon tree amplitude factors in the following way:

$$\mathcal{A}_n^{\text{tree}}(p_1, \epsilon_1, \ldots, p_n, \epsilon_n) = g^{n-2} \sum_{\sigma} \text{Tr}(T^{a_{\sigma(1)}} T^{a_{\sigma(2)}} \cdots T^{a_n}) A_n^{\text{tree}}(p_{\sigma(1)}, \epsilon_{\sigma(1)}, \ldots, p_{\sigma(n)}, \epsilon_{\sigma(n)}) \quad (2.3.4)$$

where the coupling constant $g^2/(4\pi) = \alpha_s$ and σ is the set of all non-cyclic permutations of the external momenta. More formally, $\sigma = S_n/Z_n$ where S_n is the set of all permutations of n elements and Z_n is the set of cyclic permutations of n elements. The A_n^{tree} are known as the *color-ordered* or *partial* amplitudes. They are functions of the kinematic information and are dressed by single trace factors consisting of a product of the generators. These amplitudes are known as *color-ordered* because the external gluons are labeled with a specific ordering (not necessarily sequential!). To calculate the partial amplitude, we find every diagram with the desired color-ordering and include all copies of those diagrams where the labels are cyclically permuted. *Color-ordered* amplitudes contain all contributions with a specific cyclic ordering of the external gluons. We will be interested in computing *color-ordered* partial amplitudes and often refer to them as amplitudes.

Color ordering of the external gluons leads to useful properties. Partial amplitudes are invariant under cyclic permutations and parity transformations (flipping the helicities). Color ordering also imposes strict constraints on the partial amplitude singularity structure. We will touch more on this later. At loop level, we can extend the color decomposition for pure-gluon amplitudes. Looking at the color factors for various terms, many color factors are inversely proportional to powers of the number of colors N_c. Taking the limit of large N_c, the non-planar diagrams vanish since their color factors are proportional to $1/N_c$. This limit is known as the planar limit. In the planar limit, the diagrams that survive have a specific ordering of external legs and can then be labeled. Color ordered Feynman rules can be constructed without the appearance of color factors. More generic QCD amplitudes can also be calculated using the color decomposition method that we applied to pure-gluon amplitudes. However, we will not need these techniques.

Despite the simplicity obtained by considering partial amplitudes and taking the planar limit, using the colored-ordered Feynman rules for QCD amplitudes is still a rather cumbersome process for even relatively simple scattering gluon scattering amplitudes. As a result of this complexity, amplitudes are calculated in a simpler theory known as $\mathcal{N} = 4$ Super-Yang-Mills (SYM). Computations in $\mathcal{N} = 4$ SYM can shed light onto the more complicated QCD amplitudes. In the following

section, $\mathcal{N}=4$ SYM theory will be reviewed and its connection to QCD scattering amplitudes will be discussed. We will see that tree level all gluon amplitudes in $\mathcal{N}=4$ SYM theory are identical to the tree level QCD results.

2.4 $\mathcal{N}=4$ Super-Yang-Mills Theory

$\mathcal{N}=4$ Super-Yang-Mills Theory is a supersymmetric pure Yang-Mills theory. We study $\mathcal{N}=4$ because it contains the maximal amount of supersymmetry allowed in four dimensions. In $\mathcal{N}=4$ SYM , each gluon has four fermionic superpartners. To close the supersymmetry we also need to introduce six scalar fields. The particle content of $\mathcal{N}=4$ SYM consists of two gluons $G^{\pm}$ (bosons), six scalars (bosons), and eight gluinos (fermions). Helicities are ± 1, $\pm 1/2$, and 0 for gluons, gluinos, and scalars respectively.

The $\mathcal{N}=4$ SYM action is given by [13]

$$S = \frac{1}{g_{\rm YM}^2}\int d^4x \mathrm{Tr}\left(-\frac{1}{4}F_{\mu\nu}F^{\mu\nu} - (D_\mu\phi_{AB})D^\mu\phi^{AB} - \frac{1}{2}[\phi_{AB},\phi_{CD}][\phi^{AB},\phi^{CD}] \right.$$
$$\left. + \overline{\psi}^A_{\dot\alpha}\sigma^{\dot\alpha\alpha}_\mu D^\mu\psi_{\alpha A} - \frac{i}{2}\psi^\alpha_A[\phi^{AB},\psi_{\alpha B}] - \frac{i}{2}\overline{\psi}^A_{\dot\alpha}[\phi_{AB},\overline{\psi}^{\dot\alpha B}]\right) \tag{2.4.1}$$

where $g_{\rm YM}$ is the Yang-Mills coupling constant, ϕ are the antisymmetric scalars an ψ are the gluinos. The greek letters $\alpha,\dot\alpha$ run over $1,2$ and the latin letters A,B,C,D run over $1,2,3,4$.

$\mathcal{N}=4$ SYM is a conformal theory with SU(N) gauge invariance. The theory remains conformal after quantization because the coupling constant is not renormalized. As a result, $\mathcal{N}=4$ SYM is free from ultraviolet (UV) divergences. However, the theory still suffers from infrared (IR) divergences resulting from radiative corrections. Throughout the course of this work we will be discussing $\mathcal{N}=4$ SYM in the planar limit. We will be interested specifically in loop amplitudes. We now review scattering amplitudes in $\mathcal{N}=4$ SYM .

2.4.1 Amplitudes in $\mathcal{N}=4$ SYM

As we saw earlier, a general n-particle scattering amplitude in the planar limit of $\mathcal{N}=4$ SYM has the following form [14]:

$$\mathcal{A}_n\left(\{p_i,h_i,a_i\}\right) = (2\pi)^4\,\delta^4\left(\sum_{i=1}^n p_i\right)\sum_{\sigma\in S_n/Z_n} 2^{n/2}g^{n-2}\mathrm{tr}[t^{a_{\sigma(1)}}\cdots t^{a_{\sigma(n)}}]A_n\left(\sigma(1^{h_1},\ldots,n^{h_n})\right) \tag{2.4.2}$$

Here we have explicitly included a delta function to enforce conservation of momenta ($p_i^2 = 0$). Here we focus on the *color-ordered* amplitudes $A_n\left(\sigma(1^{h_1}, \ldots, n^{h_n})\right)$ that depend only on the helicities h_i and momenta of the external particles. The colored-ordered partial amplitudes can be perturbatively expanded in powers of the 't Hooft coupling constant $a = g_{\rm YM}^2 N/(8\pi^2)$.

Gluon amplitudes are the most commonly studied amplitudes in $\mathcal{N} = 4$ SYM. We begin with the simplest non-vanishing MHV tree-level amplitudes. A concise formula for the MHV tree amplitude for n-gluons was formulated by Parke and Taylor [8] and proven by Berends and Giele [15]

$$A_{n;0}^{\rm MHV} = A_n\left(1^+ \ldots i^- \ldots j^- \ldots n^+\right) = \frac{\langle ij\rangle^4}{\langle 12\rangle\langle 23\rangle \cdots \langle n1\rangle} \tag{2.4.3}$$

Note: this factor only depends on the angle brackets. The $\overline{\rm MHV}$ tree-level is found by replacing the angle brackets with square brackets. After perturbatively expanding the full n-gluon amplitude, the Parke-Taylor factor, eq. (2.4.3), appears at all orders in the 't Hooft coupling

$$A_n^{\rm MHV}\left(1^+ \ldots i^- \ldots j^- \ldots n^+\right) = A_{n;0}^{\rm MHV} + aA_{n;1}^{\rm MHV} + a^2 A_{n;2}^{\rm MHV} + \mathcal{O}(a^3) = A_{n;0}^{\rm MHV} M_n^{\rm MHV} \tag{2.4.4}$$

and can be factored out. The function $M_n^{\rm MHV}$ depends on the Mandelstam invariants and the 't Hooft coupling constant, but does not depend on the positions of the negative helicity gluons i and j. Calculating the MHV amplitude becomes the problem of determining $M_n^{\rm MHV}$ to all orders in the coupling constant a.

Going beyond MHV, the perturbative expansions of NMHV amplitudes no longer contain the tree-level Parke-Taylor factor. The tree-level amplitude $A_{n;0}^{\rm NMHV}$ now depends on both the angle and square brackets. Very often the angle and bracket spinor are represented using λ and $\tilde{\lambda}$ respectively. Perturbatively expanding the NMHV amplitude in the coupling constant,

$$A_n^{\rm NMHV}\left(1^+ \ldots i^- \ldots j^- \ldots k^- \ldots n^+\right) = A_{n;0}^{\rm NMHV}(\lambda, \tilde{\lambda}) + a\sum_l A_{n;1}^{{\rm NMHV},(l)}(\lambda, \tilde{\lambda}) M_{n;1}^{{\rm NMHV},(l)} + \mathcal{O}(a^2) \tag{2.4.5}$$

the new factors ($A_{n;0}^{\rm NMHV}$, $A_{n;1}^{{\rm NMHV},(l)}$) and the scalar Feynman integrals $M_{n;1}^{{\rm NMHV},(l)}$ do not retain the simple properties observed in the MHV case. All of these functions must be calculated for each helicity configuration because they depend on the positions of the negative helicity gluons [4, 16, 17, 18, 19].

As one might expect, N^{k}MHV amplitudes for $k > 1$ are more complex than NMHV amplitudes. In [17] a general one-loop NMHV gluon amplitude was found. Using traditional unitarity cuts, ex-

plicit next-to-next-to-MHV results were obtained by calculating scalar box integrals and the rational function coefficients [18]. Often times these computations are challenging and so non-MHV results for a given number of external particles are not as commonly computed as MHV amplitudes.

The simplicity of the MHV amplitudes led amplitudeologists to wonder if NMHV amplitudes could also be written in a compact form. As it turns out, the discovery of a hidden symmetry, dual (super)conformal symmetry [14], allowed NMHV amplitudes to be expressed in significantly simpler forms than the forms computed using unitarity cuts. In order to understand how this symmetry was realized and then utilized, we first review the on-shell superamplitude construction.

2.4.2 On-Shell Superamplitude Formulation

The space described in terms of the massless angle and square spinors is known as the "on-shell" space because the particles are on-shell (p_i^2=0). In order to construct an on-shell superamplitude, we first package the field content into a single superfield Φ, as was done by Nair [20]. We introduce Grassmann variables η_i^A for each external particle with an $SU(4)$ index $A = 1, \ldots, 4$. Using these Grassmann variables, all of the fields can be combined into a superfield Φ defined by

$$\Phi = G^+ + \eta^A \psi_A + \frac{1}{2}\eta^A\eta^B\phi_{AB} + \frac{1}{3!}\eta^A\eta^B\eta^C\epsilon_{ABCD}\overline{\psi}^D + \frac{1}{4!}\eta^A\eta^B\eta^C\eta^D\epsilon_{ABCD}G^- \tag{2.4.6}$$

where each of the fields where introduced at the beginning of this section. We define the superamplitude as

$$\mathcal{A}_n(\lambda, \tilde{\lambda}, \eta) = \mathcal{A}_n\left(\Phi_1, \ldots, \Phi_n\right) \tag{2.4.7}$$

Any amplitude can be extracted from the superamplitude above by taking derivatives with respect to the Grassmann variables η_{iA} and then setting the remaining Grassmann variables to zero. For example, the MHV amplitude can be obtained by

$$\mathcal{A}_n(1^+ \cdots i^- \cdots j^- \cdots n^+) = \left[\prod_{I=1}^{4}\left(\frac{\partial}{\partial\eta_i^I}\right)\prod_{J=1}^{4}\left(\frac{\partial}{\partial\eta_j^J}\right)\mathcal{A}_n\left(\Phi_1, \ldots, \Phi_n\right)\right]\Big|_{\eta_k^K \to 0} \tag{2.4.8}$$

Another way to think about this is that the superamplitude $\mathcal{A}_n$ contains the MHV pure gluon amplitude as the term multiplying a specific product of the Grassmann variables. Explicitly,

$$\mathcal{A}_n = \frac{1}{4!}\eta_i^A\eta_i^B\eta_i^C\eta_i^D\epsilon_{ABCD}\frac{1}{4!}\eta_j^A\eta_j^B\eta_j^C\eta_j^D\epsilon_{ABCD}\mathcal{A}_n(1^+ \cdots i^- \cdots j^- \cdots n^+) + \cdots \tag{2.4.9}$$

The superamplitude also contains all of the amplitudes with fermions and scalars as well. The supersymmetric version of the MHV tree level amplitude (eq. (2.4.3)) is [20]

$$\mathcal{A}_{n;0}^{\mathrm{MHV}} = \frac{\delta^{(4)}\left(\sum_{j=1}^{n} p_j\right)\delta^{(8)}\left(\sum_{i=1}^{n}\lambda_i^{\alpha}\eta_i^{A}\right)}{\langle 12\rangle\langle 23\rangle\cdots\langle n1\rangle} \tag{2.4.10}$$

where $\delta^8\left(\sum_{i=1}^{n}\lambda_i^{\alpha}\eta_i^{A}\right) = \prod_{\alpha=1,2}\prod_{A=1}^{4}\lambda_i^{\alpha}\eta_i^{A}$. The term inside this delta function is the supermomentum and the extra delta function enforces supermomentum conservation. The full tree-level superamplitude contains both MHV and all possible N^kMHV superamplitudes as well.

When expressing the full tree-level superamplitude, the MHV superamplitude is factored out in the following way

$$\mathcal{A}_{n;0} = \mathcal{A}_{n;0}^{\mathrm{MHV}}\mathcal{P}_{n;0} \tag{2.4.11}$$

where $\mathcal{P}_{n;0}$ can be expanded in terms of functions with varying Grassmann weight.

$$\mathcal{P}_{n;0} = 1 + \mathcal{P}_{n;0}^{\mathrm{NMHV}} + \mathcal{P}_{n;0}^{\mathrm{N^2MHV}} + \cdots + \mathcal{P}_{n;0}^{\overline{\mathrm{MHV}}} \tag{2.4.12}$$

In [14], the NMHV tree-level superamplitude was conjectured

$$\mathcal{A}_{n;0}^{\mathrm{NMHV}} = \mathcal{A}_{n;0}^{\mathrm{MHV}}\sum_{1<s<t<n} R_{n;st} \tag{2.4.13}$$

and the form above was proven in [21]. In [22], tree-level superamplitudes in $\mathcal{N}=4$ SYM were determined for all n. The $R_{n;st}$, known as R-invariants, are dual superconformal invariants that will be defined later. First, we must introduce the dual coordinates and the associated symmetry.

2.4.3 Dual Conformal Symmetry

The conformal symmetry of $\mathcal{N}=4$ SYM theory is only half of the story. In addition to the standard conformal symmetry, planar $\mathcal{N}=4$ SYM has a hidden symmetry known as dual superconformal symmetry. When formulated in the appropriate dual superspace, all tree level MHV and NMHV amplitudes in $\mathcal{N}=4$ SYM are found to have a dual superconformal symmetry. This new symmetry is distinct from the typical conformal symmetry of $\mathcal{N}=4$ SYM theory. After introducing *dual* coordinates $x_{\alpha\dot{\alpha}}$ expressed in terms of the particle momenta, a $SO(2,4)$ conformal group can be defined with a linear action on the dual space coordinates. From the definition, the action of the dual conformal symmetries on the spinor variables can be derived. We first introduce the dual

coordinates.

Dual coordinates arise as an equivalent representation for the standard momenta. The dual coordinates x_i are defined to relate to the momenta by

$$p_i^\mu = x_{i+1}^\mu - x_i^\mu \tag{2.4.14}$$

for $i = 1, \ldots, n$ where $\alpha, \dot{\alpha}$ are the same $SU(2)$ indices we saw for the bispinors. As a result, the $x_i^{\alpha\dot{\alpha}}$ are relate to the momentum bispinor $p_i^{\alpha\dot{\alpha}}$ in an analogous way.

$$p_i^{\alpha\dot{\alpha}} = x_{i+1}^{\alpha\dot{\alpha}} - x_i^{\alpha\dot{\alpha}} \tag{2.4.15}$$

The dual coordinates satisfy momentum conservation by requiring $x_{n+1} = x_1$. Note these dual coordinates are not spacetime coordinates. Since we will be computing superamplitudes, it is convenient to also introduce dual fermionic supermomenta $\theta_i^{\alpha A}$ defined by

$$q_i^{\alpha A} = |\theta_{i+1}^{\alpha A}\rangle - |\theta_i^{\alpha A}\rangle \tag{2.4.16}$$

$i = 1, \ldots, n$ where $\alpha, \dot{\alpha}$ are $SU(2)$ indices and A are the $SU(4)$ indices of the Grassmann η_i. Supermomentum conservation requires $|\theta_{n+1}^{\alpha A}\rangle = |\theta_1^{\alpha A}\rangle$.

The 'dual' conformal symmetry is best presented in the dual space where the angle brackets and η_i have been replaced with the dual momenta and supermomenta. When expressed in the dual superspace, all tree-level MHV and NMHV amplitudes in $\mathcal{N} = 4$ super-Yang-Mills theory exhibit dual superconformal symmetry [14]. To explicitly construct the conformal group, we first need conformal inversion. Conformal inversion of the dual coordinates is defined in a similar way to standard conformal inversion.

$$I\big[x_{\alpha\dot{\beta}}\big] = \frac{x_{\beta\dot{\alpha}}}{x^2} \tag{2.4.17}$$

The special conformal generators K^μ are found by after performing an inversion, an infinitesimal translations, and another inversion. The rest of the conformal algebra is found by commuting the special conformal generators with the infinitesimal generator of translation. More details regarding how conformal inversion is defined for other quantities, like the momenta spinors, can be found in [14].

Since we are interested in the conformal symmetry associated with Lorentz invariant scattering

amplitudes, it is sufficient to provide the following conformal inversion properties

$$I\left[x_{ij}^2\right] = \frac{x_{ij}^2}{x_i^2 x_j^2} \tag{2.4.18}$$

$$I\left[\langle ii{+}1\rangle\right] = \left(x_i^2\right)^{-1} \langle ii{+}1\rangle \tag{2.4.19}$$

$$I\left[[ii{+}1]\right] = \left(x_{i+2}^2\right)^{-1} [ii{+}1] \tag{2.4.20}$$

More complicated dual conformally covariant quantities can be constructed, but we will not do so here. Now that we have defined the dual coordinates, we still need twistors before defining the R-invariants as they appear in eq. (2.4.13).

2.5 Twistor Space

While the spinor variables proved to be extremely useful to simplify scattering amplitudes, many modern amplitude calculations are not written in the spinor variables. Instead, they are expressed in terms of twistor variables and other physical variables constructed from twistors. With the conformal group acting linearly in configuration space, the action in momentum space is rather complicated because conformal boosts are generated by a second-order differential operator. In general, the generators are functions of the spinor variables. The goal of introducing twistors is to introduce a set of variables where the generators are linearized.

The complex projective three-space $\mathbb{P}^3$ is known as twistor space. The introduction of twistor space to scattering amplitudes was first made by Penrose [23] where he detailed a twistor description that is equivalent to complex Minkowski space-time (completed by a null cone at infinity). In his twistor representation, a null line in complex Minkowski space-time is represented by a pair of two component spinors packaged into a four component object called a twistor. One of the spinors defines the direction of the line and the other can be geometrically interpreted as its moment about an origin. In [11], Witten introduced his twistor string theory with tree-level amplitudes matching those of $\mathcal{N} = 4$ SYM theory. In this work, we will not stress the geometric interpretation of twistor variables. Instead, we will use twistors constructed from the momenta spinors as a useful change of variables that simplifies the form of scattering amplitudes.

Momentum twistors are not twistors associated with Minkowski space-time. Rather momentum twistors are formed exactly like the twistors introduced by Penrose, but the dual coordinates are used instead of the space-time coordinates. For this reason, they are referred to as momentum twistors. Momentum twistors were introduced in [24]. Momentum twistors are four component objects formed

from two spinors. In certain signatures, one of the two spinors packaged into a momentum twistor can be thought of as a Fourier transform on the angle spinors. Momentum twistors are defined by

$$Z_i^I = (|i\rangle^{\dot{a}}, [\mu_i|^a) \tag{2.5.1}$$

where $I = (\dot{a}, a)$ is an SU(2,2) index. The new spinor $[\mu_i|^a$ is defined by the following equations

$$[\mu_i|^a = \langle i|_{\dot{a}} x_i^{\dot{a}a} = \langle i|_{\dot{a}} x_{i+1}^{\dot{a}a} \tag{2.5.2}$$

known as the incidence relations.

After defining the momenta twistors Z_i^I, the square brackets can be expressed in terms of the angle brackets and the new $[\mu_i|^a$ spinors. Let's look at how the usual square and angle bracket products can be expressed in the language of momenta twistors. Using a special skew two-index twistor appearing in the twistor algebra I_{AB}, we can write the angle and square brackets as

$$\langle ij\rangle = I_{AB} Z_1^A Z_2^B \tag{2.5.3}$$

$$[ij] = I^{AB} W_{1A} W_{2B} \tag{2.5.4}$$

where W are dual twistors that can be defined in terms of the Zs (definition can be found in [24]). We can also define dual conformal invariants from momentum twistors using the Levi-Civita ϵ_{ABCD} in the following way

$$\langle ijkl\rangle = \epsilon_{ABCD} Z_i^A Z_j^B Z_k^C Z_l^D \tag{2.5.5}$$

where the quantity $\langle ijkl\rangle$ is known as a four-bracket. The four-bracket is an extremely important quantity that appears throughout the study of scattering amplitudes.

To form momentum twistors from the bosonic coordinates, the angle brackets were replaced with the variables $[\mu_i|$ defined by the incidence relations. Following the same definition of the new bosonic spinors, we can similarly define a new Grassmann variable χ_i^A that is the fermionic analog of the $[\mu_i|$ variables. The χ_i^A are defined according to the incidence relations

$$\chi_i^A = \langle i|\theta_i^A\rangle = \langle i|\theta_{i+1}^A\rangle \tag{2.5.6}$$

We can package the momentum twistors with the new Grassmann variables χ_i^A into a quantity

known as a momentum supertwistor. The momentum supertwistors are defined as

$$\mathcal{Z}_i = \left(Z_i^a, \chi_i^A\right) = \left(\lambda_i^\alpha, x_i^{\alpha\dot{\alpha}}\lambda_{i\alpha}, \theta_i^{\alpha A}\lambda_{i\alpha}\right) \tag{2.5.7}$$

As we can see, the momentum supertwistors are formed from the angle spinors, the dual coordinates $x_i^{\alpha\dot{\alpha}}$, and the fermionic Grassmann variables $\theta_i^{\alpha A}$.

As we saw earlier, dual superconformal invariants appear at tree-level amplitudes as soon as NMHV processes are considered. Now that we have introduced momentum supertwistors, we can define R-invariants.

$$R_{n;jk} = -\frac{\delta^4\left(\langle j{-}1, j, k{-}1, k\rangle\chi_n + \text{cyclic}\right)}{\langle n, j{-}1, j, k{-}1\rangle\langle j{-}1, j, k{-}1, k\rangle\langle j, k{-}1, k, n\rangle\langle k{-}1, k, n, j{-}1\rangle\langle k, n, j{-}1, j\rangle} \tag{2.5.8}$$

Since the R-invariant definition is cyclic in the labels, we define a five-bracket $[n, j-1, j, k-1, k]$ where

$$R_{n;jk} = [n, j-1, j, k-1, k] \tag{2.5.9}$$

With these five-brackets, the tree-level n-gluon NMHV superamplitude can be written as

$$\mathcal{A}_{n;0}^{\text{NMHV}} = \mathcal{A}_{n;0}^{\text{MHV}} \sum_{j=2}^{n-3} \sum_{k=j+2}^{n} [n, j-1, j, k-1, k] \tag{2.5.10}$$

At this point we have introduced most of the momenta variables we will need to describe the scattering amplitudes presented in this work. We now review how loop amplitudes are formulated.

2.6 Loop Amplitudes in Planar $\mathcal{N} = 4$ SYM Theory

Loop amplitudes in gauge theories have been the focus of much of modern scattering amplitude research. In fact, there are many research programs dedicated to constructing loop integrands. We will only touch upon work relevant to gluon scattering amplitudes. The first one-loop amplitude for four external gluons $\mathcal{N} = 4$ SYM theory was calculated in 1982 by Green, Schwarz, and Brink as the low energy limit of a superstring amplitude [25]. In 1994, Bern, Dixon, Dunbar, and Kowoser constructed an ansätze for n-point one-loop amplitudes and determined a general n-point gluon one-loop amplitude in $\mathcal{N} = 4$ SYM theory [3]. In this section, we will review some of the most important advancements in loop calculations in the study of planar $\mathcal{N} = 4$ SYM theory. We start with the method of generalized unitarity and progress to multi-loop calculations.

The method of generalized unitarity has played a crucial role in loop order computations. Generalized unitarity is the process of constructing the full loop amplitude from unitarity cuts. By sending loop momenta on-shell (known as a unitarity cut), loop amplitudes can be written as products of lower weight amplitudes. Starting with a complete basis of integrals, computing a loop amplitude can be reduced to the problem of computing the coefficients in the complete basis. The coefficients can be determined by taking sets of unitarity cuts of the general ansatz in the complete integral basis and comparing to the factorization of the loop amplitude into lower-point amplitudes. We will not go into more details about the method of generalized unitarity, but more details can be found in textbooks like [13].

Now we want to focus on planar $\mathcal{N} = 4$ SYM loop amplitudes. As we saw earlier, $\mathcal{N} = 4$ SYM is a conformal theory free of ultraviolet divergences which cancel order by order in perturbation theory. However, loop amplitudes in planar $\mathcal{N} = 4$ SYM theory do have infrared divergences. The IR divergences can be interpreted as loop-momenta becoming *collinear* with external momenta. Typically one of the loop momenta going $soft$ leads to a $1/\epsilon$ factor. When one of each of the loop-momenta become $soft$, the $1/\epsilon^{2L}$ behavior is obtained for an L-loop amplitude. Soft and collinear limits have been well studied in massless gauge theories like $\mathcal{N} = 4$ SYM. A modern treatment can be found in the review article [26].

To handle the IR divergences, amplitudes are computed using $D = 4 - 2\epsilon$ dimensional regularization where they are well understood. Dimensional regularization breaks the conformal and dual conformal symmetries. Therefore, the complete loop order amplitudes are not (dual) conformally invariant due to the IR divergent components. While this might sound like the the end of the conformal and dual conformal symmetries, we can construct IR-finite quantities. The IR divergences in $\mathcal{N} = 4$ SYM amplitudes have a universal form. After computing the 2-loop 4-point MHV amplitude, Anastasiou, Bern, Dixon, and Kosower (ABDK) conjectured that higher loop MHV amplitudes could be expressed in terms of the one-loop results [27]. Bern, Dixon, and Smirnov observed that the iterative structure found by ABDK continued in the 3-loop 4-point computation [28]. The resulting pattern was shown to exponentiate leading to the well-known ABDK/BDS ansatz

$$\mathcal{M}_n^{\text{MHV,BDS}}(\epsilon) = \exp \sum_{L=1}^{\infty} a^L \left(f^{(L)}(\epsilon) \mathcal{M}_{n;1}^{\text{MHV}}(L\epsilon) + C^{(L)} \right) \tag{2.6.1}$$

where $\mathcal{M}_n^{\text{MHV}} = \frac{\mathcal{A}_n^{\text{MHV}}}{\mathcal{A}_{n;0}^{\text{MHV}}}$ and ϵ is the dimensional regularization parameter. The remaining functions will be explicitly defined later.

The 2-loop 5-point MHV amplitude [29, 30] matched the prediction from the BDS ansatz. At

six-points and higher, the BDS ansatz fails to produce the correct result. Fortunately, the BDS ansatz correctly captures the IR divergences and the ansatz can be corrected to match higher loop results. The correction factor, known as the remainder function R_n, is a function of dual conformally invariant cross ratios. R_n is defined as

$$\mathcal{A}_n^{\text{MHV}} = \mathcal{A}_n^{\text{MHV,BDS}} \exp\left(R_n\right) \tag{2.6.2}$$

The remainder function at loop order L is the difference between the amplitude and the BDS ansatz

$$R_{n;L} = \mathcal{M}_{n;L}^{\text{MHV}}(\epsilon) - \mathcal{M}_{n;L}^{\text{MHV,BDS}}(\epsilon) \tag{2.6.3}$$

Paired with the BDS ansatz, the L-loop remainder function is sufficient to compute the n-point L-loop MHV amplitude.

For NMHV superamplitudes the story is very similar because NMHV amplitudes have the same infrared-divergent structure as MHV amplitudes. Dual conformal invariants can be constructed by taking a ratio of the loop level and the tree-level superamplitudes. This ratio is known as the ratio function $\mathcal{P}$ where

$$\mathcal{A}_n^{\text{NMHV}} = \mathcal{A}_n^{\text{MHV}} \mathcal{P}_n \tag{2.6.4}$$

Ratio functions, like remainder functions, are IR-finite. The ratio functions at tree-level can be constructed from the R-invariants defined in eq. (2.5.8). Moving to loop level, the ratio function is given by R-invariants multiplied by transcendental functions of dual conformal invariants. New techniques for computing these loop level remainder and ratio functions will be presented in subsequent chapters. In the following chapter, the mathematical machinery needed to calculate these types of amplitudes will be discussed.

Chapter 3

Amplitude Toolbox

Many advances in $\mathcal{N} = 4$ SYM scattering amplitude calculations have been pioneered by identifying important mathematical and physical properties they satisfy. MHV and NMHV amplitudes exhibit remarkable mathematical structure beyond dual conformal invariance. In order to understand this underlying structure, we must borrow results from mathematics. Amplitude research is growing rapidly and new mathematical techniques are being applied to computations daily. Much of this mathematical formalism is hiding in highly technical papers and at this point in time cohesive reviews do not exist for many important topics. In this chapter, I hope to briefly provide some of the essentials that will be needed to understand the cluster bootstrap computations and cluster algebra structure presented in this thesis. An advanced reader could skip this chapter and move on to the results presented in Chapters 4 and 5.

3.1 Polylogarithms

Polylogarithms functions play a crucial role in the scattering amplitude story for $\mathcal{N} = 4$ SYM scattering amplitudes. In planar $\mathcal{N} = 4$ SYM theory, the rational functions appearing in the remainder and ratio functions are often classical polylogarithms. It is believed that all L-loop MHV and NMHV scattering amplitudes in planar $\mathcal{N} = 4$ SYM can be represented as linear combinations of weight $2L$ polylogarithms. Like typical classes of functions, there are many types of different polylogarithms. First, we will discuss classical polylogarithms.

A classical polylogarithm is an iterative integral of logarithms. The weight of a classical polylogarithm can be thought of as the number of integrations from the starting $1/(1-z)$ function. A

classical polylogarithms of weight k is defined by

$$\mathrm{Li}_k(z) = \int_0^z \mathrm{Li}_{k-1}(t)\mathrm{dlog}(t) \tag{3.1.1}$$

where

$$\mathrm{Li}_1(z) = -\log(1-z) \tag{3.1.2}$$

Another class of polylogarithms appearing in amplitudes are known as Goncharov's multiple polylogarithms [31] defined by

$$G(\overrightarrow{w}; z) = \int_0^z \frac{dt}{t-a} G(\overrightarrow{w}'; z) \tag{3.1.3}$$

where $\overrightarrow{w} = (a, \overrightarrow{w}')$

$$G(\overrightarrow{0_n}; z) = \frac{1}{n!}\ln^n(z) \tag{3.1.4}$$

In the case of Goncharov's multiple polylogarithms, the weight is equal to the number of elements of $\overrightarrow{w}$.

Polylogarithms satisfy complicated multiplicative (functional) identities. In [32], Golden et. al. present a 40 term trilogarithm identity. These nontrivial identities make working with analytic forms difficult. When the six-point two-loop remainder function was presented [33, 34], it was a seventeen page long expression in terms of the multiple polylogarithms defined above. It turns out that the gigantic expression presented could actually be written in terms of classical polylogarithms. By employing this mathematical tool called the **symbol**, Goncharov, Spradlin, Vergu, and Volovich were able to reduce the 17 page long expression of the six-point two-loop remainder function to an expression spanning only a few lines [35]. With higher loop computations depending on the more complicated generalized polylogarithms, the symbol is a crucial tool.

3.2 Symbol

The symbol is a mathematical tool used to represent transcendental functions that appear in scattering amplitudes. Some of the first works using symbols in physics can be found in [35, 36]. We start by assuming that we have an arbitrary function F of weight k that can be represented by iterative integrals in the following way

$$F = \int_a^b \mathrm{dlog}F_1 \cdots \mathrm{dlog}F_k \tag{3.2.1}$$

where

$$\int_a^b \mathrm{dlog}F_1 \cdots \mathrm{dlog}F_k = \int_a^b \left(\int_a^t \mathrm{dlog}F_1 \cdots \mathrm{dlog}F_{k-1} \right) \mathrm{dlog}F_k(t) \tag{3.2.2}$$

Given such a function, the symbol of F is defined by

$$S(F) = F_1 \otimes F_2 \otimes \cdots \otimes F_k \tag{3.2.3}$$

As we can see, the symbol of a weight k function is a k-fold tensor product. From the definition of a classical polylogarithm, we see that

$$d\mathrm{Li}_k(x) = -\mathrm{dlog}(1-x)\mathrm{dlog}(x) \cdots \mathrm{dlog}(x) \tag{3.2.4}$$

ad the symbol is given by

$$S(\mathrm{Li}_k(x)) = -(1-x) \otimes \underbrace{x \otimes \cdots \otimes x}_{k-1 \text{ times}} \tag{3.2.5}$$

Using the definition of symbol, the symbols for more complicated polylogarithm functions can be found be writing the function explicitly in the form of eq. 3.2.1.

Symbols in scattering amplitudes are used primarily to simplify complicated polylogarithm functions. The symbol for a function is found by applying the definition and writing the k-fold tensor product. Then a few mathematical properties are applied to the symbol. Terms in the symbol that are products can be split apart in the following way

$$AB \otimes C \otimes D = A \otimes C \otimes D + B \otimes C \otimes D \tag{3.2.6}$$

If one of the elements in the product is a constant, the same rule applies except the term containing the constant disappears. This makes sense since each element of the symbol corresponds to a differential term in the functional representation and the differential of a constant is zero.

$$cA \otimes B \otimes D = A \otimes B \otimes D \tag{3.2.7}$$

These two rules are applied and the symbol is expanded out. In the process, many terms end up canceling. Complicated, many-term polylogarithm identities are trivialized to algebraic identities at the symbol level.

Given that functions composed of transcendental functions can be expressed in many ways, it is sometimes difficult to determine if two functions are equivalent. Fortunately, symbols are uniquely

defined. There is only one symbol for a given function. If two functions have different symbols, the functions are not equivalent. A statement of equivalence of two symbols does not mean that the two functions are equivalent. Often times the products of lower weight functions are removed to simplify the overall symbol algebra. When this is done, two functions with identical symbols are only equivalent up to products of lower weight functions. Reconstruction of a full amplitude from its symbol is a nontrivial step. In the process of expanding the symbol, constant terms are lost. Only a subset of all symbols even correspond to functions and those that do are known as integrable functions. There are numerous methods for determining the beyond the symbol terms and rational functions, but the details will not be covered here.

3.3 u Variables

As seen from dual conformal symmetry [37, 38, 39, 40, 41, 42, 43, 14], the n-particle SYM scattering amplitude depends on $3(n-5)$ dual conformal cross-ratios. These cross ratios are algebraically independent and constructed by taking ratios of x_{ij}^2 where $x_{ij} = x_i - x_j$. Many modern amplitudes are expressed in terms of variables known as u variables. They are defined as ratios of the squares of the dual coordinates in the following way

$$u_{ij} = \frac{x_{i,j+1}^2 x_{i+1,j}^2}{x_{i,j}^2 x_{i+1,j+1}^2}, \qquad u_i \equiv u_{i+1,i+4} = \frac{x_{i+1,i+5}^2 x_{i+2,i+4}^2}{x_{i+1,i+4}^2 x_{i+2,i+5}^2} \tag{3.3.1}$$

where the indices are mod n. Each of the squares of the dual coordinates can be directly related to the spinor variables or the familiar Mandelstam invariants.

$$s_{i\ldots j-1} = (p_i + p_{i+1} + \cdots + p_{j-1})^2 = x_{ij}^2 = \frac{\langle i{-}1ij{-}1j\rangle}{\langle i{-}1i\rangle\langle j{-}1j\rangle} \tag{3.3.2}$$

The four-brackets are Plücker coordinates. The seven-point amplitudes will be expressed in another set of variables known as cluster-$\mathcal{A}$ coordinates. These variables are known as cluster coordinates because of their direct connection to cluster algebras, which we discuss now.

3.4 Cluster Algebras

Cluster algebras play a central role in planar $\mathcal{N} = 4$ SYM theory because of the special functional dependence of amplitudes on the momenta variables. Cluster algebras were first introduced in mathematics literature in [44, 45] and their appearance in planar $\mathcal{N} = 4$ SYM has recently been

detailed in [32, 46, 47]. Cluster algebras have beautiful connections to Stasheff polytopes as well as many other useful properties. In Chapter 5, some results describing the cluster algebraic structure of two-loop six- and seven-point amplitudes will be presented. A more complete treatment of the cluster structure of planar $\mathcal{N} = 4$ SYM scattering amplitudes can be found in [32].

Here, we aim to give a simple definition of a cluster algebra and the types of coordinates. Formally, a cluster algebra is a commutative ring. The rank n of the cluster algebra is the number of subsets known as *clusters*. Replacing an element from a cluster with an element related by an exchange relation yields another cluster. The elements of a cluster can then be related to the elements of another cluster through a series of replacements using the exchange relation. For a finite cluster algebra, this means that there are a finite number of variables existing within the clusters that can related through the exchange relation.

We will focus on only a couple of the cluster algebras relevant to $\mathcal{N} = 4$ SYM amplitudes for six and seven particles. We start with one of the simplest cluster algebras known as A_2. Starting with a cluster consisting of two variables x_1 and x_2, we can mutate on one of the two variables in the cluster using the mutation rule

$$x_{m+1} = \frac{1 + x_m}{x_{m-1}} \tag{3.4.1}$$

In each cluster, we can mutate on the variable that was not previously mutated. Repeating this process we generate the remaining cluster variables

$$x_3 = \frac{1 + x_2}{x_1} \tag{3.4.2}$$

$$x_4 = \frac{1 + x_1 + x_2}{x_1 x_2} \tag{3.4.3}$$

$$x_5 = \frac{1 + \frac{1+x_1+x_2}{x_1 x_2}}{\frac{1+x_2}{x_1}} = \frac{1 + x_1}{x_2} \tag{3.4.4}$$

Figure 3.4.1, on the next page shows the resulting A_2 cluster algebra.

Now, we can construct the A_3 cluster algebra in the same way starting with a cluster containing $\{x_1, x_2, x_3\}$. After performing all of the possible mutations on the cluster variables in each cluster, we find there are 15 unique variables. The variables, known as *cluster-χ coordinates*, are defined in [46]. The *cluster χ-coordinates* live on the configuration space $\mathrm{Conf}_n(\mathbb{P}^3)$. More details about how these cluster coordinates are formed from the momenta variables we have discussed so far is provided in Section 5.1. We now take detour and discuss the Steinmann Relations.

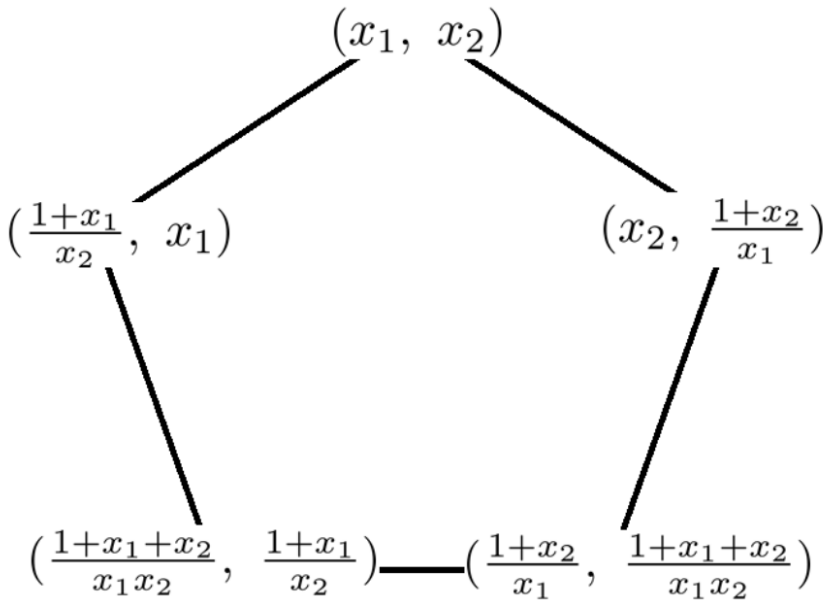

Figure 3.4.1: The figure shows the A_2 cluster algebra. Each pair of coordinates form the clusters.

3.5 Steinmann Relations

The *Steinmann relations* provide information about the allowed discontinuity structure of scattering amplitudes. Specifically, these relations restrict the space of allowed physical functions by imposing constraints on the double discontinuities that may appear in an amplitude. Here a double discontinuity is the discontinuity of a function after taking a discontinuity. As we have known for quite some time, scattering amplitudes can have poles when consecutive momenta go on-shell. An equivalent statement in the language of s-invariants would be that the amplitude is allowed to have physical poles when s-invariants go to zero. When an amplitude factors into two lower point amplitudes, we will say that a cut is not kinematically realizable if the factored amplitudes do not depend on a particular s-invariant of interest.

The *Steinmann relations* forbid the appearance of a certain discontinuities following the discontinuity in one channel (i.e. restricts which double discontinuities may appear). After taking a discontinuity when an s-invariant goes to zero, the amplitude factors into a left amplitude dependent on the the s-invariant and a right amplitude dependent on the remaining momenta and the s-invariant. The factorization of the amplitude into lower point amplitudes then prohibits the appearance of discontinuities that “cross" the factorization because the factored amplitude can only have physical poles when consecutive momenta within the left or right amplitude go to zero. In other words, we do not expect to see remaining discontinuities from s-invariants which share momenta across the

factorization.

Let us consider the behavior of the scattering of six particles when discontinuities arise from three particle invariants becoming zero. These relations prevent functions like $ln(s_{123})ln(s_{234})$ from appearing because the factored amplitude (after the s_{123} cut) cannot have a dependence on s_{234}. We say that the s_{234} cut is not kinematically realizable after the s_{123} cut. At this point, we will not consider discontinuities arising from two particle invariants because the restrictions provided are not well understood. By studying the three particle s-invariants discontinuity structure of scattering amplitude functions, we can implement powerful constraints on the space of functions. At the symbol level these restrictions constrain the s-invariants that may appear in the second entry based on the first entry in the symbol. The restrictions from Steinmann relations are not too powerful when considering the weight 2 hexagon functions, but are far more useful when looking into heptagon functions.

3.5.1 Hexagon Functions

The symbol of hexagon functions (those appearing in six-point amplitudes) have entries drawn from the nine-letter set:

$$\{u, v, w, 1-u, 1-v, 1-w, y_u, y_v, y_w\} \tag{3.5.1}$$

These are the standard u's and y's used by Dixon et al [48, 49, 50, 51]. From their work, we know that there are nine possible weight 2 hexagon functions. Out of the nine possible weight 2 hexagons, only six of these functions are allowed by the Steinmann relations. The following functions are allowed:

$$\mathrm{Li}_2(1-\frac{1}{u_i}) \tag{3.5.2}$$

$$\ln^2\left(\frac{u_i u_{i+2}}{u_{i+1}}\right) \tag{3.5.3}$$

where $i = 1, 2, 3$ and the indices are mod 3. Consecutive u_i are related by a cyclic permutation of the momenta. The u_i can be expressed in terms of Mandelstam invariants by

$$u_1 = \frac{s_{34}s_{61}}{s_{234}s_{345}}, \qquad u_2 = \frac{s_{12}s_{45}}{s_{123}s_{345}}, \qquad u_3 = \frac{s_{23}s_{56}}{s_{234}s_{456}} = \frac{s_{23}s_{56}}{s_{123}s_{234}} \tag{3.5.4}$$

and in terms of momentum twistors by

$$u_1 = \frac{\langle 3456\rangle\langle 1236\rangle}{\langle 1346\rangle\langle 2356\rangle}, \qquad u_2 = \frac{\langle 1234\rangle\langle 1456\rangle}{\langle 1245\rangle\langle 1346\rangle}, \qquad u_3 = \frac{\langle 2345\rangle\langle 1256\rangle}{\langle 2356\rangle\langle 1245\rangle} \tag{3.5.5}$$

From these forms, we can see that functions of three particle invariants may have discontinuities when one or more of the three particle invariants go to zero.

Let's look at the first set of allowed weight 2 hexagon functions given by eq. (3.5.2). To consider the discontinuity structure, we will look at the symbol of the functions. Recall that the symbol of a classical polylogarithm is given by

$$S\left[\mathrm{Li}_n(z)\right] = -(1-z) \otimes \underbrace{z \otimes \cdots \otimes z}_{n-1 \text{ times}} \tag{3.5.6}$$

Therefore, the symbol of the functions in eq. (3.5.2) is given by

$$S\left[\mathrm{Li}_2(1-\frac{1}{u_i})\right] = -\frac{1}{u_i} \otimes (1-\frac{1}{u_i}) = u_i \otimes (1-\frac{1}{u_i}) \tag{3.5.7}$$

Since $\mathrm{Li}_n(z)$ has a branch cut at $z=1$, there will be a discontinuity in the $\mathrm{Li}_2(1-\frac{1}{u_i})$ function when $u_i \to \infty$ or one of the three particle invariants goes to zero. As $u_i \to \infty$, the second entry in the symbol remains finite (it goes to 1). This can be seen by noticing that the second entry of the symbol $\mathrm{Li}_2(1-\frac{1}{u_1})$ is

$$1 - \frac{s_{234}s_{345}}{s_{34}s_{61}} \tag{3.5.8}$$

which inversely proportional to u_i, placing the three particle invariants in the numerator. A three particle invariant going to zero no longer produces a discontinuity in this term, so these types of functions are allowed by the Steinmann relations.

Let's look at the functions in eq. (3.5.3). Recall that the symbol of a product of natural logs is given by the shuffle product of the arguments. Therefore,

$$S\left[\ln A \ln B\right] = A \sqcup\!\sqcup B = A \otimes B + B \otimes A \tag{3.5.9}$$

For the natural log squared terms, the symbol is given by

$$S\left[\ln^2\left(\frac{u_i u_{i+2}}{u_{i+1}}\right)\right] = 2\frac{u_i u_{i+2}}{u_{i+1}} \otimes \frac{u_i u_{i+2}}{u_{i+1}} \tag{3.5.10}$$

We will consider the case of $i=1$ since the others are obtained by permuting the indices. First, let's express this product in terms of s-invariants as

$$\frac{u_2 u_1}{u_3} = \frac{s_{12}s_{45}}{s_{123}s_{345}}\frac{s_{34}s_{61}}{s_{345}s_{234}}\frac{s_{234}s_{123}}{s_{23}s_{56}} = \frac{s_{12}s_{45}s_{34}s_{61}}{s_{23}s_{56}s_{345}^2} \tag{3.5.11}$$

where this product of u_i only depends on one three particle invariant. One of the properties of symbols allows entries to be inverted with a resulting negative sign. Signs inside the symbol don't matter, so the symbol of $S\left[\ln^2\left(\frac{u_i u_{i+2}}{u_{i+1}}\right)\right]$ can be equivalently expressed as

$$S\left[\ln^2\left(\frac{u_2u_1}{u_3}\right)\right] = 2\frac{u_3}{u_2u_1}\otimes\frac{u_3}{u_2u_1} = 2\frac{s_{23}s_{56}s_{345}^2}{s_{12}s_{45}s_{34}s_{61}}\otimes\frac{s_{23}s_{56}s_{345}^2}{s_{12}s_{45}s_{34}s_{61}} \tag{3.5.12}$$

The natural logarithm of the complex variable z, $\ln(z)$, has a branch cut starting at $z = 0$. As we take the limit $s_{345} \to 0$, we run into a discontinuity. Upon first glance this may seem problematic because we have a discontinuity in the second entry of the symbol. However, the discontinuity in the second entry is the same discontinuity in the first entry, so the Steinmann relations do not rule this type of term from appearing in the second entry.

Finally, we may wonder about terms like $\ln^2 u_i$ or $\ln u_i \ln u_j$ for $i \neq j$. Each u_i contains two overlapping three particle invariants. This prohibits the $\ln^2 u_i$ terms from appearing because the second entry in the symbol would have a discontinuity in an overlapping three particle invariant, which is ruled out by the Steinmann relations. Similarly, u_i and u_j for $i \neq j$ also have overlapping three particle invariants so these terms suffer from the same exact problem. Now that we have a handle on the six point case, let's consider the seven point case.

3.5.2 Heptagon Functions

The story becomes more interesting at seven points because there are more independent three particle invariants than there were in the six point case. Let us first define the commonly used u_i variables used for seven points. The u_i are

$$u_1 = \frac{s_{34}s_{671}}{s_{234}s_{345}}, \qquad u_2 = \frac{s_{45}s_{712}}{s_{345}s_{456}}, \qquad u_3 = \frac{s_{56}s_{123}}{s_{456}s_{567}}, \qquad u_4 = \frac{s_{67}s_{234}}{s_{567}s_{671}}, \tag{3.5.13}$$

$$u_5 = \frac{s_{71}s_{345}}{s_{671}s_{712}}, \qquad u_6 = \frac{s_{12}s_{456}}{s_{712}s_{123}}, \qquad u_7 = \frac{s_{23}s_{567}}{s_{123}s_{234}} \tag{3.5.14}$$

These can be rewritten in terms of momenta twistors as

$$u_1 = \frac{\langle 3456\rangle\langle 2367\rangle}{\langle 2356\rangle\langle 3467\rangle}, \qquad u_2 = \frac{\langle 4567\rangle\langle 1347\rangle}{\langle 3467\rangle\langle 1457\rangle}, \qquad u_3 = \frac{\langle 1567\rangle\langle 1245\rangle}{\langle 1457\rangle\langle 1256\rangle} \tag{3.5.15}$$

$$u_4 = \frac{\langle 1267\rangle\langle 2356\rangle}{\langle 1256\rangle\langle 2367\rangle}, \qquad u_5 = \frac{\langle 1237\rangle\langle 3467\rangle}{\langle 2367\rangle\langle 1347\rangle}, \qquad u_6 = \frac{\langle 1234\rangle\langle 1457\rangle}{\langle 1347\rangle\langle 1245\rangle} \tag{3.5.16}$$

$$u_7 = \frac{\langle 2345\rangle\langle 1256\rangle}{\langle 1245\rangle\langle 2356\rangle} \tag{3.5.17}$$

When the alternate a_{ij} variables are introduced, expressions for u_i in terms of a_{ij} will be provided.

Just like in the six point case, we are interested in determining all the weight 2 functions that are allowed by the Steinmann relations. As discussed earlier, the Steinmann relations provide restrictions on the three particle invariants that can appear within the discontinuity structure. Let's consider the types of classical polylogarithms that may exist at weight 2. Recall that terms with two overlapping three particle invariants are allowed to appear inside a classical polylogarithm as long as the second entry of the symbol doesn't have discontinuities when a three particle invariant goes to zero. Specific products of the u_i can be taken to produce terms with only two three particle invariants in the denominator. For example,

$$u_1 u_4 = \frac{s_{34}s_{671}}{s_{234}s_{345}}\frac{s_{67}s_{234}}{s_{567}s_{671}} = \frac{s_{34}s_{67}}{s_{345}s_{567}} \tag{3.5.18}$$

and its cyclic images can appear inside a polylogarithm. Therefore, the allowed weight two classical polylogarithms are

$$\mathrm{Li}_2\left(1-\frac{1}{u_1}\right), \qquad \mathrm{Li}_2\left(1-\frac{1}{u_1 u_4}\right) \tag{3.5.19}$$

and their cyclic images. The symbols are given by

$$u_1 \otimes \left(1-\frac{1}{u_1}\right), \qquad u_1 u_4 \otimes \left(1-\frac{1}{u_1 u_4}\right) \tag{3.5.20}$$

respectively. In terms of momenta twistors,

$$S\left[\mathrm{Li}_2\left(1-\frac{1}{u_i}\right)\right] = \frac{\langle 3456\rangle\langle 2367\rangle}{\langle 2356\rangle\langle 3467\rangle} \otimes \frac{\langle 2346\rangle\langle 3467\rangle}{\langle 3456\rangle\langle 2367\rangle} \tag{3.5.21}$$

$$S\left[\mathrm{Li}_2\left(1-\frac{1}{u_1 u_4}\right)\right] = \frac{\langle 3456\rangle\langle 2671\rangle}{\langle 3467\rangle\langle 2561\rangle} \otimes \frac{\langle 6(12)(34)(57)\rangle}{\langle 3456\rangle\langle 2671\rangle} \tag{3.5.22}$$

where $\langle a(bc)(de)(fg)\rangle = \langle abde\rangle\langle acfg\rangle - \langle acde\rangle\langle abfg\rangle$. The $\mathrm{Li}_2\left(1-\frac{1}{u_i}\right)$ are allowed by the Steinmann relations for the exact same reason they were allowed in the six point example. Note these types of arguments still cannot exist in log squared terms because they share overlapping three particle invariants.

Now, we want to construct the weight two functions formed by taking products of natural logarithms. Products of natural logarithms of the momenta invariants that do not get eliminated by the Steinmann relations must only be dependent on a single three particle invariant. For example,

$$\frac{u_1 u_4 u_7}{u_2 u_6} = \frac{s_{23}s_{34}s_{67}}{s_{45}s_{12}s_{234}} \tag{3.5.23}$$

together with its cyclic images are valid entries inside a natural logarithm squared term because it contains only a single three particle invariant. A product of natural logarithms would be allowed if the arguments of the two logarithms do not have overlapping momenta. For example, cycling the product above, eq. (3.5.23), by three gives

$$\frac{u_4 u_7 u_3}{u_5 u_2} = \frac{s_{56} s_{67} s_{23}}{s_{71} s_{45} s_{567}} \tag{3.5.24}$$

which only depends on the three invariant s_{567}. Then the product

$$\ln\left(\frac{u_1 u_4 u_7}{u_2 u_6}\right) \ln\left(\frac{u_4 u_7 u_3}{u_5 u_2}\right) \tag{3.5.25}$$

and its cyclic images are acceptable weight 2 functions because the two arguments of the natural logarithms have discontinuities when non-overlapping three particle invariants go to zero. Cycling eq. (3.5.23) by four would also produce a term containing a non-overlapping three particle invariant s_{456}. That would suggest that

$$\ln\left(\frac{u_1 u_4 u_7}{u_2 u_6}\right) \ln\left(\frac{u_5 u_1 u_4}{u_6 u_3}\right) \tag{3.5.26}$$

is also a valid weight two function. Indeed this is a valid weight two function, but it is a cyclic image of eq. (3.5.25) (cycling by four). Now, the valid weight 2 functions that are products of natural logarithms are given by

$$\ln\left(\frac{u_1 u_4 u_7}{u_2 u_6}\right) \ln\left(\frac{u_4 u_7 u_3}{u_5 u_2}\right), \qquad \ln^2\left(\frac{u_1 u_4 u_7}{u_2 u_6}\right) \tag{3.5.27}$$

plus cyclic images. The symbols are given by

$$\left(\frac{u_1 u_4 u_7}{u_2 u_6}\right) \otimes \left(\frac{u_4 u_7 u_3}{u_5 u_2}\right) + \left(\frac{u_4 u_7 u_3}{u_5 u_2}\right) \otimes \left(\frac{u_1 u_4 u_7}{u_2 u_6}\right), \qquad 2\left(\frac{u_1 u_4 u_7}{u_2 u_6}\right) \otimes \left(\frac{u_1 u_4 u_7}{u_2 u_6}\right) \tag{3.5.28}$$

respectively. In terms of momenta twistors,

$$S\left[\ln\left(\frac{u_1 u_4 u_7}{u_2 u_6}\right) \ln\left(\frac{u_4 u_7 u_3}{u_5 u_2}\right)\right] = \frac{\langle 3456\rangle\langle 1267\rangle\langle 2345\rangle}{\langle 2356\rangle\langle 1234\rangle\langle 4567\rangle} \otimes \frac{\langle 1267\rangle\langle 2345\rangle\langle 1567\rangle}{\langle 1256\rangle\langle 1237\rangle\langle 4567\rangle} \tag{3.5.29}$$

$$+ \frac{\langle 1267\rangle\langle 2345\rangle\langle 1567\rangle}{\langle 1256\rangle\langle 1237\rangle\langle 4567\rangle} \otimes \frac{\langle 3456\rangle\langle 1267\rangle\langle 2345\rangle}{\langle 2356\rangle\langle 1234\rangle\langle 4567\rangle} \tag{3.5.30}$$

$$S\left[\ln^2\left(\frac{u_1 u_4 u_7}{u_2 u_6}\right)\right] = 2\frac{\langle 3456\rangle\langle 1267\rangle\langle 2345\rangle}{\langle 2356\rangle\langle 1234\rangle\langle 4567\rangle} \otimes \frac{\langle 3456\rangle\langle 1267\rangle\langle 2345\rangle}{\langle 2356\rangle\langle 1234\rangle\langle 4567\rangle} \tag{3.5.31}$$

In summary, there are 28 weight two functions that satisfy the Steinmann relations out of the

42 integrable weight two functions. They are given by the following four functions and their cyclic images

$$\text{Li}_2\left(1-\frac{1}{u_1}\right),\ \text{Li}_2\left(1-\frac{1}{u_1u_4}\right),\ \ln\left(\frac{u_1u_4u_7}{u_2u_6}\right)\ln\left(\frac{u_4u_7u_3}{u_5u_2}\right),\ \ln^2\left(\frac{u_1u_4u_7}{u_2u_6}\right) \tag{3.5.32}$$

As shown by the reduction in the number of functions, the Steinmann relations significantly constrains the space of physical functions.

It is convenient to work with a set of projectively invariant ratios constructed out of the 42 n=7 cluster $\mathcal{A}$-coordinates. The 42 cluster $\mathcal{A}$-coordinates are given by

$$\langle 2367\rangle,\quad \langle 2567\rangle,\quad \langle 2347\rangle,\quad \langle 2457\rangle,\quad \langle 1(23)(45)(67)\rangle,\quad \langle 1(34)(56)(72)\rangle \tag{3.5.33}$$

plus cyclic copies where $Z_i \to Z_{i+1}$. A convenient set of invariant ratios is formed by multiplying the cluster $\mathcal{A}$-coordinates with the appropriate $\langle i\, i{+}1\, i{+}2\, i{+}3\rangle$ Plücker coordinate factors. The ratios are referred to as the a_{ij} variables and can expressed using momentum twistors in the following way

$$a_{11} = \frac{\langle 1234\rangle\langle 1567\rangle\langle 2367\rangle}{\langle 1237\rangle\langle 1267\rangle\langle 3456\rangle}, \qquad a_{41} = \frac{\langle 2457\rangle\langle 3456\rangle}{\langle 2345\rangle\langle 4567\rangle}, \tag{3.5.34}$$

$$a_{21} = \frac{\langle 1234\rangle\langle 2567\rangle}{\langle 1267\rangle\langle 2345\rangle}, \qquad a_{51} = \frac{\langle 1(23)(45)(67)\rangle}{\langle 1234\rangle\langle 1567\rangle}, \tag{3.5.35}$$

$$a_{31} = \frac{\langle 1567\rangle\langle 2347\rangle}{\langle 1237\rangle\langle 4567\rangle}, \qquad a_{61} = \frac{\langle 1(34)(56)(72)\rangle}{\langle 1234\rangle\langle 1567\rangle} \tag{3.5.36}$$

Notice each of the 42 cluster $\mathcal{A}$-coordinates are dressed by $\langle i\, i{+}1\, i{+}2\, i{+}3\rangle$ Plücker coordinate factors. The entire set of 42 a_{ij} are found from the a_{i1} listed above by cyclically permuting the momenta. Mathematically, the cyclic permutations are represented by

$$a_{ij} = a_{i1}\big|_{Z_k \to Z_{k+j-1}} \tag{3.5.37}$$

Since the Steinmann relations are expressed in the language of Mandelstam invariants, we can express the a_{1j} in the following way

$$a_{11} = \frac{s_{23}s_{67}s_{712}}{s_{12}s_{71}s_{45}} \tag{3.5.38}$$

with the a_{1j} given by cyclic permutations of a_{11}. The remaining a_{ij} for $i \neq 1$ are not dependent on three particle invariants.

We are interested in expressing the Steinmann relations in the language of the 42 a_{ij} because these coordinates are far more convenient to use. Remembering that the Steinmann relations provide three

particle invariant restrictions, the relations only prohibit the appearance of three particle momenta in the second entry of the symbol of weight 2 functions if it contains a forbidden double discontinuity. In the language of a_{ij}, Steinmann relations only prohibit specific a_{1j} from appearing in the second entry. The forbidden a_{1j} are dependent on the a_{1i} that appear in the first entry of the symbol. Let's formulate the restrictions in a more coherent fashion. Each a_{1i} is proportional to a single three particle invariant $s_{i-2,i-1,i}$. If a_{1i} appears in the first entry of the symbol, then the second entry must not depend on a three particle invariant containing overlapping momenta ($i-2$, $i-1$, or i). However, the second entry is not prohibited from depending on the same three particle invariant, so it is allowed to be a_{1i}. The only other possibilities with non-overlapping momenta are $a_{1,i+3}$ and $a_{1,i+4}$. The first entry condition forces the first entry of the symbol of heptagon functions to be one of the a_{1i}. Assuming the first entry of the symbol of a heptagon function is given by a_{1i}, the second entry of the symbol is not allowed to be a_{1j} unless $j = i$, $j = i+3$, or $j = i+4$. This statement is the formulation of the Steinmann relations in the language of the a_{ij} variables.

Now, let's go back and verify that our formulation of the Steinmann relations in the a_{ij} language agrees with the functions that live in the weight 2 Steinmann space. In order to do this, the u_i must be expressed in terms of the a_{ij} as

$$u_1 = \frac{a_{17}}{a_{13}a_{14}}, \qquad u_2 = \frac{a_{11}}{a_{14}a_{15}}, \qquad u_3 = \frac{a_{12}}{a_{15}a_{16}}, \qquad u_4 = \frac{a_{13}}{a_{16}a_{17}} \tag{3.5.39}$$

$$u_5 = \frac{a_{14}}{a_{11}a_{17}}, \qquad u_6 = \frac{a_{15}}{a_{11}a_{12}}, \qquad u_7 = \frac{a_{16}}{a_{12}a_{13}} \tag{3.5.40}$$

The special products of u_i in the a_{ij} are

$$u_1u_4 = \frac{1}{a_{14}a_{16}}, \qquad \frac{u_1u_4u_7}{u_2u_6} = \frac{1}{a_{13}}, \qquad \frac{u_4u_7u_3}{u_5u_2} = \frac{1}{a_{16}} \tag{3.5.41}$$

Now we express the symbols of the weight 2 functions living in the Steinmann space in our new variables

$$S\left[\mathrm{Li}_2\left(1-\frac{1}{u_1}\right)\right] = \frac{a_{17}}{a_{13}a_{14}} \otimes \frac{a_{24}a_{33}}{a_{17}} \tag{3.5.42}$$

$$S\left[\mathrm{Li}_2\left(1-\frac{1}{u_1u_4}\right)\right] = \frac{1}{a_{14}a_{16}} \otimes a_{65} = a_{14}a_{16} \otimes a_{65} \tag{3.5.43}$$

$$S\left[\ln^2\left(\frac{u_1u_4u_7}{u_2u_6}\right)\right] = 2\frac{1}{a_{13}} \otimes \frac{1}{a_{13}} = 2a_{13} \otimes a_{13} \tag{3.5.44}$$

$$S\left[\ln\left(\frac{u_1u_4u_7}{u_2u_6}\right)\ln\left(\frac{u_4u_7u_3}{u_5u_2}\right)\right] = a_{13} \otimes a_{16} + a_{16} \otimes a_{13} \tag{3.5.45}$$

It is easy to see that these weight 2 symbols are allowed by the Steinmann relations as formulated in the a_{ij} language. Starting with the complete set of 42 functions weight 2 functions, this basis could be found by applying the formulation of the Steinmann relations in the language of the a_{ij} variables. Now, we are ready to apply the Steinmann relations to obtain heptagon functions.

Chapter 4

Heptagons from the Steinmann Cluster Bootstrap

The desire to construct general scattering amplitudes from their analytic and physical properties has been a goal since the birth of the analytic S-matrix program (see e.g. ref. [52]). More recently, such a procedure has been applied in a perturbative context and referred to as bootstrapping. Aspects of this approach have been applied to theories such as quantum chromodynamics at one loop [53, 54, 55] and more recently at two loops [56, 57, 58]. However, the most powerful applications to date have been to the planar limit of $\mathcal{N} = 4$ super-Yang-Mills (SYM) theory in four dimensions [2, 59]. Fueled by an increased understanding of the classes of analytic functions appearing in amplitudes in general quantum field theories, as well as the stringent constraints obeyed by amplitudes in planar $\mathcal{N} = 4$ SYM, it has been possible to advance as far as five loops [49, 60, 61, 62, 47, 5]. These results in turn provide a rich mine of theoretical data for understanding how scattering amplitudes behave.

The planar limit of a large number of colors in $\mathcal{N} = 4$ SYM has received a great deal of attention because of the remarkable properties it exhibits. In addition to superconformal symmetry it respects a dual conformal symmetry [43, 37, 38, 63, 42], and amplitudes are dual to polygonal light-like Wilson loops [39, 40, 64, 41, 43, 65, 66]. Dual (super)conformal symmetry fixes the four-point and five-point amplitudes uniquely to match the Bern-Dixon-Smirnov (BDS) ansatz [28], which captures all the infrared divergences of planar scattering amplitudes. Starting at six points, the BDS ansatz receives corrections from finite functions of dual conformal invariants [67, 68, 66, 65]. The correction to the maximally helicity violating (MHV) amplitude has traditionally been expressed in terms of a (BDS) remainder function [65, 66, 49, 50, 61], while the correction to the next-to-maximally helicity

violating (NMHV) amplitude has traditionally been expressed in terms of the infrared-finite NMHV ratio function [14, 21, 69, 48, 60, 70].

The cluster bootstrap program is built on the idea that certain scattering amplitudes can be determined order by order in perturbation theory using a set of basic building blocks known as cluster coordinates [71, 72]. Inspired by the results of refs. [35, 32], the bootstrap approach developed in refs. [49, 60, 61, 62, 47, 5] assumes that the MHV and NMHV amplitudes at each loop order belong to a particular class of iterated integrals, or generalized polylogarithms. More specifically, the L-loop contribution to the remainder and ratio functions is expected to lie within the space spanned by polylogarithms of weight $2L$ [73] whose symbols can be written in terms of cluster $\mathcal{A}$-coordinates. A further constraint on the relevant space of functions comes from the restriction that only physical branch cuts can appear in the remainder and ratio functions [36].

To make use of this expectation, in the bootstrap program one first constructs a general linear combination of the above set of functions to serve as an ansatz. Then one tries to determine all free coefficients in the ansatz by imposing analytic and physical constraints. This procedure becomes increasingly computationally expensive at higher loop orders, largely due to the fact that the number of relevant functions increases exponentially with the weight. It is hoped that one day a constructive procedure for determining these amplitudes can be developed that does not require constructing the full weight-$2L$ space as an intermediate step. A promising candidate in this respect is the Wilson loop Operator Product Expansion (OPE) [74, 36, 75] and the Pentagon OPE program [76, 77, 78, 79, 80, 81, 82] which provides finite-coupling expressions for the amplitudes as an expansion around (multi-)collinear kinematics. The main challenge in this framework is to resum the infinite series around these kinematics; there has been progress recently in this direction at weak coupling [83, 84, 85]. Another potential constructive approach could involve the Amplituhedron [86, 87] description of the multi-loop integrand. Perhaps one can extend the methods of ref. [88] for reading off the branch-point locations, in order to enable reading off the entire function.

To date, six- and seven-point amplitudes have been computed in the cluster bootstrap program through the study of so-called hexagon and heptagon functions. Both helicity configurations of the six-point amplitude have been determined through five loops [5], while the MHV seven-point amplitude has been determined at symbol level through three loops [61]. The seven-point NMHV amplitude has not yet received attention in the bootstrap program, but it has been calculated through two loops using slightly different methods [89]. Surprisingly, bootstrapping the seven-point remainder function has thus far proven to be conceptually simpler (i.e. requiring the imposition of fewer constraints) than bootstrapping its six-point counterpart. The collinear limit of the seven-point

remainder function must be nonsingular and a well-defined hexagon function. This requirement is so restrictive that it entirely determines the two-loop heptagon remainder function, up to an overall scale. It similarly determines the three-loop remainder function, once the full implications of dual superconformal symmetry are taken into account [61]. The corresponding hexagon remainder function symbols may then be obtained by taking a collinear limit.

In a recent breakthrough [5], the classic work of Steinmann [90, 91] on the compatibility of branch cuts in different channels has been used to supercharge the hexagon function bootstrap program. The Steinmann relations dramatically reduce the size of the functional haystack one must search through in order to find amplitudes, putting higher-loop amplitudes that were previously inaccessible within reach. In this chapter we reformulate the heptagon bootstrap of ref. [61] to exploit the power of the Steinmann relations. With their help, we are able to fully determine the symbol of the seven-point three-loop NMHV and four-loop MHV amplitude in planar $\mathcal{N} = 4$ SYM, using only a few simple physical and mathematical inputs. In a separate paper [92], we will investigate various kinematical limits of these amplitudes in more detail, including the multi-Regge limit [68, 93, 94, 95, 96, 97, 98, 99, 100, 101, 102, 103], the OPE limit [74, 36, 75, 76, 77, 78, 79, 80], and the self-crossing limit [104, 105]. In this chapter, we study one of the simpler limits, where the NMHV seven-point amplitude factorizes on a multi-particle pole.

This chapter is organized as follows. In section 4.1 we begin by reviewing the general structure of seven-particle MHV and NMHV (super)amplitudes, and different schemes for subtracting their infrared divergences. Section 4.2 discusses the essential ingredients of the amplitude bootstrap for constructing heptagon functions, which are believed to describe the nontrivial kinematical dependence of these amplitudes. Section 4.3 focuses on the additional physical constraints that allow us to single out the MHV or NMHV amplitude from this space of functions.

Our main results, including the analysis of the general space of heptagon symbols, and the determination of the three-loop NMHV and four-loop MHV amplitude symbols, are presented in section 4.4. Section 4.5 describes a sample kinematical limit, the behavior of the NMHV amplitude as a multi-particle Mandelstam invariant vanishes. Finally, section 4.6 contains our conclusions, and discusses possible avenues for future study.

Many of the analytic results in this chapter are too lengthy to present in the manuscript. Instead, computer-readable files containing our results can be downloaded from [106].

4.1 Seven-Particle Scattering Amplitudes

4.1.1 MHV: The Remainder Function

In planar $\mathcal{N} = 4$ SYM, n-particle amplitudes are completely characterized by the color-ordered partial amplitudes A_n, which are the coefficients of specific traces $\mathrm{Tr}(T^{a_1}T^{a_2}\cdots T^{a_n})$ in the color decomposition of the amplitudes. The MHV helicity configuration has precisely two gluons with negative helicity and $(n-2)$ with positive helicity (in a convention where all particles are outgoing). The MHV amplitude is encoded in the remainder function R_n, which is defined by factoring out the BDS ansatz A_n^{BDS} [28] (reviewed in appendix A):

$$A_n^{\mathrm{MHV}} = A_n^{\mathrm{BDS}} \exp\left[R_n\right]. \tag{4.1.1}$$

The BDS ansatz captures all the infrared and collinear divergences [107, 108, 109] in the planar amplitude, so the remainder function is infrared finite. It is also invariant under dual conformal transformations [37, 38, 39, 63, 43]. Moreover, since the BDS ansatz accounts for collinear factorization to all orders in perturbation theory [28], the n-point remainder function smoothly tends to the $(n-1)$-point remainder function in its collinear limits, a fact that will prove to be an important ingredient in the bootstrap program.

In the definition (4.1.1), R_n is the finite-coupling (or all-loop) remainder function. Here we will be interested in its perturbative expansion. For any function F of the coupling, we denote the coefficients of its perturbative expansion with a superscript according to the definition

$$F = \sum_{L=0}^{\infty} g^{2L} F^{(L)}, \tag{4.1.2}$$

where $g^2 = g_{YM}^2 N/(16\pi^2)$, g_{YM} is the Yang-Mills coupling constant, and N is the number of colors. Elsewhere in the literature, the coupling constant $a = 2g^2$ is often used. The L-loop contribution to the remainder function, $R_n^{(L)}$, is expected to be a weight-$2L$ iterated integral.

The remainder function vanishes for the four- and five-particle amplitudes, because dual conformally invariant cross ratios cannot be formed with fewer than six external lightlike momenta (in other words, the BDS ansatz is correct to all loop orders for $n = 4$ or 5) [67, 66, 65]. The first nontrivial case, the six-point remainder function, has been successfully computed at two loops [35], three loops [49, 89, 50], four loops [51] and recently five loops [5]. At seven points, the remainder function has been computed at two loops [110, 89, 111, 112] and its symbol has been computed at

three loops [61]. The symbol of the four-loop seven-point MHV remainder function $R_7^{(4)}$ is one of the main results of this chapter.

4.1.2 NMHV: The Ratio Function and R-invariants

Beyond the MHV case, scattering amplitudes in SYM theory are most efficiently organized by exploiting the (dual) superconformal symmetry [14] of the theory, as reviewed in ref. [113].

In a nutshell, one starts by packaging the on-shell particle content of the theory into a single superfield Φ with the help of four Grassmann variables η^A, whose index transforms in the fundamental representation of the $SU(4)$ R-symmetry group. In other words, all external states, gluons $G^{\pm}$, fermions Γ_A and $\bar{\Gamma}^A$, and scalars S_{AB}, can be simultaneously described by the superfield

$$\Phi = G^+ + \eta^A \Gamma_A + \tfrac{1}{2!}\eta^A\eta^B S_{AB} + \tfrac{1}{3!}\eta^A\eta^B\eta^C \epsilon_{ABCD}\bar{\Gamma}^D + \tfrac{1}{4!}\eta^A\eta^B\eta^C\eta^D\epsilon_{ABCD}G^- \,, \tag{4.1.3}$$

which allows us to combine all n-point amplitudes into a superamplitude $\mathcal{A}_n(\Phi_1, \ldots, \Phi_n)$.

Expanding the superamplitude in the Grassmann variables separates out its different helicity components. The MHV amplitude is contained in the part of $\mathcal{A}_n^{\text{MHV}}$ with 8 powers of Grassmann variables, or Grassmann degree 8. Specifically, the MHV amplitude discussed in the previous subsection is given in the MHV superamplitude by the term

$$\mathcal{A}_n^{\text{MHV}} = (2\pi)^4 \delta^{(4)}\Big(\sum_{i=1}^n p_i\Big) \sum_{1\le j<k\le n} (\eta_j)^4 (\eta_k)^4 A_n^{\text{MHV}}(1^+ \ldots j^- \ldots k^- \ldots n^+) + \ldots, \tag{4.1.4}$$

where we have shown only the pure-gluon terms explicitly. Similarly, the terms of Grassmann degree 12 make up the NMHV superamplitude. Since NMHV amplitudes in this theory have the same infrared-divergent structure as MHV amplitudes, the two superamplitudes can be related by

$$\mathcal{A}_n^{\text{NMHV}} = \mathcal{A}_n^{\text{MHV}}\, \mathcal{P}_n \,, \tag{4.1.5}$$

where the infrared-finite quantity $\mathcal{P}_n$ is called the NMHV ratio function and has Grassmann degree 4. On the basis of tree-level and one-loop amplitude computations, it was argued in ref. [14] that $\mathcal{P}_n$ is dual conformally invariant.

At tree level, the dual conformal symmetry is enhanced to dual superconformal symmetry, and the ratio function can be written as a sum of *dual superconformal invariants* or '*R-invariants*' [14, 21]. These quantities, which carry the dependence on the fermionic variables, are algebraic functions of

the kinematics and can be written as Grassmannian contour integrals [114]. From this representation it is also possible to prove their invariance under ordinary superconformal transformations [115, 116], or in other words their Yangian invariance [117].

As shown in ref. [114], R-invariants are most easily expressed in terms of the momentum supertwistors $\mathcal{Z}_i$ defined by[1] [24]

$$\mathcal{Z}_i = (Z_i \,|\, \chi_i)\,, \qquad Z_i^{\alpha,\dot{\alpha}} = (\lambda_i^\alpha, x_i^{\beta\dot{\alpha}}\lambda_{i\beta})\,, \qquad \chi_i^A = \theta_i^{\alpha A}\lambda_{i\alpha}\,. \tag{4.1.6}$$

Their fermionic components χ_i are associated with the fermionic dual coordinates θ_i in the same way that the bosonic twistors Z_i are associated with the bosonic dual coordinates x_i. Differences between color-adjacent dual coordinates x_i and θ_i are related to the external momenta p_i and supermomenta q_i, respectively:

$$p_i^{\alpha\dot{\alpha}} = \lambda_i^\alpha \tilde{\lambda}_i^{\dot{\alpha}} = x_{i+1}^{\alpha\dot{\alpha}} - x_i^{\alpha\dot{\alpha}}\,, \qquad q_i^{\alpha A} = \lambda_i^\alpha \eta_i^A = \theta_{i+1}^{\alpha A} - \theta_i^{\alpha A}\,. \tag{4.1.7}$$

Given any set of five supertwistors $\mathcal{Z}_a, \mathcal{Z}_b, \mathcal{Z}_c, \mathcal{Z}_d, \mathcal{Z}_e$, we may define a corresponding NMHV R-invariant as a 5-bracket

$$[abcde] = \frac{\delta^{0|4}\big(\chi_a\langle bcde\rangle + \text{cyclic}\big)}{\langle abcd\rangle\langle bcde\rangle\langle cdea\rangle\langle deab\rangle\langle eabc\rangle}\,, \tag{4.1.8}$$

in terms of dual conformally invariant bosonic 4-brackets

$$\langle ijkl\rangle \equiv \langle Z_i Z_j Z_k Z_l\rangle = \epsilon_{ABCD} Z_i^A Z_j^B Z_k^C Z_l^D = \det(Z_i Z_j Z_k Z_l)\,, \tag{4.1.9}$$

and a fermionic delta function $\delta^{0|4}(\xi) = \xi^1\xi^2\xi^3\xi^4$ for the different $SU(4)$ components of ξ. The original definition of the R-invariants [14, 21] (there denoted $R_{r;ab}$) in normal twistor space corresponds to the special case $R_{r;ab} = [r,\, a{-}1,\, a,\, b{-}1,\, b]$.

From the definition (4.1.8), we can see that R-invariants are antisymmetric in the exchange of any pair of supertwistor indices (hence also invariant under cyclic permutations). They are also manifestly dual conformally invariant, since they don't depend on spinor products $\langle ij\rangle$. The aforementioned Grassmannian contour integral representation in momentum twistor space [114] makes the full dual conformal invariance manifest. It also allows one to prove more transparently the following important identity between R-invariants: Given any six momentum supertwistors

[1] The indices $\alpha, \dot{\alpha} = 1, 2$ denote the components of the spinor representation of the Lorentz group $SO(3,1) \simeq SL(2,\mathbb{C})$.

$\mathcal{Z}_a, \mathcal{Z}_b, \mathcal{Z}_c, \mathcal{Z}_d, \mathcal{Z}_e, \mathcal{Z}_f$, their R-invariants are related by [14]

$$[abcde] - [bcdef] + [cdefa] - [defab] + [efabc] - [fabcd] = 0\,. \tag{4.1.10}$$

For n-particle scattering, there exist $\binom{n}{6}$ such equations for the $\binom{n}{5}$ distinct R-invariants; however, it turns out that only $\binom{n-1}{5}$ are independent. So in the end we are left with

$$\#\text{ linearly independent } n\text{-particle } R\text{-invariants} = \binom{n}{5} - \binom{n-1}{5} = \binom{n-1}{4}\,. \tag{4.1.11}$$

For example, there are 5, 15, and 35 independent R-invariants relevant for 6-, 7- and 8-particle NMHV scattering amplitudes, respectively.

Let us now focus on the seven-particle NMHV superamplitude. For compactness we may express the corresponding R-invariants in terms of the particle indices that are *not* present in the 5-brackets (4.1.8), for example

$$[12345] = (67) = (76)\,, \tag{4.1.12}$$

where (by convention) the 5-bracket on the left-hand side of this definition is always ordered, so ordering on the right-hand side doesn't matter.

In this notation, the representation for the tree-level ratio function found in ref. [21] may be rewritten as

$$\mathcal{P}_7^{(0)} = \frac{3}{7}\,(12) + \frac{1}{7}\,(13) + \frac{2}{7}\,(14) \;\; + \text{cyclic}\,. \tag{4.1.13}$$

Following the same reference, we find it convenient to use a basis of 15 independent R-invariants consisting of $\mathcal{P}_7^{(0)}$ together with $(12), (14)$, and their cyclic permutations. (Because $\mathcal{P}_7^{(0)}$ is totally symmetric, it has no independent cyclic images.) In particular, the remaining R-invariants $(i, i+2)$ are related to this set by

$$(13) = -\,(15) - (17) - (34) - (36) - (56) + \mathcal{P}_7^{(0)}\,, \tag{4.1.14}$$

plus the cyclic permutations of this identity.

Beyond tree level, the independent R-invariants are dressed by transcendental functions of dual conformal invariants, and the ratio function can be put in the form

$$\mathcal{P}_7 = \mathcal{P}_7^{(0)}\, V_0 + \big[(12)\, V_{12} + (14)\, V_{14} \;\; + \text{cyclic}\big]\,. \tag{4.1.15}$$

As we will review in section 4.3.2, $\mathcal{P}_7$ is symmetric under the dihedral group D_7. The component V_0 inherits the full dihedral symmetry of $\mathcal{P}_7^{(0)}$, whereas V_{12} and V_{14} are only invariant under the flip $i \to 3-i$ and $i \to 5-i$ of their momentum twistor labels, respectively.

The dependence of $\mathcal{P}_7$ on the coupling enters only through the functions V_0 and V_{ij}. Their L-loop contributions, $V_0^{(L)}$ and $V_{ij}^{(L)}$, like the remainder function, $R_7^{(L)}$, are expected to be weight-$2L$ iterated integrals. Using the notation introduced in eq. (4.1.2) we must have

$$V_0^{(0)} = 1\,, \quad V_{12}^{(0)} = V_{14}^{(0)} = 0 \tag{4.1.16}$$

at tree level. At one loop, these functions become [21]

$$\begin{aligned}
V_0^{(1)} &= \mathrm{Li}_2\,(1-u_1) - \mathrm{Li}_2\,(1-u_1u_4) - \log u_1 \log u_3 + \text{ cyclic}\,,\\
V_{12}^{(1)} &= -\mathrm{Li}_2\,(1-u_6) + \mathrm{Li}_2\,(1-u_1u_4) + \mathrm{Li}_2\,(1-u_2u_6) + \mathrm{Li}_2\,(1-u_3u_6)\,,\\
&\quad + \log u_1 \log u_2 - \log u_3 \log u_2 + \log u_4 \log u_2 + \log u_1 \log u_3 + \log u_3 \log u_4\\
&\quad + \log u_1 \log u_6 + \log u_4 \log u_6 - \zeta_2\,,\\
V_{14}^{(1)} &= \mathrm{Li}_2\,(1-u_1u_4) + \mathrm{Li}_2\,(1-u_3u_6) + \log u_1 \log u_3 + \log u_4 \log u_3 + \log u_1 \log u_6\\
&\quad + \log u_4 \log u_6 - \zeta_2\,.
\end{aligned} \tag{4.1.17}$$

See also ref. [118] for a more recent, compact representation of the same amplitude. In the above relations and everything that follows, the cross ratios u_i are defined by,

$$u_{ij} = \frac{x_{i,j+1}^2\, x_{i+1,j}^2}{x_{i,j}^2\, x_{i+1,j+1}^2}\,, \qquad u_i = u_{i+1,i+4} = \frac{x_{i+1,i+5}^2\, x_{i+2,i+4}^2}{x_{i+1,i+4}^2\, x_{i+2,i+5}^2}\,. \tag{4.1.18}$$

The u_i are dual conformally invariant combinations of the Mandelstam invariants, see eq. (4.1.7) and also eq. (4.2.1) below.

Finally, the symbol of the two-loop NMHV heptagon has been computed in ref. [89] using the same choice of independent R-invariants as in eq. (4.1.15), with the help of an anomaly equation for the $\bar{Q}$ dual superconformal symmetry generators. Here we will use the Steinmann cluster bootstrap to push to three loops: The symbols of the functions $V_0^{(3)}$, $V_{12}^{(3)}$, and $V_{14}^{(3)}$ constituting the three-loop seven-point NMHV ratio function are another of the main results of this work.

4.1.3 The BDS- and BDS-like Normalized Amplitudes

In the previous sections we mentioned that MHV and NMHV amplitudes have the same infrared-divergent structure, which is accurately captured by the BDS ansatz. This fact allows us to define the MHV and NMHV *BDS-normalized* superamplitudes,

$$\mathcal{B}_n \equiv \frac{\mathcal{A}_n^{\text{MHV}}}{\mathcal{A}_n^{\text{BDS}}} = \frac{A_n^{\text{MHV}}}{A_n^{\text{BDS}}} = \exp\left[R_n\right], \tag{4.1.19}$$

$$B_n \equiv \frac{\mathcal{A}_n^{\text{NMHV}}}{\mathcal{A}_n^{\text{BDS}}} = \frac{\mathcal{A}_n^{\text{NMHV}}}{\mathcal{A}_n^{\text{MHV}}} \frac{\mathcal{A}_n^{\text{MHV}}}{\mathcal{A}_n^{\text{BDS}}} = \mathcal{P}_n \, \mathcal{B}_n \,, \tag{4.1.20}$$

where $\mathcal{A}_n^{\text{BDS}}$ is the superamplitude obtained from the bosonic BDS ansatz by replacing the tree-level MHV Parke-Taylor factor [8, 15] it contains with its supersymmetrized version [20]. Indeed, normalizations (4.1.19), (4.1.20) were found to be more natural for the study of the dual superconformal symmetry anomaly equation [89].

In what follows, it will prove greatly beneficial to define yet another set of infrared-finite quantities, using an alternate normalization factor that is compatible with the Steinmann relations. The BDS ansatz is essentially the exponential of the full one-loop amplitude, which includes a finite part with nontrivial dependence on Mandelstam invariants involving all possible numbers of external momenta. Dividing by the BDS ansatz produces a quantity with altered dependence on three-particle Mandelstam invariants. As we will see, such a quantity does not satisfy the Steinmann relations. In the case of seven-particle scattering (indeed, whenever n is not a multiple of four), all the dependence on the three-particle invariants (and higher-particle invariants) can be assembled into a dual conformally invariant function Y_n, which we may remove from the one-loop amplitude in order to define a *BDS-like* ansatz,

$$\mathcal{A}_n^{\text{BDS-like}} \equiv \mathcal{A}_n^{\text{BDS}} \exp\left[\frac{\Gamma_{\text{cusp}}}{4} Y_n\right], \tag{4.1.21}$$

where

$$Y_6 = -\operatorname{Li}_2\left(1-\frac{1}{u}\right) - \operatorname{Li}_2\left(1-\frac{1}{v}\right) - \operatorname{Li}_2\left(1-\frac{1}{w}\right), \tag{4.1.22}$$

$$Y_7 = -\sum_{i=1}^{7}\left[\operatorname{Li}_2\left(1-\frac{1}{u_i}\right) + \frac{1}{2}\log\left(\frac{u_{i+2}u_{i-2}}{u_{i+3}u_i u_{i-3}}\right)\log u_i\right], \tag{4.1.23}$$

and

$$\Gamma_{\text{cusp}} = \sum_{L=1}^{\infty} g^{2L}\Gamma_{\text{cusp}}^L = 4g^2 - \frac{4\pi^2}{3}g^4 + \frac{44\pi^4}{45}g^6 - 4\left(\frac{73\pi^6}{315} + 8\zeta_3^2\right)g^8 + \mathcal{O}(g^{10}), \tag{4.1.24}$$

is the cusp anomalous dimension in the normalization of e.g. [77].[2] In eq. (4.1.22), u, v, w are the three cross ratios for six-point kinematics, defined below in eq. (4.5.1). The difference between the BDS- and BDS-like-normalized ansätze for seven-point kinematics is reviewed in more detail in appendix A. The utility of the BDS-like ansatz was first noticed in the strong coupling analysis of amplitudes via the AdS/CFT correspondence [119] (see also ref. [120]). At weak coupling, it was found to simplify the six-point multi-particle factorization limit [60], self-crossing limit [105] and NMHV $\bar{Q}$ relations [70], before its role in applying the six-point Steinmann relations was noticed [5]. We will see its advantages as well in our seven-point analysis.

When n is a multiple of four it is not possible to simultaneously remove the dependence on all three-particle and higher-particle Mandelstam invariants in a conformally invariant fashion [121]. However, for $n = 8$ it is still possible to separately remove the dependence of all three-particle invariants, *or* of all four-particle invariants, giving rise to two different BDS-like ansätze.

Restricting our attention to the case $n \neq 4$, we may thus define the *BDS-like-normalized* MHV and NMHV amplitudes as

$$\begin{aligned}
\mathcal{E}_n &\equiv \frac{\mathcal{A}_n^{\text{MHV}}}{\mathcal{A}_n^{\text{BDS-like}}} = \frac{\mathcal{A}_n^{\text{MHV}}}{\mathcal{A}_n^{\text{BDS}}} \frac{\mathcal{A}_n^{\text{BDS}}}{\mathcal{A}_n^{\text{BDS-like}}} = \mathcal{B}_n \exp\left[-\frac{\Gamma_{\text{cusp}}}{4} Y_n\right] = \exp\left[R_n - \frac{\Gamma_{\text{cusp}}}{4} Y_n\right], \\
E_n &\equiv \frac{\mathcal{A}_n^{\text{NMHV}}}{\mathcal{A}_n^{\text{BDS-like}}} = \frac{\mathcal{A}_n^{\text{NMHV}}}{\mathcal{A}_n^{\text{BDS}}} \frac{\mathcal{A}_n^{\text{BDS}}}{\mathcal{A}_n^{\text{BDS-like}}} = B_n \exp\left[-\frac{\Gamma_{\text{cusp}}}{4} Y_n\right] = \mathcal{P}_n \, \mathcal{E}_n \,,
\end{aligned} \tag{4.1.25}$$

where we have also spelled out their relation to the previously-considered normalizations. Note that

$$\mathcal{E}_n^{(1)} = -Y_n \,, \tag{4.1.26}$$

since R_n starts at two loops.

Because we will focus almost exclusively on heptagon amplitudes in this chapter, we will usually drop the particle index n from of all of its associated quantities in order to avoid clutter, e.g. $\mathcal{P}_7 \to \mathcal{P}$, $\mathcal{E}_7 \to \mathcal{E}$ and $E_7 \to E$. In the NMHV case we will instead use subscripts to denote components multiplying the different R-invariants. For example, the BDS-normalized and BDS-like-normalized analogs of eq. (4.1.15) are

$$B = \mathcal{P}^{(0)} \, B_0 + \big[(12) \, B_{12} + (14) \, B_{14} + \text{ cyclic}\big] \,, \tag{4.1.27}$$

$$E = \mathcal{P}^{(0)} \, E_0 + \big[(12) \, E_{12} + (14) \, E_{14} + \text{ cyclic}\big] \,. \tag{4.1.28}$$

[2] In particular, $\Gamma_{\text{cusp}} = \gamma_K/2$ compared to the normalization of [28] and subsequent papers of Dixon and collaborators.

It is important to note that because the R-invariants are coupling-independent, the same coupling-dependent factor that relates NMHV superamplitudes in different normalizations will also relate the respective coefficient functions of the R-invariants. In other words,

$$E_* = B_* \exp\left[-\frac{\Gamma_{\text{cusp}}}{4} Y\right] = \mathcal{E}\, V_*\,, \tag{4.1.29}$$

where $*$ can be any index, 0 or ij.

Given that in this chapter we will be focusing exclusively on symbols, it's also worth emphasizing that when expanding eq. (4.1.25) or equivalently eq. (4.1.29) at weak coupling, we may replace $\Gamma_{\text{cusp}} \to 4g^2$, as a consequence of the fact that the symbol of any term containing a transcendental constant, such as ζ_n, is zero. Thus, the conversion between the BDS-like-normalized quantities $F \in \{\mathcal{E}, E, E_0, E_{ij}\}$ and the corresponding BDS-normalized quantities $\mathcal{F} \in \{\mathcal{B}, B, B_0, B_{ij}\}$ at symbol level and at fixed order in the coupling, simply becomes

$$F^{(L)} = \sum_{k=0}^{L} \mathcal{F}^{(k)} \frac{(-Y_n)^{L-k}}{(L-k)!}\,, \qquad \mathcal{F}^{(L)} = \sum_{k=0}^{L} F^{(k)} \frac{Y_n^{L-k}}{(L-k)!}\,. \tag{4.1.30}$$

In particular, for R_7, which sits in the exponent, its analogous conversion to $\mathcal{E}_7$ through four loops is given by

$$\begin{aligned}
\mathcal{E}_7^{(2)} &= R_7^{(2)} + \frac{1}{2}\Big(\mathcal{E}_7^{(1)}\Big)^2\,,\\
\mathcal{E}_7^{(3)} &= R_7^{(3)} + \mathcal{E}_7^{(1)} R_7^{(2)} + \frac{1}{6}\Big(\mathcal{E}_7^{(1)}\Big)^3\,,\\
\mathcal{E}_7^{(4)} &= R_7^{(4)} + \frac{1}{2}\Big(R_7^{(2)}\Big)^2 + \mathcal{E}_7^{(1)} R_7^{(3)} + \frac{1}{2}\Big(\mathcal{E}_7^{(1)}\Big)^2 R_7^{(2)} + \frac{1}{24}\Big(\mathcal{E}_7^{(1)}\Big)^4\,.
\end{aligned} \tag{4.1.31}$$

In summary, all the nontrivial kinematic dependence of seven-particle scattering can be encoded in the four transcendental functions R_7, B_0, B_{12} and B_{14} using BDS normalization, or equivalently $\mathcal{E}, E_0, E_{12}$ and E_{14} using BDS-like normalization. (The other E_{ij} that are needed are related to E_{12} and E_{14} by cyclic permutations.) These functions are all expected to belong to a very special class of transcendental functions called heptagon functions, whose definition and construction we turn to in the next section. However, we will see that it is only the BDS-like-normalized amplitudes that inherit a specific analytic property from the full amplitudes: they satisfy the Steinmann relations. Taking this restriction into account hugely trims the space of heptagon functions needed to bootstrap the BDS-like normalized functions, thus allowing for a far more efficient construction of the amplitude.

4.2 The Steinmann Cluster Bootstrap

The heptagon bootstrap approach we use in this chapter is a slight refinement of that used in ref. [61], which in turn is a generalization of the hexagon function bootstrap [49, 48, 50, 51, 60, 62]. We begin this section by reviewing some basics of the bootstrap approach and defining heptagon functions. Then we express the seven-point Steinmann relations in the language of cluster $\mathcal{A}$-coordinates. We assume a basic working knowledge of both symbols [35, 122, 123, 124, 125, 126, 32, 46] and momentum twistor notation [24].

4.2.1 Symbol Alphabet

In the cluster bootstrap program for n-point amplitudes in planar SYM theory, we assume that the symbol alphabet consists of certain objects known as cluster $\mathcal{A}$-coordinates. These coordinates have been discussed extensively in the context of scattering amplitudes; see for example ref. [32]. Here we will only briefly recall that the kinematic data for a scattering process in planar SYM theory may be specified by a collection of n momentum twistors [24], each of which is a homogeneous coordinate Z_i on $\mathbb{P}^3$. The configuration space for SYM theory is $\text{Conf}_n(\mathbb{P}^3) = \text{Gr}(4,n)/(\mathbb{C}^*)^{n-1}$, and cluster $\mathcal{A}$-coordinates on this space can be expressed in terms of the Plücker coordinates of 4-brackets $\langle ijkl\rangle$, which we defined in eq. (4.1.9).

Mandelstam invariants constructed from sums of cyclically adjacent external momenta $p_i, p_{i+1}, \ldots, p_{j-1}$ can be expressed nicely in terms of dual coordinates x_i satisfying the relation $p_i = x_{i+1} - x_i$. Using the notation $x_{ij} = x_i - x_j$, the Mandelstam invariant $s_{i,\ldots,j-1}$ can be written as

$$s_{i,\ldots,j-1} = (p_i + p_{i+1} + \cdots + p_{j-1})^2 = x_{ij}^2 = \frac{\langle i{-}1\, i\, j{-}1\, j\rangle}{\langle i{-}1\, i\rangle\langle j{-}1\, j\rangle}\,. \tag{4.2.1}$$

Here we have also shown how to express the Mandelstam invariant $s_{i,\ldots,j-1}$ in terms of Plücker coordinates and the usual spinor products $\langle ij\rangle = \epsilon_{\alpha\beta}\lambda_i^\alpha\lambda_j^\beta$, see also eq. (4.1.7). The denominator factors in eq. (4.2.1) drop out of any dual conformally invariant quantity and so may be ignored for our purposes. We will use eq. (4.2.1) to establish the connection between the cluster $\mathcal{A}$-coordinates (defined in terms of Plücker coordinates) and the Steinmann relations (formulated in terms of Mandelstam invariants). More general Plücker coordinates $\langle ijkl\rangle$ not of the form $\langle i{-}1\, i\, j{-}1\, j\rangle$ have more complicated (algebraic) representations in terms of Mandelstam invariants. (A systematic approach for finding such representations was discussed in the appendix of ref. [127].)

In this chapter we focus on $n = 7$ where there are a finite number of $\mathcal{A}$-coordinates. In addi-

tion to the Plücker coordinates $\langle ijkl\rangle$ there are 14 Plücker bilinears of the form $\langle a(bc)(de)(fg)\rangle \equiv \langle abde\rangle\langle acfg\rangle - \langle abfg\rangle\langle acde\rangle$. A convenient complete and multiplicatively independent set of 42 dual conformally invariant ratios, introduced in ref. [61], is given in terms of these building blocks by

$$\begin{aligned} a_{11} &= \frac{\langle 1234\rangle\langle 1567\rangle\langle 2367\rangle}{\langle 1237\rangle\langle 1267\rangle\langle 3456\rangle}\,, & a_{41} &= \frac{\langle 2457\rangle\langle 3456\rangle}{\langle 2345\rangle\langle 4567\rangle}\,, \\ a_{21} &= \frac{\langle 1234\rangle\langle 2567\rangle}{\langle 1267\rangle\langle 2345\rangle}\,, & a_{51} &= \frac{\langle 1(23)(45)(67)\rangle}{\langle 1234\rangle\langle 1567\rangle}\,, \\ a_{31} &= \frac{\langle 1567\rangle\langle 2347\rangle}{\langle 1237\rangle\langle 4567\rangle}\,, & a_{61} &= \frac{\langle 1(34)(56)(72)\rangle}{\langle 1234\rangle\langle 1567\rangle}\,, \end{aligned} \tag{4.2.2}$$

with a_{ij} for $1 < j \leq 7$ given by cyclic permutation of the particle labels; specifically,

$$a_{ij} = a_{i1}\big|_{Z_k \to Z_{k+j-1}}\,. \tag{4.2.3}$$

The Steinmann relations, to be reviewed in section 4.2.4, are expressed simply in terms of Mandelstam invariants. We therefore note that with the help of eq. (4.2.1) we can express a_{1j} quite simply as

$$a_{11} = \frac{s_{23}s_{67}s_{712}}{s_{12}s_{71}s_{45}}\,, \tag{4.2.4}$$

with the remaining six a_{1j} again given by cyclic permutations. The remaining 35 cluster $\mathcal{A}$-coordinates do not admit simple representations in terms of Mandelstam invariants because they involve brackets not of the form $\langle i{-}1\, i\, j{-}1\, j\rangle$.

Finally, it is useful to relate the cross ratios u_i, defined in eq. (4.1.18), to the letters a_{ij}. Eq. (4.2.4) can alternatively be written as

$$a_{11} = \frac{x_{24}^2 x_{61}^2 x_{73}^2}{x_{13}^2 x_{72}^2 x_{46}^2}\,. \tag{4.2.5}$$

Combining this equation with cyclic permutations of it, and using eq. (4.1.18), we find that

$$\frac{a_{11}}{a_{14}a_{15}} = \frac{x_{73}^2 x_{46}^2}{x_{74}^2 x_{36}^2} = u_{36} = u_2\,, \tag{4.2.6}$$

plus cyclic permutations of this relation. Note that, although we can define 7 of these cross ratios u_i in seven-point kinematics, an n-point scattering process in this theory only has $3n-15$ algebraically independent dual conformal invariants. Thus only 6 of the 7 u_i (or a_{1i}) are algebraically independent. The seven u_i obey a single algebraic equation, the condition that a particular Gram determinant vanishes, which restricts the kinematics to a six-dimensional surface within the seven-dimensional space of cross ratios. We will not need the explicit form of the Gram determinant in this work.

4.2.2 Integrability

The heptagon bootstrap is based on the working hypothesis that any seven-point L-loop amplitude in planar $\mathcal{N} = 4$ SYM theory can be expressed as a linear combination of weight-$2L$ generalized polylogarithm functions written in the 42-letter alphabet shown in eq. (4.2.2). Using this alphabet one can write 42^k distinct symbols of weight k. Fortunately, relatively few linear combinations of these 42^k symbols are actually the symbol of some function. A symbol $\mathcal{S}$ of the form

$$\mathcal{S}(f_k) = \sum_{\alpha_1,\ldots,\alpha_k} f_0^{(\alpha_1,\ldots,\alpha_k)}(\phi_{\alpha_1} \otimes \cdots \otimes \phi_{\alpha_k}), \tag{4.2.7}$$

where the ϕ_{α_j} are letters, corresponds to an actual function only if it satisfies the integrability condition

$$\sum_{\alpha_1,\ldots,\alpha_k} f_0^{(\alpha_1,\ldots,\alpha_k)} \underbrace{(\phi_{\alpha_1} \otimes \cdots \otimes \phi_{\alpha_k})}_{\text{omitting } \alpha_j \otimes \alpha_{j+1}} d\log\phi_{\alpha_j} \wedge d\log\phi_{\alpha_{j+1}} = 0 \quad \forall j \in \{1, 2, \ldots, k-1\}\,. \tag{4.2.8}$$

A conceptually simple method for determining all integrable symbols of a given weight k is discussed in appendix B, where the definition of the wedge product appearing in the above equation is also given. The symbols of physical amplitudes have several additional properties, to which we will now turn our attention.

4.2.3 Symbol Singularity Structure

Locality requires that amplitudes can only have singularities when an intermediate particle goes on-shell. In a planar theory the momenta of intermediate particles can always be expressed as a sum of cyclically adjacent momenta, and thresholds in massless theories are always at the origin. Hence perturbative amplitudes in planar SYM theory can only have branch points when the corresponding Mandelstam invariants $s_{i,\ldots,j-1} = x_{ij}^2$ vanish.

When some letter ϕ appears in the first entry of a symbol it indicates that the corresponding function has branch points at $\phi = 0$ and $\phi = \infty$. Therefore the first entry of a symbol that corresponds to a physical scattering amplitude must be a ratio of products of x_{ij}^2 [36]. We see from eqs. (4.2.1) and (4.2.2) that only the seven a_{1j} are valid first entries. The remaining 35 cluster $\mathcal{A}$-coordinates contain terms that may be zero (or infinite) without any intermediate particles going on-shell. There is no possibility of cancellation in a sum over terms in a symbol since the letters of the alphabet are multiplicatively independent. The restriction that the first entry of the symbol of

any seven-point amplitude must be one of the seven a_{1j} is called the first-entry condition.

4.2.4 Steinmann Relations

The classic work of Steinmann provided powerful restrictions on the analytic form of discontinuities [90]. Expanding upon his work, Cahill and Stapp found that the generalized Steinmann relations hold and that double discontinuities vanish for any pair of overlapping channels [128].[3] A channel is labelled by a Mandelstam invariant, but it also corresponds to an assignment of particles to incoming and outgoing states. Two channels overlap if the four sets into which they divide the particles – (incoming,incoming), (incoming,outgoing), (outgoing,incoming) and (outgoing,outgoing) – are all non-empty. Fig. 4.2.1 shows a pair of overlapping channels for the seven-point process, s_{345} and s_{234}. They overlap because they divide the seven particles into the four non-empty sets $\{2\}$, $\{3,4\}$, $\{5\}$, and $\{6,7,1\}$.

Unlike two-particle invariants, three-particle invariants can cross zero "gently", without any other invariants having to change sign. Fig. 4.2.1 is drawn for the $3 \to 4$ configuration with particles 1, 2 and 3 incoming. Within that configuration, the left panel shows that s_{345} can be either negative or positive. As s_{345} moves from negative to positive, a branch cut opens up, due to one or more on-shell particles being allowed to propagate between the two blobs. The discontinuity in the amplitude across the branch cut is given by the sum of all such on-shell intermediate-state contributions, integrated over their respective phase space. The same is true for the s_{234} discontinuity illustrated in the right panel. However, once one takes the s_{345} discontinuity, the resulting function cannot have a second discontinuity in the s_{234} channel, because it is impossible for states to propagate on-shell simultaneously in both the s_{345} and s_{234} "directions". Thus we require the Steinmann conditions,

$$\mathrm{Disc}_{s_{i+1,i+2,i+3}}\left[\mathrm{Disc}_{s_{i,i+1,i+2}}F\right] = \mathrm{Disc}_{s_{i+2,i+3,i+4}}\left[\mathrm{Disc}_{s_{i,i+1,i+2}}F\right] = 0, \tag{4.2.9}$$

to hold for all $i = 1, 2, \ldots 7$.

In contrast, the s_{234} channel does not overlap the s_{567} channel (or the s_{671} channel). For example, in the right panel of the figure, one can have a second discontinuity, after taking $\mathrm{Disc}_{s_{234}}$, in the s_{567} channel, as particle 1 and the particles crossing the s_{234} cut rescatter into another set of intermediate states, which then materializes into particles 5, 6 and 7. That is, the following double discontinuities

[3] The implications of the Steinmann relations for the multi-Regge limit of amplitudes in planar $\mathcal{N} = 4$ SYM have been analyzed in refs. [129, 130, 68, 93].

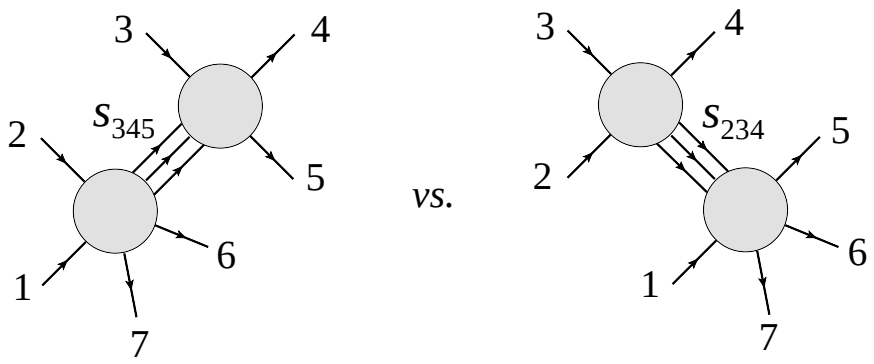

Figure 4.2.1: The figure on the left (right) shows the discontinuity of an amplitude in the s_{345} (s_{234}) channel due to the respective intermediate states. These two channels overlap, which implies that the states that cross the first cut cannot produce a discontinuity in the second channel (or vice versa).

can be nonvanishing,

$$\text{Disc}_{s_{i+3,i+4,i+5}}\left[\text{Disc}_{s_{i,i+1,i+2}}F\right] \neq 0, \qquad \text{Disc}_{s_{i+4,i+5,i+6}}\left[\text{Disc}_{s_{i,i+1,i+2}}F\right] \neq 0, \tag{4.2.10}$$

and they provide us with no useful constraints. Also, the "self" double discontinuities are nonvanishing,

$$\text{Disc}_{s_{i,i+i,i+2}}\left[\text{Disc}_{s_{i,i+1,i+2}}F\right] \neq 0, \tag{4.2.11}$$

and are not of use to us. A recent analysis of the Steinmann relations, focusing on the six-point case, can be found in ref. [5].

We will only consider restrictions imposed on the symbol letters a_{ij} by the Steinmann relations on overlapping three-particle cuts, eq. (4.2.9). If there are any restrictions imposed by using two-particle cuts, they are considerably more subtle for generic kinematics. Flipping the sign of a two-particle invariant generally entails moving a particle from the initial state to the final state, or vice versa, and other invariants can flip sign at the same time, making it hard to assess the independence of the two-particle discontinuities.

Because the discontinuities of a symbol are encoded in its first entries, double discontinuities are encoded by the combinations of first and second entries that appear together. Correspondingly, the Steinmann relations tell us that the symbol of an amplitude cannot have any terms in which overlapping three-particle Mandelstam invariants appear together as first and second entries. Eqs. (4.2.1)–(4.2.2) imply that this only imposes a constraint on the letters a_{1j}, since the other letters do not contain three-particle Mandelstam invariants $s_{i-1,i,i+1} \propto \langle i{-}2\, i{-}1\, i{+}1\, i{+}2\rangle$. More specifically, we see in eq. (4.2.4) that each a_{1i} is proportional to a single three-particle invariant

$s_{i-1,i,i+1}$, so a first entry of a_{1i} cannot be followed by a second entry of $a_{1,i+1}, a_{1,i+2}, a_{1,i+5}$, or $a_{1,i+6}$, all of which contain a three-particle invariant involving p_{i-1}, p_i, or p_{i+1}. A first entry of a_{1i} *can* be followed by a second entry of a_{1i}, $a_{1,i+3}$, $a_{1,i+4}$, or any a_{ki} for $k > 1$ (subject to the constraint of integrability).

Everything stated thus far about the Steinmann constraint applies to full, infrared-divergent amplitudes. However, the BDS-like-normalized amplitudes straightforwardly inherit this constraint, due to the fact that the BDS-like ansatz, given explicitly in eqs. (A.0.14) and (A.0.15), contains no three-particle invariants; it therefore acts as a spectator when taking three-particle discontinuities, e.g.

$$\text{Disc}_{s_{i-1,i,i+1}} \mathcal{A}_7^{\text{MHV}} = \text{Disc}_{s_{i-1,i,i+1}} \left[\mathcal{A}_7^{\text{BDS-like}} \, \mathcal{E} \right] = \mathcal{A}_7^{\text{BDS-like}} \, \text{Disc}_{s_{i-1,i,i+1}} \mathcal{E} \, . \tag{4.2.12}$$

This is no longer true for the BDS-normalized amplitude, which according to eq. (4.1.25) comes with an extra factor of $\exp[\frac{\Gamma_{\text{cusp}}}{4} Y_n]$. When expanded at weak coupling this factor will produce powers of Y_n. The function Y_n is itself Steinmann since $Y_n = -\mathcal{E}_n^{(1)}$. However, products of Steinmann functions are not generically Steinmann functions, because overlapping discontinuities can arise from different factors in the product. Indeed, once we observe that Y_n has a cut in one three-particle channel, and that it is dihedrally invariant, we know it has cuts in all three-particle channels. Whereas Y_n itself is a *sum* of terms having cuts in overlapping channels, it is the *cross terms* in $(Y_n)^2$, or higher powers of Y_n, that violate the Steinmann relations. Similarly, the ratio function $V_* = E_*/\mathcal{E}$, when expanded out perturbatively, contains products of Steinmann functions and therefore does not obey the Steinmann relations. The lesson here is that the proper normalization of the amplitude is critical for elucidating its analytic properties.

To summarize, the Steinmann relations require that any BDS-like-normalized seven-point function F, such as $\mathcal{E}_7$ or E_7, must satisfy

$$\text{Disc}_{a_{1i}} \left[\text{Disc}_{a_{1j}} F \right] = 0 \quad \text{if } j \neq i, i+3, i+4 \, . \tag{4.2.13}$$

At the level of the symbol, this statement is equivalent to requiring that the symbol of F contains no first entries a_{1i} followed by second entries $a_{1,i+1}$, $a_{1,i+2}$, $a_{1,i+5}$, or $a_{1,i+6}$.

4.2.5 Absence of Triple Discontinuity Constraints

At the seven-point level, it is interesting to ask whether there could be new constraints on amplitudes of the following type:

$$\mathrm{Disc}_{a_{17}}\Big[\mathrm{Disc}_{a_{14}}\Big[\mathrm{Disc}_{a_{11}}F\Big]\Big] \stackrel{?}{=} 0. \tag{4.2.14}$$

The three-particle channels corresponding to a_{11} and a_{14} do not overlap, nor do the channels corresponding to a_{14} and a_{17}. The channels corresponding to a_{11} and a_{17} *do* overlap, but the two discontinuities are separated by the a_{14} discontinuity in between. (An analogous situation never arises for three-particle cuts in the six-point case, because the only allowed double three-particle cut in that case involves cutting the same invariant twice.) We have inspected the symbols of the MHV and NMHV seven-point amplitudes, and we find that eq. (4.2.14) is generically non-vanishing. The act of taking the non-overlapping second discontinuity of the amplitude apparently alters the function's properties enough that the third discontinuity is permitted.

4.2.6 Steinmann Heptagon Functions

We define a heptagon function of weight k to be a generalized polylogarithm function of weight k whose symbol may be written in the alphabet of 42 cluster $\mathcal{A}$-coordinates, eq. (4.2.2), and which satisfies the first entry condition. These functions have been studied in ref. [61], where it was found that the vector space of heptagon function symbols at weight $k = 1, 2, 3, 4, 5$ has dimension 7, 42, 237, 1288, 6763, respectively.

In this chapter our goal is to sharpen the heptagon bootstrap of ref. [61] by taking advantage of the powerful constraint provided by the Steinmann relations. We thus define Steinmann heptagon functions to be those heptagon functions that additionally satisfy the Steinmann relations (4.2.13). This corresponds to a restriction on the second entry of their symbols, as discussed in section 4.2.4. We stress again that while both BDS-normalized and BDS-like-normalized amplitudes are heptagon functions, only the BDS-like-normalized ones, $\mathcal{E}$, E_0, and E_{ij}, are Steinmann heptagon functions.

We will see in subsection 4.4.1 that a drastically reduced number of heptagon functions satisfy the Steinmann relations. The reduction begins at weight 2, where there are 42 heptagon function symbols, but only 28 that obey the Steinmann relations. The corresponding 28 functions fall into 4 orbits:

$$\mathrm{Li}_2\left(1-\frac{a_{13}a_{14}}{a_{17}}\right), \quad \mathrm{Li}_2\left(1-a_{14}a_{16}\right), \quad \log^2 a_{13}, \quad \log a_{13}\log a_{16}, \tag{4.2.15}$$

together with their cyclic permutations. This fractional reduction, by one third, is the same as in the

hexagon case [5], where the number of weight-2 functions was reduced from 9 to 6. At higher weight, we will see that the reductions are much more dramatic, and even more so for heptagon functions than hexagon functions. This reduction in the number of relevant functions vastly decreases the size of our ansatz, making this version of the bootstrap program more computationally tractable than its predecessor.

4.3 MHV and NMHV Constraints

In appendix B we provide an algorithm for generating a basis for the symbols of weight-k Steinmann heptagon functions, which serve as ansätze for the MHV and NMHV amplitudes. We then impose known analytic and physical properties as constraints in order to identify the amplitudes uniquely. Here we review these properties and the constraints they impose.

4.3.1 Final Entry Condition

The final entry condition is a restriction on the possible letters that may appear in the final entry of the symbol of an amplitude. As a consequence of the dual superconformal symmetry of SYM, the differential of an MHV amplitude must be expressible as a linear combination of $d\log\langle i\,j{-}1\,j\,j{+}1\rangle$ factors [110]. The differential of a generalized polylogarithm of weight k factors into linear combinations of weight-$(k{-}1)$ polylogarithms multiplied by $d\log\phi$ terms where ϕ is the final entry of the symbol. Therefore the final entries of the symbol of an MHV amplitude must be composed entirely of Plücker coordinates with three adjacent momentum twistors, $\langle i\,j{-}1\,j\,j{+}1\rangle$. In the symbol alphabet (4.2.2) we have chosen, the final entries can only be drawn from the set of 14 letters $\{a_{2j}, a_{3j}\}$.

The MHV final entry condition we just described can be derived from an anomaly equation for the $\bar{Q}$ dual superconformal generators [89]. The same anomaly equation can also be used to constrain the final entries of the symbol of the NMHV superamplitude E. In particular, using as input the leading singularities of the N^{2}MHV 8-point amplitude obtained from the Grassmannian [115], and refining the $\bar{Q}$ equation so as to act on the BDS-like normalized amplitude rather than the BDS-normalized one, Caron-Huot has found [131] that only 147 distinct (R-invariant) $\times$ (final entry)

combinations are allowed in E, namely these 21:

$$\begin{gathered}
(34)\log a_{21},\quad (14)\log a_{21},\quad (15)\log a_{21},\quad (16)\log a_{21},\quad (13)\log a_{21},\quad (12)\log a_{21},\\
(45)\log a_{37},\quad (47)\log a_{37},\quad (37)\log a_{37},\quad (27)\log a_{37},\quad (57)\log a_{37},\quad (67)\log a_{37},\\
(45)\log\frac{a_{34}}{a_{11}},\quad (14)\log\frac{a_{34}}{a_{11}},\quad (14)\log\frac{a_{11}a_{24}}{a_{46}},\quad (14)\log\frac{a_{14}a_{31}}{a_{34}},\\
(24)\log\frac{a_{44}}{a_{42}},\qquad (56)\log a_{57},\qquad (12)\log a_{57},\qquad (16)\log\frac{a_{67}}{a_{26}},\\
(13)\log\frac{a_{41}}{a_{26}a_{33}}+((14)-(15))\log a_{26}-(17)\log a_{26}a_{37}+(45)\log\frac{a_{22}}{a_{34}a_{35}}-(34)\log a_{33}\,,
\end{gathered}\tag{4.3.1}$$

together with their cyclic permutations.[4]

4.3.2 Discrete Symmetries

The n-particle superamplitudes $\mathcal{A}_n$ are invariant under dihedral transformations acting on the external particle labels. The generators of the dihedral group D_n are the cyclic permutation $i \to i+1$ and the flip permutation $i \to n+1-i$ of the particle labels, or equivalently of the momentum twistors. For the heptagon a-letters (4.2.2), these correspond to

$$\begin{aligned}
&\text{Cyclic transformation:}\quad a_{li} \to a_{l,i+1}\,,\\
&\text{Flip transformation:}\begin{cases} a_{2i} \leftrightarrow a_{3,8-i} \\ a_{li} \to a_{l,8-i} \quad \text{for} \quad l \neq 2,3\,. \end{cases}
\end{aligned}\tag{4.3.2}$$

MHV and $\overline{\text{MHV}}$ amplitudes differ only in their tree-level prefactors. Hence the functions $\mathcal{E}_n$ and R_n must remain invariant under spacetime parity transformations. Parity maps NMHV amplitudes to $\overline{\text{NMHV}}$ ones and therefore acts nontrivially on E_0, E_{12} and E_{14}. In the language of our symbol alphabet (4.2.2), a parity transformation leaves the letters a_{1i} and a_{6i} invariant. The remaining letters transform under parity according to

$$\text{Parity transformation:}\quad a_{21} \longleftrightarrow a_{37},\qquad a_{41} \longleftrightarrow a_{51},\tag{4.3.3}$$

and the cyclic permutations thereof.

The parity and dihedral symmetries of the (super)amplitude are inherited by its BDS(-like) normalized counterpart because the BDS(-like) ansätze are also dihedrally invariant.

[4]We thank Simon Caron-Huot for sharing these results with us.

4.3.3 Collinear Limit

So far we have primarily focused on the BDS-like normalized amplitude and the Steinmann functions describing it. However for the study of collinear limits it proves advantageous to switch, using eq. (4.1.30), to the BDS-normalized amplitude, since in the limit the former becomes divergent, whereas the latter remains finite.

In more detail, the BDS ansatz A_n^{BDS} entering eq. (4.1.1) is defined in such a way that the n-point BDS-normalized amplitude (or equivalently the remainder function for MHV) reduces to the same quantity but with one fewer particle:

$$\begin{aligned} \lim_{i+1||i} R_n &= R_{n-1}\,, \\ \lim_{i+1\|i} B_n &= B_{n-1}\,. \end{aligned} \tag{4.3.4}$$

To take one of these collinear limits, one of the $s_{i,i+1}$ must be taken to zero. From eq. (4.2.1), we see that this can be accomplished by taking a limit of one of the momentum twistor variables. In the case of the NMHV superamplitude we also need to specify the limit of the fermionic part of the supertwistors (4.1.6). The (MHV degree preserving) 7||6 collinear limit can be taken by sending

$$\mathcal{Z}_7 \to \mathcal{Z}_6 + \epsilon\frac{\langle 1246\rangle}{\langle 1245\rangle}\mathcal{Z}_5 + \epsilon\tau\frac{\langle 2456\rangle}{\langle 1245\rangle}\mathcal{Z}_1 + \eta\frac{\langle 1456\rangle}{\langle 1245\rangle}\mathcal{Z}_2\,, \tag{4.3.5}$$

for fixed τ, and by taking the limit $\eta \to 0$ followed by $\epsilon \to 0$.

Of course for bosonic quantities, only the bosonic part $\mathcal{Z}_i \to Z_i$ of the supertwistor is relevant. As noted in ref. [61], in the limit (4.3.5) the heptagon alphabet (4.2.2) reduces to the hexagon alphabet, plus the following 9 additional letters,

$$\begin{gathered} \eta\,, \quad \epsilon\,, \quad \tau\,, \quad 1+\tau\,, \\ \langle 1235\rangle\langle 1246\rangle + \tau\langle 1236\rangle\langle 1245\rangle\,, \quad \langle 1245\rangle\langle 3456\rangle + \tau\langle 1345\rangle\langle 2456\rangle\,, \\ \langle 1246\rangle\langle 2356\rangle + \tau\langle 1236\rangle\langle 2456\rangle\,, \quad \langle 1246\rangle\langle 3456\rangle + \tau\langle 1346\rangle\langle 2456\rangle\,, \\ \langle 1235\rangle\langle 1246\rangle\langle 3456\rangle + \tau\langle 1236\rangle\langle 1345\rangle\langle 2456\rangle\,. \end{gathered} \tag{4.3.6}$$

Therefore the collinear limits of heptagon functions are not generically hexagon functions. We say that a heptagon symbol has a well-defined 7||6 limit only if in this limit it is independent of all 9 of the additional letters (4.3.6).

We must also take the limit (4.3.5) of the R-invariants. Since these invariants are antisymmetric

under the exchange of any pair of twistor indices, the invariants that contain both indices 6 and 7 will vanish. All other invariants reduce to six-point R-invariants. Denoting the six-point invariants by

$$[12345] = (6) \tag{4.3.7}$$

and its cyclic permutations (under the six-point dihedral group), and solving the single identity of type (4.1.10) among them to eliminate (6), we deduce that

$$\begin{aligned}\lim_{7\|6} B =&(1)[\hat{B}_{17} + \hat{B}_{67} + \hat{B}_0] + (2)[\hat{B}_{26} - \hat{B}_{67}] + (3)[\hat{B}_{36} + \hat{B}_{37} + \hat{B}_{67} + \hat{B}_0] \\ &+ (4)[\hat{B}_{47} - \hat{B}_{67}] + (5)[\hat{B}_{56} + \hat{B}_{67} + \hat{B}_0]\,,\end{aligned} \tag{4.3.8}$$

where the hats denote the collinear limit of the corresponding bosonic functions.

Finally, we should note that in this work we will be focusing on collinear limits of dihedrally invariant functions. Therefore it will be sufficient to consider the $7||6$ limit shown above, and the remaining $i{+}1 \parallel i$ collinear limits will be automatically satisfied as a consequence of dihedral symmetry.

4.4 Results

4.4.1 Steinmann Heptagon Symbols and Their Properties

As defined in section 4.2.6, a Steinmann heptagon function of weight k is a polylogarithm of weight k that has a symbol satisfying the following properties:

(i) it can be expressed entirely in terms of the heptagon symbol alphabet of eq. (4.2.2),

(ii) only the seven letters a_{1i} appear in its first entry,

(iii) a first entry a_{1i} is not followed by a second entry a_{1j} with $j \in \{i+1, i+2, i+5, i+6\}$.

We will frequently use the term 'Steinmann heptagon symbol' to mean the symbol of a Steinmann heptagon function. We begin by investigating how the number of Steinmann heptagon symbols compares to the number of heptagon symbols reported in ref. [61] through weight 5.

Table 4.1 presents the number of Steinmann heptagon symbols through weight 7, computed using the bootstrapping procedure outlined in appendix B. The total number of Steinmann symbols through weight 5 can be compared to $7, 42, 237, 1288$, and 6763 linearly independent heptagon symbols at weights 1 through 5, respectively [61]. By weight 5, the size of the Steinmann heptagon space

Weight $k =$	1	2	3	4	5	6	7	$7''$
parity +, flip +	4	16	48	154	467	1413	4163	3026
parity +, flip −	3	12	43	140	443	1359	4063	2946
parity −, flip +	0	0	3	14	60	210	672	668
parity −, flip −	0	0	3	14	60	210	672	669
Total	7	28	97	322	1030	3192	9570	7309

Table 4.1: Number of Steinmann heptagon symbols at weights 1 through 7, and those satisfying the MHV next-to-final entry condition at weight 7.

has already been reduced by a factor of six compared to the size of the standard heptagon space! (The corresponding reduction factor for hexagon symbols at weight 5 is only about 3.5.)

The total number of Steinmann heptagon symbols at each weight was calculated without imposing spacetime parity or dihedral symmetries. The first four rows show the number of Steinmann heptagon symbols that have the specified eigenvalue under the $\mathbb{Z}_2 \times \mathbb{Z}_2$ generators of parity and the dihedral flip symmetry. There are many more parity even (parity +) Steinmann heptagon functions than parity odd. At each weight there are approximately the same number of flip + as flip −. Up through weight 7, there are an equal number of flip + and flip − parity odd functions.

Table 4.1 has two columns for weight 7. The column $7''$ counts the number of weight 7 symbols that satisfy an additional constraint we call the MHV next-to-final entry condition. Paired with the MHV final entry condition, which requires the final entry of the symbol to be a_{2j} or a_{3j}, integrability imposes an additional constraint that prohibits the seven letters a_{6i} from appearing in the next-to-final entry of any MHV symbol. Symbols satisfying this additional constraint are useful for bootstrapping the four-loop MHV heptagon, to be discussed in subsection 4.4.3 below.

The fact that there are many more parity-even than parity-odd Steinmann heptagon functions is also true in the hexagon case [5]. In that case, it is possible to give a closed-form construction of an infinite series of parity-even "K" functions. The K functions apparently saturate the subspace of Steinmann hexagon functions having no parity-odd letters. This series of functions can also be repurposed, with appropriate arguments, to describe some, but not all, of the Steinmann heptagon symbols having no parity-odd letters.

Before concluding this section, let us emphasize that we are here counting integrable symbols, not functions. We expect each such symbol to be completable into a function. However, there are other functions (with vanishing symbol) obtained by multiplying lower-weight functions by multiple zeta values. When we impose physical constraints on the full function space, parameters associated

with these additional functions will also have to be determined. On the other hand, sometimes the function-level constraints are more powerful than the symbol-level constraints. As first observed in the case of the 3-loop MHV hexagon [49, 50], the number of n-gon functions obeying additional constraints, such as well-defined collinear limits, may be smaller than the number of the corresponding symbols. That is, completing a symbol to a function with proper branch cuts may require adding to it functions of lower weight that don't have a well-defined collinear limit, even if the symbol does. We leave the problem of upgrading our heptagon bootstrap from symbol to function level to a later work.

4.4.2 The Three-Loop NMHV Heptagon

Once we have constructed the Steinmann heptagon symbol space, we can assemble it into an ansatz for the seven-particle amplitude and apply the constraints outlined in section 4.3 to fix the free parameters. Let us describe the steps of this computation in the NMHV case.

Loop order $L =$	1	2	3
Steinmann symbols	15×28	15×322	15×3192
NMHV final entry	42	85	226
Dihedral symmetry	5	11	31
Well-defined collinear	0	0	0

Table 4.2: Number of free parameters after applying each of the constraints in the leftmost column, to an ansatz for the symbol of the L-loop seven-point NMHV BDS-like-normalized amplitude. The first row in column L is equal to the last line of column $k = 2L$ of table 4.1, multiplied by 15 for the 15 linearly independent R-invariants.

The NMHV amplitude is a linear combination of 15 transcendental functions multiplying the independent R-invariants. Therefore the initial number of free parameters at L loops, shown in table 4.2, is given by 15 times the entry in table 4.1 that counts the total number of Steinmann heptagon symbols of weight $2L$.[5]

We then impose the heptagon NMHV final entry condition discussed in subsection 4.3.1. Similarly to the NMHV hexagon case [70], the list of allowed final entries in eq. (4.3.1) can be translated into relations between the 42 different $\{k-1, 1\}$ coproduct components for each of the 15 functions multiplying the independent R-invariants, for a total of $42 \times 15 = 630$ independent objects. Note that

[5] If we had imposed dihedral symmetry first, we would have had only three independent functions E_0, E_{12} and E_{14} to parametrize, each with some dihedral symmetry, and there would have been fewer than 3 times the number of independent Steinmann heptagon symbols in the first line of the table. This part of the computation is not a bottleneck either way. This alternative procedure would also give rise to a different set of numbers in the second line of table 4.2.

eq. (4.3.1) contains all 21 distinct R-invariants, so in order to obtain the aforementioned equations we first need to eliminate the dependent R-invariants with the help of eqs. (4.1.13) and (4.1.14).

In principle, one can impose the NMHV final entry equations at $L = k/2$ loops on the ansatz of weight-k integrable symbols appearing in the first line of table 4.2. In practice, we have found it more efficient to solve these equations simultaneously with the weight-k integrability equations (4.2.8), namely the equations imposing integrability on the last two slots of an ansatz for E. The number of free parameters after imposing this condition (using either method) is reported in the second line of table 4.2. We see that the final entry condition is already very restrictive; out of the 47880 possible NMHV symbols with generic final entry at three loops, only 226 of them obey the NMHV final entry. Next we impose invariance of E under dihedral transformations, as discussed in subsection 4.3.2. The dihedral restriction leads to the small number of remaining free parameters reported in the third line of table 4.2.

We then examine the behavior of the amplitude in the collinear limit. To this end, we recall from subsection 4.3.3 that it is advantageous to convert to the BDS normalization, since the BDS-normalized amplitude is finite in the collinear limit, while the BDS-like normalized one becomes singular. Converting our partially-determined ansatz for E to an equivalent ansatz for B with the help of eq. (4.1.30), we then take its collinear limit using eq. (4.3.5).

Quite remarkably, demanding that the right-hand side of eq. (4.3.8) be well-defined, namely independent of the spurious letters (4.3.6) (and thus also finite), suffices to uniquely fix B through 3 loops! Even an overall rescaling is not allowed in the last line of table 4.2, because the condition of well-defined collinear limits, while homogeneous for BDS-normalized amplitudes, is inhomogeneous for the BDS-like normalization with which we work. We did not need to require that the collinear limit (4.3.8) of the solution agrees with the six-point ratio function computed at three loops in ref. [60], but of course we have checked that it does agree.

In this manner, we arrive at a unique answer for the symbol of the NMHV heptagon through three loops. Our results can be downloaded in a computer-readable file from [106]. The one- and two-loop results match the amplitudes computed in refs. [21] and [89], respectively. The fact that six-point boundary data is not even needed to fix the symbol through three loops points to a strong tension between the Steinmann relations, dual superconformal symmetry (in the guise of the final entry condition), and the collinear limit.

4.4.3 The Four-Loop MHV Heptagon

For the MHV remainder function at $L = k/2$ loops, we could in principle start from an ansatz for $\mathcal{E}_7^{(L)}$ involving all heptagon Steinmann symbols of weight k. As with the NMHV case, however, it is simpler to impose the MHV final-entry condition discussed in section 4.3.1 at the same time as integrability on the last two entries of the symbol. In fact, our initial four-loop MHV ansatz was constructed using not just the MHV final-entry condition, but also the MHV next-to-final entry condition discussed in section 4.4.1.

Loop order $L =$	1	2	3	4
Steinmann symbols	28	322	3192	?
MHV final entry	1	1	2	4
Well-defined collinear	0	0	0	0

Table 4.3: Free parameter count after applying each of the constraints in the leftmost column to an ansatz for the symbol of the L-loop seven-point MHV BDS-like-normalized amplitude.

In the first line of table 4.3, we reiterate the number of Steinmann heptagon functions with general final entry. In the second line of the table, we report the number of symbols that satisfy the MHV final entry condition. Clearly, there are only a few Steinmann heptagon functions at each weight that satisfy even these few constraints. Note that we have not even imposed dihedral invariance, nor that the symbol have even spacetime parity.

To determine the third line of the table, we convert the ansatz to one for the BDS normalized amplitude, using eq. (4.1.30) and the symbol of Y_7. We then ask that this quantity have a well-defined collinear limit. As in the NMHV case, there is a unique solution to this constraint, this time through four loops, as reported in the last line of table 4.3; this unique solution must be the symbol of $\mathcal{E}_7^{(L)}$. Our results can be downloaded in computer-readable files from [106]. Again the overall normalization is fixed because the last constraint is an inhomogeneous one for a BDS-like normalized amplitude. The symbols of the two- and three-loop seven-point BDS remainder functions $R_7^{(2)}$, $R_7^{(3)}$ are known [110, 61]. We have converted these quantities to the BDS-like normalization with the help of eq. (4.1.31), and they agree with our unique solutions. At four loops, when we convert our unique solution for $\mathcal{E}_7^{(4)}$ (which has 105,403,942 terms) to $R_7^{(4)}$ (which has 899,372,614 terms), we find that its well-defined collinear limit agrees perfectly with the symbol of the four-loop six-point MHV remainder function $R_6^{(4)}$ computed in ref. [51]. Because we did not need to impose dihedral invariance, nor spacetime parity, we can say that even less input is needed to fix the symbol of the MHV amplitude through four loops than was needed for the three-loop NMHV amplitude!

Before concluding, let us note that although we used the Steinmann constraint to tightly constrain the space of symbols through which we had to sift in order to find the four-loop MHV heptagon, it is possible that the same result could have been obtained (in principle, with much more computer power), without it. In the second row of table 4.3 we see, for example, that at weight 6 there are precisely 2 Steinmann heptagon symbols satisfying the MHV final-entry condition. Ref. [61] imposed the MHV final-entry condition, without considering the Steinmann relations, and found 4 different symbols at weight 6: $(Y_7)^3$, $Y_7\, R_7^{(2)}$, $R_7^{(3)}$ and one more. Modulo the reducible (product) functions $(Y_7)^3$ and $Y_7\, R_7^{(2)}$, heptagon functions satisfying the MHV final-entry condition automatically satisfy the Steinmann relations as well, at least at weight 6! We cannot rule out the possibility that the Steinmann constraint is also superfluous at weight 8 (or, perhaps, even higher), but certainly the complexity of the computation is significantly reduced if one allows oneself to input this knowledge.

4.4.4 Three Loops from Dihedral Symmetry

In this subsection we consider dropping the final entry condition, which derives from dual superconformal invariance. One motivation for doing this is to check independently the NMHV final entry conditions detailed in eq. (4.3.1). Another possible motivation, in the MHV case, is to try to widen the applicability of the bootstrap approach to the study of (bosonic) light-like Wilson loops in weakly-coupled conformal theories with less supersymmetry than $\mathcal{N} = 4$ SYM.

Let us consider adding general L-loop Steinmann heptagon symbols $\tilde{\mathcal{E}}_7^{(L)}$ (with no restrictions on the final entry) to the known answer $\mathcal{E}_7^{(L)}$ and see whether we can preserve the conditions of dihedral symmetry and good collinear behavior. We can ask this question through three loops, because we have a complete basis of Steinmann heptagon symbols up to (and beyond) weight six. Since such symbols appear additively in the BDS-normalized quantity $\mathcal{B}_7^{(L)}$, we need the Steinmann symbols $\tilde{\mathcal{E}}_7^{(L)}$ themselves to be well-defined in the collinear limit. The numbers of Steinmann heptagon symbols obeying the successive conditions of cyclic invariance, flip symmetry, and well-defined collinear behavior are detailed in table 4.4.

We find that the first dihedrally invariant Steinmann symbol with well-defined collinear limits appears at weight six, i.e. at three loops. We denote this symbol by $\tilde{\mathcal{E}}_7$. In fact the collinear limit of $\tilde{\mathcal{E}}_7$, which we denote by $\tilde{\mathcal{E}}_6$, automatically turns out to possess six-point dihedral invariance as well. Furthermore the collinear limit of $\tilde{\mathcal{E}}_6$ from six points to five is vanishing. Therefore the symbol $\tilde{\mathcal{E}}_7$ could be added to that for $\mathcal{E}_7^{(3)}$ (and simultaneously $\tilde{\mathcal{E}}_6$ to $\mathcal{E}_6^{(3)}$) without breaking dihedral symmetry or good collinear behavior either at seven points or at six points.

Neither $\tilde{\mathcal{E}}_7$ nor $\tilde{\mathcal{E}}_6$ obey the MHV final entry condition, as required to be consistent with the results of section 4.4.3. Thus at the three-loop order, $\bar{Q}$-supersymmetry is really fixing only a single parameter, after the consequences of the Steinmann relations, dihedral symmetry and good collinear behavior are taken into account. A different criterion that can be used to uniquely determine $\mathcal{E}_7^{(3)}$ is that the three-loop remainder $R_6^{(3)}$ should have at most a double discontinuity around the locus $u = 0$ where u is one of three the cross ratios available at six points. The double discontinuity is in fact predicted from the original implementation of the Wilson line OPE [36], which we will not delve into here. We may simply observe that $\tilde{\mathcal{E}}_6$ has a triple discontinuity and hence we can rule out adding $\tilde{\mathcal{E}}_7$ to $\mathcal{E}_7^{(3)}$ on these grounds.

Loop order $L =$	1	2	3
Steinmann symbols	28	322	3192
Cyclic invariance	4	46	456
Dihedral invariance	4	30	255
Well-defined collinear	0	0	1

Table 4.4: Number of linearly independent Steinmann heptagon symbols obeying, respectively: cyclic invariance, dihedral invariance, and well-defined collinear behavior together with dihedral symmetry.

We may similarly examine the consequences of dihedral symmetry and collinear behavior for the NMHV amplitude. In this case there are some additional conditions which we can impose, from requiring the absence of spurious poles. We recall the form of the NMHV ratio function given in eq. (4.1.15), or equivalently the form of E given in eq. (4.1.28). The tree-level amplitude $\mathcal{P}^{(0)}$ obviously possesses only physical poles, but the individual R-invariants have spurious poles. Requiring that the NMHV amplitude as a whole has no spurious poles leads us to the following conditions:

$$\text{Spurious I:} \quad E_{47}|_{\langle 1356\rangle=0} = 0\,, \tag{4.4.1}$$

$$\text{Spurious II:} \quad E_{23}|_{\langle 1467\rangle=0} = E_{25}|_{\langle 1467\rangle=0}\,. \tag{4.4.2}$$

In table 4.5 we detail the number of Steinmann symbols obeying the successive conditions of cyclic symmetry, absence of spurious poles, well-defined collinear behavior, and flip symmetry. At weight two, we find a single combination obeying all conditions, which is precisely the combination $B^{(1)}$ itself, which is therefore determined up to an overall scale by these conditions. Note that unlike the $B^{(L)}$ for $L > 1$, the function $B^{(1)}$ obeys the Steinmann relations.

At weight four, we find no Steinmann symbols obeying all the conditions. This is not in contradiction with the results of section 4.4.2: we recall that the quantity $E^{(2)}$ does not exhibit well-defined, finite collinear behavior; rather it is the (non-Steinmann) function $B^{(2)}$ which manifests this. The zero in the final row of the $L = 2$ column in table 4.5 rather reflects the fact that there is no Steinmann symbol which could be added to $E^{(2)}$ while preserving the good collinear behavior of $B^{(2)}$, even if we are willing to abandon the NMHV final entry condition.

At weight six, we find a single Steinmann symbol with all the properties listed in table 4.5. It is precisely the same symbol $\tilde{\mathcal{E}}_7$ appearing in table 4.4 multiplied by the tree-level amplitude $\mathcal{P}^{(0)}$. Hence it only appears as a potential contribution to $E_0^{(3)}$. In other words, the symbols of $E_{12}^{(3)}$ and $E_{14}^{(3)}$ are uniquely fixed by the constraints of dihedral symmetry, absence of spurious poles and correct collinear behavior. The appearance of the same ambiguity $\tilde{\mathcal{E}}_7$ in $E_0^{(3)}$ is to be expected since the only additional criterion imposed in table 4.5, that of spurious-pole cancellation, cannot constrain potential contributions to E_0. Finally, we note that the addition of $\tilde{\mathcal{E}}_7$ in $E_0^{(3)}$ is connected to its addition to $\mathcal{E}_7^{(3)}$ by the NMHV to MHV collinear limit which relates E_7 to $\mathcal{E}_6$. Thus dropping the final entry condition from $\bar{Q}$-supersymmetry allows only a single potential contribution at weight 6 in all of the heptagon and hexagon amplitudes.

Loop order $L =$	1	2	3
Steinmann symbols	15×28	15×322	15×3192
Cyclic invariant	$4 + (2 \times 28)$	$46 + (2 \times 322)$	$456 + (2 \times 3192)$
Spurious vanishing I	$4 + 1 + 28$	$46 + 19 + 322$	$456 + 208 + 3192$
Spurious vanishing II	$4 + 6$	$46 + 89$	$456 + 927$
Well-defined collinear	1	0	11
Flip invariant	1	0	1

Table 4.5: Number of Steinmann heptagon symbols entering the NMHV amplitude obeying respectively cyclic invariance, vanishing on spurious poles, well-defined collinear behavior and flip symmetry.

We conclude that, up to three loops, starting from an ansatz of Steinmann heptagon functions, all heptagon amplitudes and hence all hexagon amplitudes (by collinear limits) in planar $\mathcal{N} = 4$ SYM can be determined just by imposing dihedral symmetry and well-defined collinear limits, combined with the requirement of no triple discontinuity in $R_6^{(3)}$ and no spurious poles in the NMHV amplitudes. These results provide an independent check of the NMHV final entry conditions (4.3.1). It would be interesting to investigate whether the ambiguity functions $\tilde{\mathcal{E}}_7$ and $\tilde{\mathcal{E}}_6$ could play a role in the perturbative expansion of any weakly-coupled conformal theories with less supersymmetry than

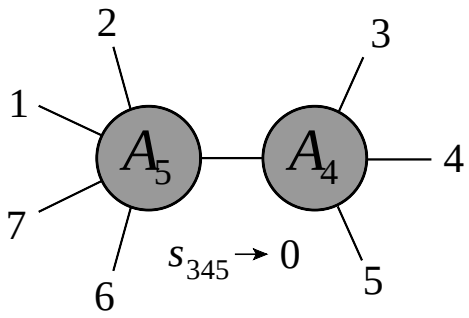

Figure 4.5.1: Factorization of a seven-point amplitude in the limit $s_{345} \to 0$. Notice that the collinear limit $p_7 \parallel p_1$ can be taken "inside" the factorization limit.

$\mathcal{N} = 4$ SYM.

4.5 The Multi-Particle Factorization Limit

One of the kinematic limits we can study using our explicit seven-point results is the multi-particle factorization limit. In this limit, one of the three-particle invariants goes on shell, $s_{i,i+1,i+2} \to 0$. Figure 4.5.1 shows the limit $s_{345} \to 0$. In this limit the seven-point NMHV amplitude factorizes at leading power into a product of four-point and five-point amplitudes, multiplied by the $1/s_{345}$ pole. The seven-point MHV amplitude vanishes at leading power. Indeed, all supersymmetric MHV amplitudes are required to vanish at leading power when a three-particle (or higher-particle) invariant goes on shell. This result holds because all possible helicity assignments for the intermediate state require at least one lower-point amplitude to have fewer than two negative-helicity gluons; such amplitudes vanish by supersymmetry Ward identities [132, 133]. For the same reason, MHV tree amplitudes [8] have no multi-particle poles.

Before turning to the behavior of the seven-point NMHV amplitude, we recall the multi-particle factorization behavior of the BDS-like-normalized six-point NMHV amplitude [60]. As $s_{345} \to 0$, two of the six-point R-invariants become much larger than the rest, and they become equal to each other. Therefore the singular behavior of the six-point amplitude is controlled by a single coefficient function, which we denote by $\mathcal{U}_6$ and whose limiting behavior takes an especially simple form.[6] Up to power-suppressed terms, the limit of $\mathcal{U}_6$ was found to be a polynomial in $\log(uw/v)$, whose coefficients are rational linear combinations of zeta values, and whose overall weight is $2L$. Here, u, v, and w are the three dual conformal invariant cross ratios for the hexagon, whose expressions in

[6]The function $\mathcal{U}_6$ can be identified with the function E in refs. [70, 5], but we prefer to adopt a different notation here to emphasize that this function is *not* the BDS-like-normalized NMHV superamplitude E_6.

terms of six-point kinematics are

$$u = \frac{x_{13}^2\, x_{46}^2}{x_{14}^2\, x_{36}^2} = \frac{s_{12}\, s_{45}}{s_{123}\, s_{345}}\,, \qquad v = \frac{x_{24}^2\, x_{51}^2}{x_{25}^2\, x_{41}^2} = \frac{s_{23}\, s_{56}}{s_{234}\, s_{123}}\,, \qquad w = \frac{x_{35}^2\, x_{62}^2}{x_{36}^2\, x_{52}^2} = \frac{s_{34}\, s_{61}}{s_{345}\, s_{234}}\,. \tag{4.5.1}$$

The six-point limit $s_{345} \to 0$ sends $uw/v \to \infty$.

The logarithm of $\mathcal{U}_6$, called U in ref. [60], has an even simpler behavior than $\mathcal{U}_6$. The L-loop contribution $U^{(L)}$ is also a polynomial in $\log(uw/v)$, but it has only degree L at L loops, for $L > 1$. This three-loop result was later found to hold also at four and five loops [70, 5]. Because $U^{(L)}$ has weight $2L$, but a maximum of L powers of $\log(uw/v)$ for $L > 1$, every term in it contains zeta values, and its symbol vanishes. The only exception is the one-loop result,

$$U^{(1)}(u,v,w) \xrightarrow{s_{345}\to 0} -\frac{1}{2}\log^2\left(\frac{uw}{v}\right) - 2\zeta_2\,, \tag{4.5.2}$$

where we have converted the result in ref. [60] to that for expansion parameter g^2. The results for $U^{(L)}$ agree with the perturbative expansion of an all-orders prediction based on the Pentagon OPE [134, 135].

Ref. [60] also made a prediction for the multi-particle factorization behavior of NMHV n-point amplitudes, which we can now test at 7 points at the symbol level. Define the factorization function F_n by

$$A_n^{\text{NMHV}}(k_i) \to A_{j-i+1}(k_i, k_{i+1}, \ldots, k_{j-1}, K)\frac{F_n(K^2, s_{l,l+1})}{K^2} A_{n-(j-i)+1}(-K, k_j, k_{j+1}, \ldots, k_{i-1})\,, \tag{4.5.3}$$

as $K^2 \to 0$, or in the seven-point case,

$$A_7^{\text{NMHV}}(k_i) \xrightarrow{s_{345}\to 0} A_5(k_6, k_7, k_1, k_2, K)\frac{F_7(K^2, s_{l,l+1})}{K^2} A_4(-K, k_3, k_4, k_5)\,, \tag{4.5.4}$$

where $K = k_3 + k_4 + k_5$, $K^2 = s_{345}$. Then F_7 was predicted to have the form

$$\begin{aligned}
[\log F_7]^{(L)}_{\text{symbol}} \;=\; \delta_{L,1}\Bigg\{ & \frac{1}{8\epsilon^2}\left[\left(\frac{(-s_{712})(-s_{34})}{(-s_{56})}\right)^{-\epsilon} + \left(\frac{(-s_{45})(-s_{671})}{(-s_{23})}\right)^{-\epsilon}\right] \\
& - \frac{1}{2}\log^2\left(\frac{(-s_{712})(-s_{34})}{(-s_{56})}\Big/\frac{(-s_{45})(-s_{671})}{(-s_{23})}\right) \\
& - \frac{1}{2}\log^2\left(\frac{x_{73}^2 x_{35}^2 x_{46}^2 x_{62}^2}{x_{57}^2 x_{24}^2 (x_{36}^2)^2}\right)\Bigg\}\,.
\end{aligned} \tag{4.5.5}$$

For simplicity, we have dropped all terms that vanish at symbol level, which kills all terms in $\log F_7$

beyond one loop, and we have converted to the g^2 expansion parameter.

We should now convert this prediction to one for the BDS-like normalized amplitude. Apart from trivial tree-level factors, we have

$$\log F_7 \;=\; \log\left(\frac{A_7^{\rm NMHV}}{A_5^{\rm BDS}\,A_4^{\rm BDS}}\right) \;=\; \log\left(\frac{A_7^{\rm NMHV}}{A_7^{\rm BDS-like}}\right) - \log\left(\frac{A_5^{\rm BDS}\,A_4^{\rm BDS}}{A_7^{\rm BDS-like}}\right). \tag{4.5.6}$$

So to obtain $\log(A_7^{\rm NMHV}/A_7^{\rm BDS-like})$ we need to add to $[\log F_7]^{(1)}$ the quantity

$$-\hat{M}_7^{(1)} + M_5^{(1)} + M_4^{(1)}\,, \tag{4.5.7}$$

where $\hat{M}_7$ is given in eq. (A.0.14), and $M_4^{(1)}$ and $M_5^{(1)}$ are the four- and five-point MHV amplitudes, for the kinematics shown in fig. 4.5.1, and normalized by their respective tree amplitudes.

Adding eqs. (4.5.6) and (4.5.7), we find, in terms of dual variables,

$$\log\left(\frac{A_7^{\rm NMHV}}{A_7^{\rm BDS-like}}\right)^{(1)} \to -\frac{1}{2}\log^2\left(\frac{x_{73}^2x_{35}^2x_{46}^2x_{62}^2}{x_{57}^2x_{24}^2(x_{36}^2)^2}\right) - \frac{1}{2}\log^2\left(\frac{x_{46}^2x_{72}^2x_{13}^2}{x_{73}^2x_{24}^2x_{61}^2}\right) - \frac{1}{2}\log^2\left(\frac{x_{35}^2x_{72}^2x_{61}^2}{x_{62}^2x_{57}^2x_{13}^2}\right), \tag{4.5.8}$$

at symbol level, and a vanishing contribution to the logarithm beyond one loop. Note that the first term in eq. (4.5.8) comes directly out of eq. (4.5.5), and is the "naive" generalization of $-\frac{1}{2}\log^2(uw/v)$ to the seven-point case. The first term diverges logarithmically as $s_{345} = x_{36}^2 \to 0$, while the last two terms are finite in this limit.

The one-loop factorization behavior in eq. (4.5.8) could have been extracted, of course, from the one-loop seven-point amplitude. Thus the symbol-level content of the prediction is really the vanishing of the logarithm beyond one loop. Beyond symbol level, the all-loop-order prediction of ref. [60] is that (up to an additive constant) the first term gets upgraded to the function appearing in the six-point limit, namely $U(x)$, where $x = (x_{73}^2x_{35}^2x_{46}^2x_{62}^2)/(x_{57}^2x_{24}^2(x_{36}^2)^2)$, while the last two terms should simply get multiplied by the cusp anomalous dimension.

Now let us test the symbol-level prediction (4.5.8) by taking the limit $s_{345} \to 0$ of the seven-point NMHV amplitude. Referring back to (4.2.1), we have

$$s_{345} = x_{36}^2 = \frac{\langle 2356\rangle}{\langle 23\rangle\langle 56\rangle} \to 0. \tag{4.5.9}$$

Keeping s_{23} and s_{56} generic requires us to take this limit by sending $\langle 2356\rangle \to 0$. This limit can be

accomplished using the replacement

$$\mathcal{Z}_2 \to \mathcal{Z}_3 + a\frac{\langle 1436\rangle}{\langle 1456\rangle}\mathcal{Z}_5 + b\frac{\langle 1453\rangle}{\langle 1456\rangle}\mathcal{Z}_6 + \epsilon\frac{\langle 3456\rangle}{\langle 1456\rangle}\mathcal{Z}_1 \tag{4.5.10}$$

where $a, b \in \mathbb{C}$ are generic and ϵ is a regulator. In the limit $\epsilon \to 0$, a_{14} vanishes while the other a_{ij} map into a space of 31 finite letters.

The map works out to be

$$\begin{aligned} a_{25} &\to \frac{a_{11}a_{17}}{a_{21}a_{24}}, \quad a_{33} \to \frac{a_{17}}{a_{24}}, \quad a_{34} \to \frac{a_{21}a_{24}}{a_{17}}, \quad a_{37} \to \frac{a_{11}a_{17}}{a_{21}} \quad a_{42} \to a_{24}, \\ a_{46} &\to \frac{a_{21}a_{24}}{a_{17}}, \quad a_{52} \to \frac{a_{17}}{a_{24}}, \quad a_{56} \to \frac{a_{11}a_{17}}{a_{21}a_{24}}, \quad a_{63} \to -1, \quad a_{65} \to -1, \end{aligned} \tag{4.5.11}$$

which removes 10 of the 42 letters, leaving a_{14} and the 31 finite letters.

We also need the limiting behavior of the seven-point R-invariants. Referring back to their definition (4.1.8), we see that the invariants (71), (14) and (47) become singular as $\langle 2356\rangle \to 0$ while all others remain finite. The finite R-invariants are suppressed in the identities (4.1.10) in this limit, giving us

$$(71)_{s_{345}\to 0} \;=\; (14)_{s_{345}\to 0} \;=\; (47)_{s_{345}\to 0}\,. \tag{4.5.12}$$

The function controlling the behavior of E_7 as $s_{345} \to 0$ is thus given by the sum of functions multiplying these singular invariants in eq. (4.1.28), corresponding to the combination

$$\mathcal{U}_7 \equiv \Big[E_{71} + E_{14} + E_{47} + E_0\Big]_{s_{345}\to 0}\,. \tag{4.5.13}$$

Note that from eq. (4.1.13), the coefficient of E_0 receives a $3/7$ contribution from (71), and $2/7+2/7$ from (14) and (47).

Ignoring the tree amplitude, the quantity $\mathcal{U}_7$ is the exponential of $\log(A_7^{\rm NMHV}/A_7^{\rm BDS-like})$, whose prediction is given in eq. (4.5.8). Using eq. (4.5.11) to compute $\mathcal{U}_7$ from eq. (4.5.13) in terms of the

letters a_{ij}, we find at one, two, and three loops,

$$\mathcal{U}_7^{(1)} = -\frac{1}{2}\log^2\left(\frac{a_{14}^2}{a_{11}a_{17}}\right) - \frac{1}{2}\log^2 a_{11} - \frac{1}{2}\log^2 a_{17}\,, \tag{4.5.14}$$

$$\mathcal{U}_7^{(2)} = \frac{\left(\mathcal{U}_7^{(1)}\right)^2}{2!}\,, \tag{4.5.15}$$

$$\mathcal{U}_7^{(3)} = \frac{\left(\mathcal{U}_7^{(1)}\right)^3}{3!}\,. \tag{4.5.16}$$

Hence $\mathcal{U}_7$ exponentiates at symbol level, as predicted by eq. (4.5.8). Substituting eq. (4.2.5) for a_{11}, and its cyclic permutations, into eq. (4.5.14), we find perfect agreement with eq. (4.5.8). We can also express the result in terms of the cross ratios u_i:

$$\mathcal{U}_7^{(1)} = -\frac{1}{2}\log^2\left(\frac{u_1u_2}{u_3u_7}\right) - \frac{1}{2}\log^2\left(\frac{u_1u_4u_5}{u_3u_6}\right) - \frac{1}{2}\log^2\left(\frac{u_2u_6u_5}{u_7u_4}\right). \tag{4.5.17}$$

Once this analysis is repeated at function level, we expect the first term in $\mathcal{U}_7^{(1)}$ to receive higher-loop zeta-valued contributions, dictated by the six-point function $U(x)$, while the last two terms simply get multiplied by the cusp anomalous dimension.

The last two terms in eq. (4.5.14) or eq. (4.5.17) do not diverge in the factorization limit. On the other hand, they play an essential role in endowing $\mathcal{U}_7$ with the correct behavior as p_7 and p_1 become collinear. Fig. 4.5.1 shows that this collinear limit is well away from the factorization pole, in the sense of color ordering. So it should be possible to take this collinear limit "inside" the $s_{345} \to 0$ multi-particle factorization limit, i.e. as a further limit of it.

The $p_7 \parallel p_1$ collinear limit takes $x_{72}^2 \to 0$, and hence the cross ratio $u_5 \to 0$. Equation (4.5.17) shows that the last two terms of $\mathcal{U}_7^{(1)}$ diverge logarithmically in this collinear limit, while the first term behaves smoothly. Recall that the n-point BDS ansatz smoothly tends to the $(n-1)$-point BDS ansatz in all collinear limits. However, this is not true for the BDS-like ansatz; that is, $Y_7 \not\to Y_6$ in collinear limits, rather it diverges logarithmically. Essentially, the last two terms of eq. (4.5.14) account for this non-smooth behavior. In the $p_7 \parallel p_1$ collinear limit,

$$-\frac{1}{2}\log^2\left(\frac{a_{14}^2}{a_{11}a_{17}}\right) \xrightarrow{p_7\parallel p_1} -\frac{1}{2}\log^2\left(\frac{uw}{v}\right), \tag{4.5.18}$$

$$-\frac{1}{2}\log^2 a_{11} - \frac{1}{2}\log^2 a_{17} + Y_7 \xrightarrow{p_7\parallel p_1} Y_6\,. \tag{4.5.19}$$

Thus the last two terms in eq. (4.5.14) precisely account for the non-smooth collinear behavior of the BDS-like-normalized amplitude at seven points, within the multi-particle factorization limit.

4.6 Discussion

Following the inclusion of the Steinmann relations in the hexagon function bootstrap program [5], we have applied these constraints to heptagon symbols, in order to drastically reduce the number of symbols needed to bootstrap seven-point scattering amplitudes. We have been able to construct a basis of Steinmann heptagon symbols through weight 7, and those which further satisfy the MHV final-entry condition at weight 8. In order to apply the Steinmann relations transparently, we have shifted our focus from the familiar BDS-normalized amplitudes to BDS-like normalized analogues. The simple conversions (4.1.30) and (4.1.31) between functions in these two normalizations allow us to simultaneously take advantage of the smaller space of Steinmann heptagon symbols, and utilize the simple behavior exhibited by BDS-normalized functions near the collinear limit. With these advances, we have completely determined, in a conceptually simple manner, the symbols of the seven-point three-loop NMHV and four-loop MHV amplitudes in planar $\mathcal{N} = 4$ SYM theory.

Calculating the symbol of these particular component amplitudes is only the tip of the Steinmann iceberg. The main limiting factor in applying the bootstrap at higher weight is the computational complexity resulting from the size of the space of Steinmann heptagon functions, which still grows close to exponentially, despite its small size relative to the general heptagon function space. This growth can be especially prohibitive when generating the general basis of Steinmann heptagon symbols at each higher weight. At the same time, nearly the entire space of Steinmann heptagon symbols is needed to describe the amplitudes we have bootstrapped – including derivatives (coproducts) of higher-loop amplitudes. That is, the full space of Steinmann heptagon symbols is spanned by the derivatives of our amplitudes at weights 2 and 3. Only 15 of the 322 Steinmann heptagon symbols are absent from the span of these derivatives at weight 4. This situation resembles what is observed in the hexagon function bootstrap [5], where the derivatives of the five-loop six-point amplitude also span the full weight-2 and weight-3 Steinmann hexagon symbol spaces, while only 3, 12, and 30 symbols are absent from the span of these derivatives at weights 4, 5, and 6. In the hexagon case, all of these symbols are observed to drop out due to lower-weight restrictions on the appearance of zeta values (i.e. the zeta values only appear in certain linear combinations with other hexagon functions, and this leads to symbol-level restrictions at higher weights). We expect that a similar set of function-level restrictions will explain why a small set of weight-4 Steinmann heptagon symbols are not needed to describe the seven-point amplitude. (Only 386 of the 1030 weight-5 Steinmann heptagon symbols are currently needed to describe the four-loop MHV and three-loop NMHV amplitudes, but here we expect significantly more of these symbols to be needed to describe coproducts

of yet higher-loop contributions.) No physical explanation for the restrictions on the occurrence of zeta values at six points has yet been discerned, indicating that there remains some physics to be discovered.

More generally, the task of upgrading our symbol-level results to full functions will be left to future work. A full functional representation would be valuable for checking seven-point predictions in both the near-collinear [75, 76, 77, 78, 79, 80, 81, 82] and multi-Regge limits [68, 93, 94, 96, 97, 98, 95, 99, 100, 101, 102, 103]. An important problem is to generalize the all-loop results for six-point scattering in the multi-Regge limit [136] to the seven-point case. The full functional form of the seven-point amplitude could assist the construction of an all-loop multi-Regge heptagon formula.

Bootstrapping amplitudes with eight or more external legs will require more than a simple extension of the heptagon bootstrap presented in this work. Both the hexagon and heptagon bootstrap approaches depend on the assumption that the weight-$2L$ generalized polylogarithms can be built from a finite symbol alphabet, corresponding to an appropriate set of cluster $\mathcal{A}$-coordinates. Going to $n = 8$, we move into a cluster algebra with infinitely many $\mathcal{A}$-coordinates. It is expected that only a finite number of letters will appear at any finite loop order, but it is currently unknown how to characterize what sets may appear. In principle, this information ought to follow from a careful consideration of the Landau singularities of these amplitudes (see for example refs. [137, 88] for recent related work). There is hope that patterns may emerge at currently accessible loop orders, which may provide insight into the letters appearing for $n > 7$.

Chapter 5

Cluster Algebra Structure Scattering Amplitudes

Several recent papers following [32] have explored the connection between (multi-loop) scattering amplitudes in planar $\mathcal{N} = 4$ super-Yang-Mills (SYM) theory and cluster algebras, a subject of great interest to mathematicians. This line of research has two closely related branches: (1) investigating purely mathematical questions having to do with the classification of functions with certain cluster algebraic properties, i.e. "how rare are special functions of the type we see in SYM theory?", and (2) exploiting these mathematical properties, together with physical input as needed, to carry out calculations of new, previously intractable amplitudes, i.e. "how far can we get by exploiting the special properties of cluster algebras?".

The most basic aspect of the observed connection, supported by all evidence available to date, is that n-point scattering amplitudes in SYM theory have singularities only at points in $\mathrm{Conf}_n(\mathbb{P}^3)$ (the space of massless n-point kinematics modulo dual conformal invariance) where some cluster coordinate of the associated $\mathrm{Gr}(4, n)$ cluster algebra vanishes. More specifically, all known multi-loop amplitudes may be expressed as linear combinations of generalized polylogarithm functions written in the symbol alphabet consisting of such cluster coordinates. We expect this to be true to all loop order for all MHV and NMHV amplitudes.

Deeper connections to the underlying cluster algebra have been found for the two-loop MHV remainder functions $R_n^{(2)}$. The algebra of generalized polylogarithm functions modulo products admits a cobracket δ satisfying $\delta^2 = 0$, giving it the structure of a Lie coalgebra [123]. It has been observed that $\delta R_n^{(2)}$ has a very rigid connection to the Poisson structure on the kinematic domain

$\mathrm{Conf}_n(\mathbb{P}^3)$. Specifically, the $(2,2)$ component of $\delta R_n^{(2)}$ can always be written as a linear combination of $\mathrm{Li}_2(-x_i) \wedge \mathrm{Li}_2(-x_j)$ for pairs of cluster coordinates having Poisson bracket $\{\log x_i, \log x_j\} = 0$, while the $(3,1)$ component can always be written as a linear combination of $\mathrm{Li}_3(-x_i) \wedge \log(x_j)$ for pairs having $\{\log x_i, \log x_j\} = \pm 1$. These mathematical properties are tightly constraining: it has been argued in [47] that, when combined with a few physical constraints, they uniquely determine the $(2,2)$ component of $\delta R_n^{(2)}$ for all n.

It is an interesting open problem to determine whether (and, if so, precisely how) the structure of more general amplitudes may be dictated by the underlying Poisson structure on $\mathrm{Conf}_n(\mathbb{P}^3)$. This is a difficult question to address because data on multi-loop amplitudes is very hard to come by—beyond the two-loop MHV amplitudes, explicit results for complete amplitudes at fixed loop order are available only for $n = 6$ [48, 49, 50, 51, 62, 60, 70] (in addition, the symbol of the two-loop $n = 7$ NMHV amplitude has been computed in [89], and that of the three-loop $n = 7$ MHV amplitude in [61]). With only a handful of results available it may be difficult to identify a pattern which might let one tease out the underlying structure. Moreover, accidental simplifications may occur at small n which can obscure the general structure. (For example, the $(2,2)$ component of $\delta R_6^{(2)}$ is identically zero [35].) It is known that the $(3,3)$ component of $\delta R_6^{(3)}$ is not expressible in terms of cluster $\mathcal{X}$-coordinates [138], but there could be some more deeply hidden structure in this amplitude.

The primary goal of this chapter is to further explore the taxonomy of two-loop cluster functions, as defined in [46], for $n = 6, 7$. We are particularly interested in the interplay between various mathematically natural but physically obscure conditions that certain functions can satisfy (such as the tight cluster constraints satisfied by all two-loop MHV amplitudes, mentioned above) and physically natural constraints, such as the requirement that amplitudes can only have physical branch points on the principal sheet (the so-called "first-entry condition" [36]). In previous work including [47] it has been remarked that the mathematical and physical constraints on MHV amplitudes seem almost orthogonal. One of our goals here is to explore this question quantitatively by fully classifying the dimensions of function spaces satisfying various properties.

We begin in Section 2 with a lightning review to set some notation and terminology. In Sections 3 and 4 respectively we exhaustively analyze the spaces of cluster functions on the $\mathrm{Gr}(4,6)$ and $\mathrm{Gr}(4,7)$ cluster algebras respectively of relevance to $n = 6, 7$-point amplitudes in planar SYM theory.

5.1 Review and Notation

A kinematic configuration of n massless on-shell particles, with a cyclic order (which comes naturally in gauge theories when one looks at planar scattering amplitudes), can be parameterized in terms of n momentum twistors [24], $Z_i \in \mathbb{P}^3$, $i = 1, \ldots, n$. The dual conformal symmetry of planar n-point amplitudes in SYM theory further implies that that they are functions not on $(\mathbb{P}^3)^n$ but on the smaller space $\mathrm{Conf}_n(\mathbb{P}^3) \cong \mathrm{Gr}(4,n)/(\mathbb{C}^*)^{n-1}$ [32].

Viewing each Z_i as a four-component vector of homogeneous coordinates, the Plücker coordinates are defined by $\langle ijkl\rangle \equiv \det(Z_i Z_j Z_k Z_l)$. Functions on $\mathrm{Conf}_n(\mathbb{P}^3)$ may be written in terms of ratios of Plücker coordinates such as

$$\frac{\langle ijkl\rangle\langle abcd\rangle}{\langle ijcd\rangle\langle abkl\rangle}\,, \tag{5.1.1}$$

or more generally in terms of ratios of homogeneous polynomials in Plücker coordinates having total weight zero under rescaling any of the Z_i.

Such objects form the building blocks for the $\mathrm{Gr}(4,n)$ Grassmannian cluster algebra [72, 139], which is the algebra generated by certain preferred sets of coordinates on $\mathrm{Gr}(4,n)$. These coordinates come in two related varieties: the $\mathcal{A}$-coordinates, which consist of the Plücker coordinates and certain homogeneous polynomials in them, and the $\mathcal{X}$-coordinates [71], which consist of certain scale-invariant ratios of $\mathcal{A}$-coordinates.

In this chapter we focus on the cases $n = 6, 7$, for which the corresponding cluster algebras have respectively 15, 49 $\mathcal{A}$-coordinates and 15, 385 $\mathcal{X}$-coordinates[1]. The reader may find these coordinates tabulated in [32]. Of course, the $\mathcal{X}$-coordinates are not algebraically independent since the dimension of $\mathrm{Conf}_n(\mathbb{P}^3)$ is only $3(n-5)$. A "cluster" is a particular choice of $3(n-5)$ cluster $\mathcal{X}$-coordinates in terms of which all others may be determined by a simple set of rational transformations called mutations.

A still mysterious but apparently important role is played by the fact that $\mathrm{Conf}_n(\mathbb{P}^3)$ admits a natural Poisson structure, which it inherits from the Grassmannian [72]. A characteristic feature of cluster coordinates is that within each cluster, the $\mathcal{X}$-coordinates are log-canonical with respect to this Poisson structure, i.e.

$$\{\log x_i, \log x_j\} = B_{ij}\,, \qquad i,j = 1, \ldots, 3(n-5)\,, \tag{5.1.2}$$

where B is an antisymmetric integer-valued matrix (which for $n = 6, 7$ only takes the values $0, \pm 1$).

[1] In some applications it is sensible to count x and $1/x$ separately, in which case these numbers would be 30, 770.

We expect all six- and seven-point L-loop scattering amplitudes in planar SYM theory to be (generalized) polylogarithm functions of uniform transcendental weight $2L$ whose symbols may be written in terms of the $\mathrm{Gr}(4,n)$ cluster coordinates. For the purpose of writing a symbol alphabet the relevant question is not how many coordinates are algebraically independent, but how many are multiplicatively independent—we say that a finite collection $\{y_1,\ldots,y_m\}$ is multiplicatively independent if there is no collection of integers $\{n_1,\ldots,n_m\}$ such that $\prod y_i^{n_i}=1$, i.e. if the collection $\{\log y_1,\ldots,\log y_m\}$ is linearly independent over $\mathbb{Z}$.

As mentioned above there are respectively 15 (385) cluster $\mathcal{X}$-coordinates x_i for $n=6$ ($n=7$), but the corresponding sets of $\log x_i$ only span spaces of dimension 9 (42). Choosing bases for these spaces provides a collection of 9 (42) multiplicatively independent ratios to serve as symbol alphabets for building cluster polylogarithm functions.

5.1.1 The $\mathrm{Gr}(4,6)$ Cluster Algebra

For six-point amplitudes the relevant cluster algebra is $\mathrm{Gr}(4,6)$, which is isomorphic to the A_3 cluster algebra. Its 15 cluster $\mathcal{A}$-coordinates are just the Plücker coordinates $\langle ijkl\rangle$. This algebra has 15 $\mathcal{X}$-coordinates. In the notation of [46] these are named $v_i, x_i^{\pm}$ for $i=1,2,3$ and e_i for $i=1,\ldots,6$.

The reader may find explicit formulas for these as ratios of Plücker coordinates in [46]. Since one of the goals of this chapter is to make contact with the work of Dixon et. al. we will instead provide this information via the connection to the variables u,v,w,y_u,y_v,y_w used in [48, 49, 50, 51, 62, 60, 70].

The three-dimensional kinematic configuration space $\mathrm{Conf}_6(\mathbb{P}^3)$ may be parameterized in terms of the three coordinates

$$y_u=\frac{\langle 1236\rangle\langle 1345\rangle\langle 2456\rangle}{\langle 1235\rangle\langle 1246\rangle\langle 3456\rangle}\,,\quad y_v=\frac{\langle 1235\rangle\langle 1456\rangle\langle 2346\rangle}{\langle 1234\rangle\langle 1356\rangle\langle 2456\rangle}\,,\quad y_w=\frac{\langle 1246\rangle\langle 1356\rangle\langle 2345\rangle}{\langle 1256\rangle\langle 1345\rangle\langle 2346\rangle}\,. \tag{5.1.3}$$

Note that a cyclic rotation $Z_i\to Z_{i+1}$ maps

$$y_u\to 1/y_v\,,\qquad y_v\to 1/y_w\,,\qquad y_w\to 1/y_u\,, \tag{5.1.4}$$

while reflection $Z_i\to Z_{1-i}$ (all indices are understood to be cyclic modulo 6) takes

$$y_u\to y_v\,,\qquad y_v\to y_u\,,\qquad y_w\to y_w\,. \tag{5.1.5}$$

The spacetime parity operator acts on momentum twistors as[2]

$$Z_i \to W_i = *(Z_{i-1} \wedge Z_i \wedge Z_{i+1})\,, \tag{5.1.6}$$

which transforms the cross-ratios defined in (5.1.3) according to

$$y_u \to 1/y_u\,, \qquad y_v \to 1/y_v\,, \qquad y_w \to 1/y_w\,. \tag{5.1.7}$$

It is a curious accident that for $n = 6$ spacetime parity reversal is equivalent on $\mathrm{Conf}_n(\mathbb{P}^3)$ to an element (namely, shift-by-three) of the cyclic group.

Three other variables used by Dixon et. al. may be defined in terms of these via

$$u = \frac{y_u(1-y_v)(1-y_w)}{(1-y_uy_v)(1-y_uy_w)}\,, \quad v = \frac{y_v(1-y_u)(1-y_w)}{(1-y_uy_v)(1-y_vy_w)}\,, \quad w = \frac{y_w(1-y_u)(1-y_v)}{(1-y_uy_w)(1-y_vy_w)}\,. \tag{5.1.8}$$

Central to our investigations is the Poisson structure on $\mathrm{Conf}_6(\mathbb{P}^3)$, which may be expressed in terms of the y variables as

$$\{\log y_u, \log y_v\} = \{\log y_v, \log y_w\} = \{\log y_w, \log y_u\} = \frac{(1-y_u)(1-y_v)(1-y_w)}{1-y_uy_vy_w}. \tag{5.1.9}$$

It is invariant under the full cyclic group (and hence, it is parity symmetric) but antisymmetric under reflection.

In terms of these variables, the cluster $\mathcal{X}$-coordinates may be expressed as

$$\begin{aligned}
v_1 &= \frac{1-v}{v}\,, & v_2 &= \frac{1-w}{w}\,, & v_3 &= \frac{1-u}{u}\,,\\
x_1^+ &= \frac{y_v(1-y_uy_w)}{1-y_v}\,, & x_2^+ &= \frac{y_w(1-y_uy_v)}{1-y_w}\,, & x_3^+ &= \frac{y_u(1-y_vy_w)}{1-y_u}\,,\\
x_1^- &= \frac{1-y_uy_w}{y_uy_w(1-y_v)}\,, & x_2^- &= \frac{1-y_uy_v}{y_uy_v(1-y_w)}\,, & x_3^- &= \frac{1-y_vy_w}{y_vy_w(1-y_u)}\,,\\
e_1 &= \frac{1-y_v}{y_v(1-y_u)}\,, & e_2 &= \frac{y_v(1-y_w)}{1-y_v}\,, & e_3 &= \frac{1-y_u}{y_u(1-y_w)}\,,\\
e_4 &= \frac{y_u(1-y_v)}{1-y_u}\,, & e_5 &= \frac{1-y_w}{y_w(1-y_v)}\,, & e_6 &= \frac{y_w(1-y_u)}{1-y_w}\,.
\end{aligned} \tag{5.1.10}$$

Note that under a cyclic shift $Z_i \to Z_{i+1}$ we have

$$v_i \to v_{i+1}\,, \qquad x_i^\pm \to x_{i+1}^\mp\,, \qquad e_i \to e_{i+1}\,, \tag{5.1.11}$$

[2]The notation means that W_i spans the one-dimensional subspace orthogonal to the 3-plane spanned by Z_{i-1}, Z_i, Z_{i+1} in $\mathbb{C}^4$.

while under parity the v_i are invariant and

$$x_i^{\pm} \to x_i^{\mp}\,, \qquad e_i \to e_{i+3}\,. \tag{5.1.12}$$

Of particular importance are pairs x_1, x_2 of distinct $\mathcal{X}$-coordinates with simple Poisson brackets. By "simple" we mean specifically that $\{\log x_1, \log x_2\}$ is either 0 or ± 1. There are three pairs with Poisson bracket zero,

$$\{\log x_i^+, \log x_i^-\} = 0\,, \tag{5.1.13}$$

and 30 pairs with Poisson bracket $+1$,

$$\{\log e_i, \log e_{i+4}\} = \{\log x_{i+1}^{\pm}, \log v_i\} = \{\log v_{i+1}, \log x_i^{\pm}\} = \{\log x_{i+1}^{\pm}, \log e_i\} = 1 \tag{5.1.14}$$

together with their cyclic images, for $6 + 6 + 6 + 12 = 30$ pairs. The remaining 72 pairs have "complicated" Poisson brackets (specifically, non-integer-valued; see for example (5.1.9)).

5.1.2 The $\mathrm{Gr}(4,7)$ Cluster Algebra

For seven-point amplitudes the relevant cluster is algebra is $\mathrm{Gr}(4,7)$, which is isomorphic to the E_6 algebra. The 49 cluster $\mathcal{A}$-coordinates consist of the 35 Plücker coordinates $\langle ijkl\rangle$ together with 14 homogeneous polynomials denoted by $\langle 1(23)(45)(67)\rangle$, $\langle 2(13)(45)(67)\rangle$ (and their cyclic images), where

$$\langle i(i{-}1,i{+}1)(j,j{+}1)(k,k{+}1)\rangle = \langle i{-}1\, i\, j\, j{+}1\rangle\langle i\, i{+}1\, k\, k{+}1\rangle - \langle i{-}1\, i\; k\, k{+}1\rangle\langle i\, i{+}1\, j\, j{+}1\rangle\,. \tag{5.1.15}$$

One can build from these 49 $\mathcal{A}$-coordinates a total of 385 cluster $\mathcal{X}$-coordinates (or 770 if we count their multiplicative inverses). These are tabulated on pages 40–41 of [32]. Out of $\frac{1}{2}\cdot 385\cdot 384 = 73920$ pairs of $\mathcal{X}$-coordinates, 2520 have Poisson bracket ± 1 while 833 have Poisson bracket zero.

5.1.3 The Cobracket and Bloch Groups

We recall that the algebra $\mathcal{A}$ of generalized polylogarithm functions admits a coproduct giving it the structure of a Hopf algebra [123]. When we work with the quotient space $\mathcal{L}$ of polylogarithm functions modulo products of functions of lower weight, the coproduct descends onto the quotient space to a cobracket δ which satisfies $\delta^2 = 0$. We review here only the barest essentials, and refer the reader to [32, 46] for additional details.

The cobracket of a weight-4 function has two components,

$$\delta \mathcal{L}_4 \in (B_3 \otimes \mathbb{C}^*) \oplus (B_2 \wedge B_2)\,, \tag{5.1.16}$$

where the Bloch group B_k is, for our purposes, the free abelian group generated by functions of the form $\{x\}_k \equiv -\mathrm{Li}_k(-x)$, where Li_k is the classical polylogarithm function and x is a function on $\mathrm{Conf}_n(\mathbb{P}^3)$ which is rational in Plücker coordinates.

The fact that $\delta^2 = 0$ and that δ has trivial cohomology means that if $a \in B_3 \otimes \mathbb{C}^*$ and $b \in B_2 \wedge B_2$, then there exists a function f whose cobracket components are $a \oplus b$ if and only if $\delta_{31}(a) + \delta_{22}(b) = 0$. As explained in [46], this condition can be used to explicitly enumerate cluster functions, at least on algebras of finite type. For such algebras $B_3 \otimes \mathbb{C}^*$ and $B_2 \wedge B_2$ are finite dimensional vector spaces on which δ acts linearly, so the space of cluster $\mathcal{A}$-functions is simply the kernel of δ.

At weight 4 a general polylogarithm can be expressed in terms of the classical functions Li_k if and only if its $B_2 \wedge B_2$ cobracket component vanishes. We will often be interested in counting the number of non-classical functions, since the classical ones (which correspond to solutions of $\delta_{31}(a) = 0$) are trivial to enumerate. To answer this question we compute the dimension of the subspace of $B_2 \wedge B_2$ such that the equation $\delta_{31}(a) + \delta_{22}(b) = 0$ is solvable for some $a \in B_3 \otimes \mathbb{C}^*$.

One final piece of terminology concerns the interplay between the Poisson structure on the Grassmannian cluster algebras and the cobracket of polylogarithm functions. We recall that two cluster $\mathcal{X}$-coordinates x, y have $\{\log x, \log y\} \in \mathbb{Z}$ only if there exists a cluster containing either x or $1/x$, and either y or $1/y$. As reviewed in [32], the combinatorics of mutations is encoded in a graph called the (generalized) Stasheff polytope associated to the algebra. We therefore say that a function has "Stasheff local" $B_2 \wedge B_2$ if it can be expressed as a linear combination of terms of the form $\{x\}_2 \wedge \{y\}_2$ for pairs having integer Poisson bracket (for $\mathrm{Gr}(4,6)$ and $\mathrm{Gr}(4,7)$, this integer will always be in the set $\{-1, 0, +1\}$).

5.2 The Cluster Structure of Hexagon Functions at Weight 4

5.2.1 Setup

In this section we consider cluster functions on the $A_3 \cong \mathrm{Gr}(4,6)$ cluster algebra. The term "cluster $\mathcal{A}$-function" introduced in [46] refers, in the present application, to an integrable symbol written in the 9-letter alphabet of cluster coordinates (specifically, this means any multiplicatively independent set of $\mathcal{X}$-coordinates; or equivalently, homogeneous ratios of $\mathcal{A}$-coordinates) on $\mathrm{Gr}(4,6)$.

Any linear combination of cluster $\mathcal{A}$-functions with the property that only the three variables u, v, w appear in the first-entry of the symbol, reflecting the physically allowed branch points for a scattering amplitude [36], is called a "physical function" or, following the terminology of [50], a "hexagon function". These have been studied through high weight in the series of papers [48, 49, 50, 51, 62, 60, 70], but we restrict our analysis to weight 4 as our aim is to explore connections between the cobrackets and the cluster Poisson structure of these functions.

Let $\mathcal{A}_k$ denote the vector space of all weight-k cluster $\mathcal{A}$-functions. Such functions are easy to count for any A_m type cluster algebra (see [124, 140]); for A_3 we have the generating function

$$f_{A_3}(t) = 1 + \sum_{k=1}^{\infty} t^k \dim(\mathcal{A}_k) = \frac{1}{1-2t}\frac{1}{1-3t}\frac{1}{1-4t}\,, \tag{5.2.1}$$

so that

$$\dim(\mathcal{A}_k) = 9, 55, 285, 1351, \ldots \qquad k = 1, 2, 3, 4, \ldots\,. \tag{5.2.2}$$

Let $\mathcal{L}_k$ denote the quotient of $\mathcal{A}_k$ by products of functions of lower weight. The number of such functions can be computed by taking the plethystic logarithm of the generating function $f_{A_3}(t)$ (see for example [141]), which gives

$$\dim(\mathcal{L}_k) = 9, 10, 30, 81, \ldots \qquad k = 1, 2, 3, 4, \ldots\,. \tag{5.2.3}$$

Finally we denote by B_k the subspace of $\mathcal{L}_k$ generated by the classical polylogarithms (we do not yet restrict their arguments to be cluster $\mathcal{X}$-coordinates). We have

$$\dim(\mathcal{B}_k) = 10, 30, 45, \ldots \qquad k = 2, 3, 4, \ldots\,. \tag{5.2.4}$$

For $k < 4$ the agreement with (5.2.3) reflects the fact that all such generalized polylogarithms can be expressed in terms of the classical functions; for higher k these numbers can be obtained by choosing a basis for $\mathcal{L}_k$ and computing $\dim\ker\delta$ as described in the previous section.

5.2.2 The Non-Classical Functions

Beginning at $k = 4$ we can distinguish between classical and non-classical functions. At weight $k = 4$, the "non-classicalness" of a function is completely characterized by its $B_2 \wedge B_2$ cobracket component (see for example [32]). Since B_2 has dimension 10 according to (5.2.4), $B_2 \wedge B_2$ evidently has dimension 45. However, a random element of this vector space is not guaranteed to be the $B_2 \wedge B_2$

cobracket component of any cluster $\mathcal{A}$-function—there is a nontrivial integrability constraint.

In fact, by comparing (5.2.4) to (5.2.3) we see that there are 81 functions in all, minus 45 classical functions, for a total of 36 non-classical functions. We conclude that in the 45-dimensional space $B_2 \wedge B_2$ spanned by objects of the form $\{x\}_2 \wedge \{y\}_2$, for cluster coordinates x and y, only the linear combinations lying in a particular 36-dimensional subspace correspond to cobracket components of actual cluster $\mathcal{A}$-functions.[3] We will shortly characterize this 36-dimensional space completely.

Let us write PB_0 to denote the subspace of $B_2 \wedge B_2$ spanned by objects of the form $\{x\}_2 \wedge \{y\}_2$ for pairs having Poisson bracket $\{\log x, \log y\} = 0$. In what follows we will for example say that a function "lives in PB_0" if its $B_2 \wedge B_2$ cobracket component can be expressed in terms of such pairs. Similarly, let PB_1 be the subspace spanned by pairs having Poisson bracket 1, and let us also use the shorthand $PB_* = B_2 \wedge B_2$, meaning that the Poisson bracket can be anything. We found in (5.1.13) and (5.1.14) that there are respectively 3, 30 pairs with Poisson bracket 0, 1. It is simple to check that the corresponding elements are linearly independent in $B_2 \wedge B_2$, so we have that $\dim PB_0 = 3$ and $\dim PB_1 = 30$, while of course $\dim PB_* = \dim B_2 \wedge B_2 = 45$.

With this notation in hand let us now summarize our findings on the 36 non-classical cluster $\mathcal{A}$-functions at weight four, which we find fall into two broad groups:

(A) 6 of these functions are the "A_2 cluster functions" introduced in [46]. There is one such function for each A_2 subalgebra of A_3; these subalgebras and the associated functions are represented visually in equation (4.3) of that paper. These six functions have additional "cluster structure": their $B_3 \otimes \mathbb{C}^*$ cobracket components can be expressed entirely in terms of cluster $\mathcal{X}$-coordinates—this means that they are "cluster $\mathcal{X}$-functions" in the terminology of [46]. General elements of this six-dimensional space are not Stasheff local—their $B_2 \wedge B_2$ cobracket components are not expressible in terms of pairs of coordinates with Poisson bracket $0, \pm 1$. Only one particular linear combination of these 6—the one called the A_3 function in [46]—has a nice $B_2 \wedge B_2$, in fact lying inside PB_0. The $B_2 \wedge B_2$ cobracket component of this A_3 function is

$$\sum_{i=1}^{3} \{x_i^+\}_2 \wedge \{x_i^-\}_2 \,. \tag{5.2.5}$$

This quantity is parity-odd so it cannot possibly appear in the two-loop six-point MHV remainder function, which is parity-even. This "explains" why the hypothesis that two-loop MHV remainder functions must live in PB_0, which we know to be true for all n [47], implies that the case $n = 6$

[3] Linear combinations which fall outside this 36-dimensional subspace are certainly integrable [142], but they integrate to functions with symbols involving letters which are not cluster coordinates, for example differences of $\mathcal{X}$-coordinates $x_i - x_j$, which does not in general factor into a product of cluster coordinates. Hence they are not cluster $\mathcal{A}$-functions.

must be classical.

(B) The remaining 30 functions are sort of the opposite: no linear combination of these 30 has a $B_3 \otimes \mathbb{C}^*$ content which can be expressed entirely in terms of $\mathcal{X}$-coordinates, so none of them are cluster $\mathcal{X}$-functions. On the other hand, all of them are Stasheff local—they all have "nice" $B_2 \wedge B_2$, in fact they span exactly the 30-dimensional subspace $PB_1 \subset B_2 \wedge B_2$.

5.2.3 The Physical (Hexagon) Functions

Dixon et. al. find that there are precisely 15 functions at weight 4 (modulo products of functions of lower weight) satisfying the first-entry condition, which they call hexagon functions. Let us put aside 9 which are purely classical and focus on the two types of functions named Ω_2 and F_1 in [50].

(A) The function F_1 is parity-odd and comes in three cyclic permutations (i.e., $i \to i{+}2$ and $i \to i{+}4$). These functions are rather interesting; each of them has a $B_2 \wedge B_2$ coproduct component given by (5.2.5) plus additional terms which cannot be expressed in terms of pairs having simple Poisson bracket. Since (5.2.5) is invariant under $i \to i{+}2$, we can throw out these terms by taking the difference between any two pairs of the three permutations of F_1. Indeed such linear combinations have appeared in the literature, as in (B.18) and (B.20) of [50] which define the function $\widetilde{V}$ by

$$8\widetilde{V} = -F_1(u,v,w) + F_1(w,u,v) + \text{products of lower-weight functions.} \tag{5.2.6}$$

Hence only two of the three distinct cyclic permutations of $\widetilde{V}$ are linearly independent.

(B) Next we look at the parity-even function Ω_2 which also comes in three cyclic permutations. At the level of $B_2 \wedge B_2$, where we can ignore all terms involving only classical polylogarithms, the function Ω_2 is equivalent (modulo an overall multiplicative factor) to the function called V by Dixon et. al.; see for example (7.1) through (7.3) of [48]. In that paper it was also observed that the three cyclic permutations of this function add up to a purely classical function, so the three different permutations of V span only a two-dimensional subset of $B_2 \wedge B_2$.

To summarize, we find that the subspace of $B_2 \wedge B_2$ spanned by physical (hexagon) functions has dimension 5. Two dimensions are spanned by the parity-even functions of type V, while three dimensions are spanned by the parity-odd functions of type F_1. Although a generic vector in the three-dimensional parity-odd subspace has terms with "bad" Poisson brackets, there is something especially nice about the subspace spanned by the permutations of V and $\widetilde{V}$ together. To see this we exhibit here a formula for their cobracket components, which we find are most simply packaged

in the formula

$$\delta|_{2,2}(V+\widetilde{V}) = \frac{1}{2}\{v_2\}_2 \wedge \{x_1^-\}_2 - \frac{1}{2}\{v_1\}_2 \wedge \{x_3^-\}_2 - \frac{1}{2}\{x_1^+\}_2 \wedge \{v_3\}_2 + \frac{1}{2}\{x_2^+\}_2 \wedge \{v_1\}_2. \quad (5.2.7)$$

Since V, $\widetilde{V}$ have parity even and odd, respectively, $\delta|_{2,2}(V-\widetilde{V})$ is given by the same formula but with $x^\pm \to x^\mp$. We now see that each term in (5.2.7) involves only the PB_1 pairs listed in (5.1.14)! Moreover, it is trivial to check directly from (5.2.7) and the cyclic transformations (5.1.11) that the six functions V, $\widetilde{V}$ altogether span only a four-dimensional subspace of PB_1.

5.2.4 Summary

The results of this section can be summarized in the following classification of weight-4 cluster functions on $A_3 \cong \mathrm{Gr}(4,6)$:

There are a total of 81 irreducible weight-four cluster $\mathcal{A}$-functions

- ↳ 45 classical, 10 of which are physical
- ↳ 36 non-classical, 5 of which are physical (three permutations of F_1 and two of Ω_2)
  - ↳ 30 PB_1 functions, 4 of which are physical (two permutations each of $V, \tilde{V}$)
  - ↳ 6 A_2 functions; these are all of the cluster $\mathcal{X}$-functions
    - ↳ 1 PB_0 function, the A_3 function
    - ↳ 5 PB_* functions

Let us emphasize that these numbers count only irreducible functions, and that starting from the third line they moreover count functions modulo the classical function Li_4 (i.e., the numbers refer to dimensions of subspaces of $B_2 \wedge B_2$). When we say that a function is physical modulo additional terms, we mean that it is possible to choose the additional terms to render the function physical.

5.2.5 The Two-Loop Hexagon MHV Amplitude

Let us now comment on the relevance of these functions to the two-loop six-point MHV remainder function $R_6^{(2)}$, which was found to be expressible in terms of the classical polylogarithm functions Li_k in [35] (a fact that we "explained" below (5.2.5)). In fact, this amplitude is even more special because it is a cluster $\mathcal{X}$-function, which means that it can be expressed in entirely in terms of the $\mathrm{Li}_k(-x)$; the $\mathrm{Li}_k(1+x)$ and $\mathrm{Li}_k(1+1/x)$ functions, whose $B_3 \otimes \mathbb{C}^*$ cobracket components are not

expressible in terms of cluster $\mathcal{X}$-coordinates, are not needed [32].

Above we tabulated our finding that (modulo products of lower-weight functions) there are only 10 physical and classical polylogarithms at weight four. In this space we now search for functions whose coproducts are expressible entirely in terms of the $\mathrm{Li}_k(-x)$. We find that there is a unique linear combination that is invariant under the discrete symmetries (parity and dihedral invariance) that MHV amplitudes must possess. That linear combination is proportional to the two-loop MHV remainder function

$$R_6^{(2)\,\mathrm{MHV}} = \sum_{i=1}^{3} \left[\mathrm{Li}_4(-x_i^+) + \mathrm{Li}_4(-x_i^-) - \frac{1}{2}\mathrm{Li}_4(-v_i) \right] + \text{products of lower-weight functions,} \quad (5.2.8)$$

in agreement with the known result [35]. (This argument, of course, does not fix the overall coefficient.) Of course, in this case it is very well known that the product terms are also completely fixed by simple considerations, but our focus in this chapter is on the leading term.

5.2.6 The Two-Loop Hexagon NMHV Amplitude

The $n = 6$ NMHV two-loop ratio function is given by [48]

$$\mathcal{P}^{(2)}_{6,\mathrm{NMHV}} = [23456][V(u,v,w) + \widetilde{V}(y_u, y_v, y_w)] + \text{cyclic} \quad (5.2.9)$$

where $[23456]$ is the R-invariant

$$[abcde] = \frac{\delta^4\left(\chi_a \langle bcde\rangle + cyclic\right)}{\langle abcd\rangle\langle bcde\rangle\langle cdea\rangle\langle deab\rangle\langle eabc\rangle} \quad (5.2.10)$$

and V, $\widetilde{V}$ are the two generalized polylogarithm functions of uniform transcendental weight four reviewed in Section 3.3 above. These two functions were computed explicitly in [48] (see also [140] for a different presentation of these functions). The $B_2 \wedge B_2$ component of the cobracket of this amplitude was computed in (5.2.7), where it was found to be expressible entirely in terms of pairs living in PB_1[4].

The NMHV ratio function provides us (at the level of $B_2 \wedge B_2$) with a total of four linearly independent non-classical functions of weight 4 (as reviewed above, each of V and $\widetilde{V}$ comes in three cyclic permutations, but the cyclic sum of each is separately zero inside $B_2 \wedge B_2$). We see from the summary in Section 5.2.4 that precisely 5 functions of this type exist. Only four linear combinations

[4]This observation was first made by C. Vergu [138].

of them, however, actually appear in the amplitude—these are precisely the four linear combinations which live in PB_1! The one additional non-classical weight-4 hexagon function which exists but does not appear in the amplitude, F_1 by itself, has terms with "bad" Poisson brackets (i.e., non-Stasheff local terms) in its $B_2 \wedge B_2$ content.

5.3 The Cluster Structure of Heptagon Functions at Weight 4

5.3.1 Setup

In this section the term "cluster function" refers to an integrable symbol written in the 42-letter alphabet of cluster coordinates on $\mathrm{Gr}(4,7)$. Any linear combination of such symbols with the property that only the Plücker coordinates of the form $\langle i\, i{+}1\, j\, j{+}1\rangle$ appear in the first entry of the symbol, reflecting the physically allowed branch points for a scattering amplitude, is called (the symbol of) a "physical function" or a "heptagon function" following the terminology of [61] where they have been studied through weight six. The analysis here, where we aim to make finer statements about the connection to the Poisson bracket of the cluster algebra, is again restricted to weight 4, of relevance to two-loop amplitudes.

Let $\mathcal{A}_k$ denote the vector space of all weight-k functions. In contrast to the A_m cluster algebras and the example shown in (5.2.1), we do not know of any generating function which counts the number of cluster functions for the E_6 algebra. These may be tabulated through weight 3 by explicit enumeration, but at higher weight these numbers must be computed by analyzing the integrability constraint. This boils down to a linear algebra problem, since counting the number of cluster functions at weight k is the same as finding how many linear combinations of the 42^k weight-k symbols satisfy the integrability constraint. (This calculation can be rendered more manageable by imposing integrability at the level of the cobracket rather than at the level of the symbol.) We have carried this out at $k = 4$ to find that

$$\dim(\mathcal{A}_k) = 42, 1035, 19536, 312578, \ldots \qquad k = 1, 2, 3, 4, \ldots . \tag{5.3.1}$$

Let $\mathcal{L}_k$ denote the quotient of $\mathcal{A}_k$ by products of functions of lower weight. As in (5.2.3) taking the plethystic logarithm [141] gives

$$\dim(\mathcal{L}_k) = 42, 132, 748, 4193, \ldots \qquad k = 1, 2, 3, 4, \ldots . \tag{5.3.2}$$

Finally we denote by B_k the subspace of $\mathcal{L}_k$ generated by the classical polylogarithms (we do not yet restrict their arguments to be cluster $\mathcal{X}$-coordinates). We have

$$\dim(\mathcal{B}_k) = 132, 748, 1155, \ldots \qquad k = 2, 3, 4, \ldots . \tag{5.3.3}$$

As mentioned before, agreement of these numbers with (5.3.2) is guaranteed for $k < 4$, and we obtained the value 1155 for $k = 4$ by computing $\dim \ker \delta$ as described in Section 2.

Before we turn to weight 4, a minor interesting comment about $k = 3$ is in order. It is simple to write down classical cluster functions of the form $\mathrm{Li}_k(-x)$, $\mathrm{Li}_k(1+x)$ and $\mathrm{Li}_k(1+1/x)$ for any weight k, where x runs over the set of 385 $\mathcal{X}$-coordinates. For $k = 3$, this set of functions is overcomplete due to the identity

$$\mathrm{Li}_3(-x) + \mathrm{Li}_3(1+x) + \mathrm{Li}_3(1+1/x) = 0 \mod \text{products of lower-weight functions.} \tag{5.3.4}$$

Among the 385 functions of type $\mathrm{Li}_3(-x)$ there are exactly 22 additional linear relations. These were discovered in [32], where they were called D_4 identities since the simplest manifestation of this identity occurs for the D_4 algebra. Altogether then these identities account for the $3\times385-385-22 = 748$ linearly independent weight-3 cluster $\mathcal{A}$-functions tabulated in (5.3.2).

5.3.2 The Non-Classical Functions

Let us now repeat the analysis done in the beginning of Section 5.2.2 for the E_6 algebra. Since B_2 has dimension 132, $B_2 \wedge B_2$ has dimension 8646. We again use the notation PB_0, PB_1, and $PB_* = B_2 \wedge B_2$ to denote the subspaces spanned by elements of the form $\{x\}_2 \wedge \{y\}_2$ for pairs x, y having Poisson bracket 0, ±1, or "anything." We find that PB_0 has dimension 455 and PB_1 has dimension 2520.

A quick glance at (5.3.2) and (5.3.3) reveals that there are $4193 - 1155 = 3038$ non-classical cluster functions at weight $k = 4$. We find that these fall into three groups:

(A) First, there are the A_2 functions. We recall from (for example) [32] that E_6 has 1071 A_2 subalgebras, so one can construct 1071 A_2 functions according to the definition given in [46], but only 448 of these are linearly independent inside $B_2 \wedge B_2$[5]. These functions are moreover cluster $\mathcal{X}$-functions: their $B_3 \otimes \mathbb{C}^*$ cobracket components can be expressed entirely in terms of cluster $\mathcal{X}$-coordinates, but their $B_2 \wedge B_2$ content is, in general, not Stasheff local—not expressible in terms of

[5]This result was first obtained in the undergraduate thesis of A. Scherlis.

pairs with Poisson bracket $0, \pm 1$.

There are no linear combinations of these 448 functions which live in PB_1—these are covered in (B) just ahead—but we find that 195 linear combinations live in PB_0. This 195-dimensional space is spanned by the set of A_3 functions associated to the various A_3 subalgebras of E_6.

(B) There are 2520 functions which span the 2520-dimensional subspace $PB_1 \subset B_2 \wedge B_2$. We found the same phenomenon in the six-point case discussed in the previous section. There we furthermore found that no linear combination of these PB_1 functions had a $B_3 \otimes \mathbb{C}^*$ component that could be expressed entirely in terms of $\mathcal{X}$-coordinates. We have not repeated this analysis for the 2520 seven-point functions; the computation seems formidable.

(C) There are an additional $3038 - 448 - 2520 = 70$ functions which we can tabulate explicitly (at least at the level of their cobrackets), but seem to have no nice characterization.

5.3.3 The Physical (Heptagon) Functions

It was found in [61] that there are precisely 1288 functions at weight 4 satisfying the first-entry condition, which are called physical, or heptagon functions. We have computed the $B_2 \wedge B_2$ cobracket of each of them, and found that there are only 126 non-zero linear combinations. This means that there are 1162 classical heptagon functions and 126 non-classical heptagon functions at weight 4. We have found that these 126 heptagon functions fall into three types:

(A) A total of 105 of these functions live in PB_0; they come in 15 families related by cyclic permutations.

(B) A total of 14 of these functions live in PB_1; they come in 2 families related by cyclic permutations.

(C) There is one remaining family of 7 functions related by cyclic permutations. No linear combination of these is Stasheff local (i.e., lives within the union of PB_0 and PB_1).

5.3.4 Summary

The results of this section can be summarized in the following classification of weight-4 cluster functions on $E_6 \cong \mathrm{Gr}(4,7)$:

There are a total of 4193 irreducible weight-four cluster $\mathcal{A}$-functions

- ↳ 1155 classical, 770 of which are physical
- ↳ 3038 non-classical, 126 of which are physical
  - ↳ 2520 PB_1 functions, 105 of which are physical
  - ↳ 448 A_2 functions; these are all of the cluster $\mathcal{X}$-functions
    - ↳ 195 PB_0 function, 14 of which are physical
    - ↳ 253 PB_* functions
  - ↳ 70 other PB_* functions

Again let us emphasize that these numbers count only irreducible functions, and that starting from the third line they moreover count functions modulo the classical function Li_4 (i.e., the numbers refer to dimensions of subspaces of $B_2 \wedge B_2$). When we say that a function is physical modulo additional terms, we mean that it is possible to choose the additional terms to render the function physical.

5.3.5 The Two-Loop Heptagon MHV Amplitude

The symbol of the two-loop seven-point MHV remainder function $R_7^{(2)}$ was computed in [110], and its cobracket was computed in [32], where it was observed to be a cluster $\mathcal{X}$-function living in PB_0. An analytic formula for $R_7^{(2)}$ was obtained in [112] and checked against the earlier numerical results of [143].

If we start from the hypothesis that $R_7^{(2)}$ should be a cluster $\mathcal{X}$-function living in PB_0, then we see from the above chart that there are only 14 physical functions with these properties. It was shown in [47] that only one linear combination of these has the dihedral symmetry required of the amplitude, is well-defined in the collinear limit, and satisfies the "last-entry" condition [110] required by supersymmetry.

In fact these constraints, while all true, are vastly stronger than necessary to pin down $R_7^{(2)}$: in [61] it was found that the symbol of $R_7^{(2)}$ is the unique weight-4 heptagon function (up to an overall multiplicative factor) which is well-defined in all $i{+}1 \parallel i$ collinear limits!

5.3.6 The Two-Loop Heptagon NMHV Amplitude

The symbol of the seven-point 2-loop NMHV ratio function $\mathcal{P}^{(2)}_{7,\mathrm{NMHV}}$ was first computed in [89]. It may be expressed as a linear combination of the 21 seven-point NMHV R-invariants (of which 15 are linearly independent), with coefficients that have uniform transcendentality weight 4. Due to the linear relations between R-invariants there is some freedom in how to represent the amplitude (i.e., one can shift terms from one transcendental function to another by adding zero to the amplitude in various ways).

Despite this freedom, we find that it impossible to write the $B_2 \wedge B_2$ cobracket of this amplitude in a Stasheff local manner, i.e. in terms of $\{x\}_2 \wedge \{y\}_2$ for pairs x, y having Poisson bracket $0, \pm 1$. The local terms having "good" Poisson brackets may be expressed (in one particular representation of the amplitude) as

$$\delta_{22}\mathcal{P}^{(2)}_{7,\mathrm{NMHV}}|_{\text{“good”}} = (f_{12}R_{12} + f_{13}R_{13} + f_{14}R_{14}) + \text{cyclic}, \tag{5.3.5}$$

where the quantities f_{12}, f_{13} and f_{13} are presented explicitly in the appendix, and R_{ij} is the R-invariant whose arguments are 1234567 (in that order) but with i and j omitted—this is the same as the notation used in [48]. Meanwhile the "bad" terms are given by:

$$\delta_{22}\mathcal{P}^{(2)}_{7,\mathrm{NMHV}}|_{\text{“bad”}} = (R_{25} - R_{26} + R_{37} - R_{47})\, B_1 + \text{cyclic} \tag{5.3.6}$$

in terms of a single element $B_1 \in B_2 \wedge B_2$ (also given in the appendix) which is not expressible solely in terms of pairs having Poisson bracket zero or one.

In fact we can point our finger directly at the "offending" function corresponding to B_1 in the summary presented at the end of Section 5.3.4. There we found that of the 126 non-classical weight-4 heptagon functions, 105 live in PB_1 while 14 live in PB_0, leaving $127 - 105 - 14 = 7$ unaccounted for. These other seven functions have $B_2 \wedge B_2$ cobracket components given exactly by B_1 in its seven cyclic arrangements.

5.4 Conclusion

In this chapter we have studied in detail the taxonomy of weight-4 cluster functions on the cluster algebras relevant for 6- and seven-point amplitudes in planar SYM theory. In particular we have counted the numbers of linearly independent functions satisfying various mathematical constraints

on their cobrackets, and the physical "first-entry" constraint which specifies the locations where amplitudes are permitted to have branch points on the principal sheet. These results are summarized in Sections 5.2.4 and 5.3.4.

For $n = 6$ the story is very simple: there is no non-classical weight-4 generalized polylogarithm function which is consistent with the discrete symmetries of the MHV amplitude and whose $B_2 \wedge B_2$ cobracket component is expressible in terms of pairs of cluster $\mathcal{X}$-coordinates having Poisson bracket 0. This "explains" why the two-loop six-point MHV remainder function "must be" expressible in terms of classical polylogarithms [35].

Meanwhile, there are precisely 4 linearly independent non-classical functions which satisfy the first-entry condition and are Stasheff local (they have $B_2 \wedge B_2$ cobracket components are expressible in terms of pairs of cluster $\mathcal{X}$-coordinates having Poisson bracket 1). These are precisely the (non-classical parts of the) 4 independent functions which appear in the two-loop six-point NMHV ratio function [48].

For $n = 7$, as has already been observed in [47, 61], the cobracket (indeed, the whole symbol) of the two-loop MHV amplitude is uniquely determined by a simple list of mathematical and physical constraints. However the story for the two-loop NMHV ratio function is a little more complicated. We find that the cobracket of this amplitude is not expressible in a Stasheff local manner (that means, in terms of pairs having Poisson bracket $0, \pm 1$). It would be very interesting to learn if there is some other question one may ask about the cluster structure of this amplitude, to which a more affirmative answer may be given. We expect to be the case since it is known that there is a cluster structure at the level of the integrand (aspects of which have been explored in [73, 144]), of which some echo ought to remain for integrated amplitudes.

One of our results might be of more mathematical than physical interest. For both the A_3 and E_6 cluster algebras, we find that for any pair of $\mathcal{X}$-coordinates with Poisson bracket $\{\log x, \log y\} = 1$, there exists a weight-4 cluster $\mathcal{A}$-function (that is, an integrable symbol whose letters are drawn from the alphabet of cluster coordinates) whose $B_2 \wedge B_2$ cobracket component is $\{x\}_2 \wedge \{y\}_2$. It would be interesting to learn if there is a mathematical explanation for this fact, and whether it is valid for more general cluster algebras (in particular, for ones of infinite type). In contrast, pairs of $\mathcal{X}$-coordinates having Poisson bracket 0 are rarely integrable in this manner; the two-loop MHV amplitudes of planar SYM theory remarkably provide functions of this relatively rare type.

In the introduction to this chapter we mentioned that in previous work including [47] it has been remarked that the mathematical and physical constraints on MHV amplitudes seem almost orthogonal. This is both good and bad. On the one hand it is good to discover a short list of

simple criteria which uniquely, or almost uniquely, determine an amplitude of interest—this is the core goal of the S-matrix program. On the other hand it is bad when there is no known formalism which simultaneously manifests both types of constraints. We do not yet know of any way, besides explicit enumeration, to actually identify and write down functions satisfying both the physical and mathematical we expect amplitudes to possess. Explicit results for higher loop planar SYM amplitudes remain, at least for the moment, difficult needles to find.

Appendix A

The BDS and BDS-like Ansätze

The BDS ansatz [28] for the n-particle MHV amplitude (with the Parke-Taylor tree amplitude scaled out) is given by

$$M_n \equiv \frac{A_n}{A_n^{(0)}} = \exp\left[\sum_{L=1}^{\infty} a^L \left(f^{(L)}(\epsilon)\frac{1}{2}M_n^{(1)}(L\epsilon) + C^{(L)}\right)\right] \tag{A.0.1}$$

with

$$f^{(L)}(\epsilon) = f_0^{(L)} + \epsilon f_1^{(L)} + \epsilon^2 f_2^{(L)}, \tag{A.0.2}$$

and where ϵ is the dimensional regularization parameter in $D = 4 - 2\epsilon$. Here $f_0^{(L)}$ is the planar cusp anomalous dimension with

$$f_0^{(L)} = \frac{1}{4}\gamma_K^{(L)} = \frac{1}{2}\Gamma_{\text{cusp}}^{(L)}\,, \tag{A.0.3}$$

according to the definition (4.1.24). However, note that in the above relation the superscript L refers to coefficients in the expansion with respect to $a = 2g^2$, and not g^2.

For $n = 7$, the BDS ansatz takes the form

$$A_7^{\text{BDS}} = A_7^{\text{MHV}(0)}\exp\left[\sum_{L=1}^{\infty} a^L \left(f^{(L)}(\epsilon)\frac{1}{2}M_7^{(1)}(L\epsilon) + C^{(L)}\right)\right]. \tag{A.0.4}$$

Here we have explicitly factored out 1/2 from the definition of $M_7^{(1)}(\epsilon)$ appearing in the original BDS paper. The seven-particle one-loop MHV amplitude (again with the tree amplitude scaled out) appearing in the BDS ansatz is given by

$$M_7^{(1)}(\epsilon) = -\frac{1}{\epsilon^2}\sum_{i=1}^{7}\left(\frac{\mu^2}{-s_{i,i+1}}\right)^{\epsilon} + F_7^{(1)}(0) + \mathcal{O}(\epsilon) \tag{A.0.5}$$

where

$$F_7^{(1)}(0) = \sum_{i=1}^{7} \left[-\log\left(\frac{-s_{i,i+1}}{-s_{i,i+1,i+2}}\right) \log\left(\frac{-s_{i+1,i+2}}{-s_{i,i+1,i+2}}\right) + D_{7,i} + L_{7,i} + \frac{3}{2}\zeta_2 \right] \tag{A.0.6}$$

with

$$D_{7,i} = -\mathrm{Li}_2\left(1 - \frac{s_{i,i+1}\, s_{i-1,i,i+1,i+2}}{s_{i,i+1,i+2}\, s_{i-1,i,i+1}}\right) \tag{A.0.7}$$

and

$$L_{7,i} = -\frac{1}{2}\log\left(\frac{-s_{i,i+1,i+2}}{-s_{i,i+1,i+2,i+3}}\right) \log\left(\frac{-s_{i+1,i+2,i+3}}{-s_{i-1,i,i+1,i+2}}\right). \tag{A.0.8}$$

Notice that all of the dependence on the three-particle Mandelstam invariants is contained within $F_7^{(1)}(0)$, so we will focus on determining its dependence. We can replace the four-particle invariants with three-particle invariants in both $D_{7,i}$ and $L_{7,i}$. The two equations then become

$$D_{7,i} = -\mathrm{Li}_2\left(1 - \frac{s_{i,i+1}s_{i+3,i+4,i+5}}{s_{i,i+1,i+2}s_{i-1,i,i+1}}\right),\ L_{7,i} = -\frac{1}{2}\log\left(\frac{s_{i,i+1,i+2}}{s_{i+4,i+5,i+6}}\right) \log\left(\frac{s_{i+1,i+2,i+3}}{s_{i+3,i+4,i+5}}\right). \tag{A.0.9}$$

At this point, it is convenient to switch to the $n = 7$ dual conformal cross ratios u_i, defined in terms of the Mandelstam variables by

$$u_i = u_{i+1,i+4} = \frac{s_{i+2,i+3}\, s_{i+5,i+6,i+7}}{s_{i+1,i+2,i+3}\, s_{i+2,i+3,i+4}}, \tag{A.0.10}$$

where all indices are understood mod 7. We can see from this definition that $D_{7,i}$ can be expressed simply in the u_i variables as $D_{7,i} = -\mathrm{Li}_2\,(1-u_{i-2})$. Using the dilogarithm identity $\mathrm{Li}_2(z) + \mathrm{Li}_2(1-1/z) = -\frac{1}{2}\log^2 z$, we then rewrite $D_{7,i} = \mathrm{Li}_2\,(1-1/u_{i-2}) + \frac{1}{2}\log^2 u_{i-2}$, and express $F_7^{(1)}(0)$ as

$$\begin{aligned} F_7^{(1)}(0) = \sum_{i=1}^{7} \Bigg[& -\log\left(\frac{s_{i,i+1}}{s_{i,i+1,i+2}}\right) \log\left(\frac{s_{i+1,i+2}}{s_{i,i+1,i+2}}\right) + \mathrm{Li}_2\,(1-1/u_i) + \frac{1}{2}\log^2 u_i \\ & -\frac{1}{2}\log\left(\frac{s_{i,i+1,i+2}}{s_{i+4,i+5,i+6}}\right) \log\left(\frac{s_{i+1,i+2,i+3}}{s_{i+3,i+4,i+5}}\right) + \frac{3}{2}\zeta_2 \Bigg]. \end{aligned} \tag{A.0.11}$$

After some algebra, $F_7^{(1)}(0)$ can be shown to be

$$\begin{aligned} F_7^{(1)}(0) \;=\; \sum_{i=1}^{7} \Bigg[& \mathrm{Li}_2\left(1-\frac{1}{u_i}\right) + \frac{1}{2}\log\left(\frac{u_{i+2}u_{i-2}}{u_{i+3}u_i u_{i-3}}\right) \log u_i \\ & + \log s_{i,i+1} \log\left(\frac{s_{i,i+1}s_{i+3,i+4}}{s_{i+1,i+2}s_{i+2,i+3}}\right) + \frac{3}{2}\zeta_2 \Bigg]. \end{aligned} \tag{A.0.12}$$

In this form, we have conveniently isolated all of the three-particle invariants in the first two terms.

Now we would like to factor out the three-particle invariants from $F_7^{(1)}(0)$ because this removes their dependence from $M_7^{(1)}$ as well. We define the function

$$Y_7 = -\sum_{i=1}^{7}\left[\mathrm{Li}_2\left(1-\frac{1}{u_i}\right)+\frac{1}{2}\log\left(\frac{u_{i+2}u_{i-2}}{u_{i+3}u_i u_{i-3}}\right)\log u_i\right] \tag{A.0.13}$$

so that adding the term Y_7 removes the three-particle invariants from $M_7^{(1)}$:

$$\begin{aligned}\hat{M}_7^{(1)}(\epsilon) &\equiv M_7^{(1)}(\epsilon)+Y_7 \\ &= \sum_{i=1}^{7}\left[-\frac{1}{\epsilon^2}\left(\frac{\mu^2}{-s_{i,i+1}}\right)^{\epsilon}+\log s_{i,i+1}\log\left(\frac{s_{i,i+1}\,s_{i+3,i+4}}{s_{i+1,i+2}\,s_{i+2,i+3}}\right)+\frac{3}{2}\zeta_2\right].\end{aligned} \tag{A.0.14}$$

The BDS-like ansatz is defined to be the BDS ansatz with $M_7^{(1)}$ replaced by with $\hat{M}_7^{(1)}$, which does not depend on any three-particle invariant:

$$A_7^{\text{BDS-like}} = A_7^{\text{MHV}(0)}\exp\left[\sum_{L=1}^{\infty}a^L\left(f^{(L)}(\epsilon)\frac{1}{2}\left(M_7^{(1)}(L\epsilon)+Y_7\right)+C^{(L)}\right)\right], \tag{A.0.15}$$

Factoring out the BDS ansatz explicitly, we have

$$A_7^{\text{BDS-like}} = A_7^{\text{BDS}}\exp\left[\sum_{L=1}^{\infty}\frac{a^L}{2}\left(f^{(L)}(\epsilon)Y_7\right)\right]. \tag{A.0.16}$$

Recall that in the BDS ansatz formulation, the limit $\epsilon \to 0$ is taken. Since Y_7 is independent of ϵ, we can set $\epsilon \to 0$ in eq. (A.0.2) and rewrite the BDS-like ansatz as simply

$$A_7^{\text{BDS-like}} = A_7^{\text{BDS}}\exp\left[\frac{Y_7}{4}\sum_{L=1}^{\infty}a^L\Gamma_{\text{cusp}}^{(L)}\right], \tag{A.0.17}$$

where we have used the definition (A.0.3). After introducing $\Gamma_{\text{cusp}} = \sum_{L=1}^{\infty}a^L\Gamma_{\text{cusp}}^{(L)}$, defined in eq. (4.1.24), we finally arrive at a simple representation of the BDS-like ansatz as a function of the BDS ansatz, the cusp anomalous dimension Γ_{cusp}, and Y_7,

$$A_7^{\text{BDS-like}} = A_7^{\text{BDS}}\exp\left[\frac{\Gamma_{\text{cusp}}}{4}Y_7\right]. \tag{A.0.18}$$

This result can be generalized to any n for which a suitable BDS-like ansatz exists, see eq. (4.1.21).

Appendix B

A Matrix Approach For Computing Integrable Symbols

We provide here a conceptually simple method for generating a basis of integrable symbols, given the set of symbol letters on which they depend. This algorithm is iterative, and assumes that one has seeded the algorithm with a basis at low weight. For general heptagon symbols, this seed is provided at weight 1 by the first entry condition reviewed in section 4.2.3. It consists of the 7 weight-1 symbols corresponding to $\log a_{1i}$. For Steinmann heptagon symbols, the seed is provided by the 28 weight-2 heptagon symbols of the functions shown in eq. (4.2.15).

Let $B^{(k)}$ denote a basis of symbols at weight k, and let $b_k = \dim B^{(k)}$. Let us also denote the i-th element of $B^{(k)}$ by $B_i^{(k)}$. Given $B^{(k)}$, we can make an ansatz for symbols of weight $(k{+}1)$ of the form

$$\sum_{i=1}^{b_k} \sum_{q=1}^{|\Phi|} c_{iq}\; B_i^{(k)} \otimes \phi_q \,, \tag{B.0.1}$$

where the sum over q runs over all letters in the symbol alphabet Φ, i.e. $\phi_q \in \Phi$, and the c_{iq} are undetermined rational coefficients. The number of letters is denoted by $|\Phi|$. The quantity (B.0.1) will be the symbol of some weight-$(k{+}1)$ function only if it satisfies the integrability constraints of eq. (4.2.8) for all j. By construction, these constraints are automatically satisfied for $j = 1, 2, \ldots, k-1$, because the elements of $B^{(k)}$ are already valid, integrable symbols. It therefore remains only to impose integrability in the final two entries at weight $(k{+}1)$, i.e. for $j = k$.

Each $B_i^{(k)}$ can of course be expressed as

$$B_i^{(k)} = \sum_{j=1}^{b_{k-1}} \sum_{p=1}^{|\Phi|} f_{ijp}\ B_j^{(k-1)} \otimes \phi_p \tag{B.0.2}$$

for some known coefficients f_{ijp}, so we can rewrite our ansatz as

$$\sum_{i=1}^{b_k} \sum_{j=1}^{b_{k-1}} \sum_{p,q=1}^{|\Phi|} c_{iq} f_{ijp}\ B_j^{(k-1)} \otimes \phi_p \otimes \phi_q \,. \tag{B.0.3}$$

Denoting

$$F_{pq} = \sum_{i=1}^{b_k} \sum_{j=1}^{b_{k-1}} c_{iq} f_{ijp}\ B_j^{(k-1)} \,, \tag{B.0.4}$$

the quantity (B.0.2) satisfies integrability in the final two entries only if

$$\sum_{p,q=1}^{|\Phi|} F_{pq}\, d\log\phi_p \wedge d\log\phi_q = 0 \,, \tag{B.0.5}$$

where the wedge product between two letters ϕ_p, ϕ_q that are functions of the independent variables x^i is defined as

$$d\log\phi_p \wedge d\log\phi_q = \sum_{m,n} \left[\frac{\partial \log\phi_p}{\partial x^m} \frac{\partial \log\phi_q}{\partial x^n} - \frac{\partial \log\phi_p}{\partial x^n} \frac{\partial \log\phi_q}{\partial x^m} \right] dx^m \wedge dx^n \,. \tag{B.0.6}$$

The term in brackets above will be a rational function of the independent variables, which can be turned polynomial by multiplying with the common denominator, without altering the equations (B.0.5). Each independent polynomial factor of the x_i times their differentials must vanish separately, which leads to distinct rational equations for the F_{pq}. If the number of linearly independent equations is r, then we may equivalently write eq. (B.0.5) as

$$\sum_{p,q=1}^{|\Phi|} F_{pq} W_{pql} = 0 \,, \quad \forall l \in \{1, 2, \ldots, r\} \,, \tag{B.0.7}$$

in terms of a rational tensor W_{pql}. Taking the tensor product of the indices p, q we may think of W as a $|\Phi|^2 \times r$ matrix, or rather a $\binom{|\Phi|}{2} \times r$ matrix after taking into account its antisymmetry in $p \leftrightarrow q$.

Since the $B_j^{(k-1)}$ are elements of the basis $B^{(k-1)}$ of weight-$(k-1)$ symbols, they are linearly independent. Each term in the sum over j in (B.0.4) must therefore vanish separately. In this

manner, we finally arrive at the following set of $r \times b_{k-1}$ linear constraints on the $|\Phi| \times b_k$ unknown coefficients c_{iq}:

$$\sum_{i=1}^{b_k} \sum_{p,q} c_{iq} f_{ijp} W_{pql} = 0\,, \qquad \forall j \in \{1, 2, \ldots, b_{k-1}\}\,, \quad l \in \{1, 2, \ldots, r\}\,. \tag{B.0.8}$$

We now specialize to the case of interest by adopting the 42-letter symbol alphabet presented in eqs. (4.2.2) and (4.2.3). There are 132 vanishing linear combinations of the 861 objects $d\log\phi_p \wedge d\log\phi_q$, i.e. there are 132 irreducible weight-2 integrable symbols (these are in correspondence with elements of the so-called Bloch group B_2; see for example ref. [32]). This means that there are $r = 861 - 132 = 729$ nontrivial integrability constraints for the heptagon symbol alphabet. In solving the linear constraints (B.0.8) for the c_{iq}, we are free to replace W by any matrix which spans the same image as W without changing the content of the constraints. It is highly advantageous to choose a basis for the image of W that is as sparse as possible, and which has numerical entries as simple as possible. In our bootstrap we used a representation of the image of W as a 861×729 matrix[1] with only 1195 nonzero entries having values ± 1.

Finally, then, the integrability constraints shown in eq. (B.0.8) take the form of $729\, b_{k-1}$ linear equations on the $42\, b_k$ unknowns c_{iq}. Finding a basis for the nullspace of this $729\, b_{k-1} \times 42\, b_k$ linear system provides a basis for $B^{(k+1)}$, the integrable symbols at weight $k+1$. For the purposes of the Steinmann heptagon bootstrap, we have further cut down the weight-2 basis yielded by this procedure to only those 28 symbols that satisfy the Steinmann relations before proceeding to weight 3. We have carried out the large linear algebra problems necessary for the heptagon bootstrap with the help of the `SageMath` system [145], which employs the `IML` integer matrix library [146]. As a double check, we also fed the weight-7 integrability constraint matrix into A. von Manteuffel's `FinRed` program, which independently generated a basis for the 9570-dimensional weight-7 Steinmann heptagon space reported in table 4.1.

B.1 Two-Loop Heptagon NMHV Coproduct Data

In the first three subsections we list the Stasheff local contributions to the $B_2 \wedge B_2$ cobracket component of the two-loop heptagon NMHV ratio function, in terms of the quantities f_{12}, f_{13}, and f_{14} appearing in (5.3.5). Specifically, these contain all terms of the form $\{x\}_2 \wedge \{y\}_2$ for pairs x, y having Poisson bracket $0, \pm 1$. The additional "bad" contributions to the cobracket are shown

[1] To orient the reader already familiar with the hexagon bootstrap: there the symbol alphabet has size $|\Phi| = 9$, and there are 10 irreducible weight-2 integrable symbols, so the W matrix for the hexagon alphabet has size 36×26.

in (5.3.6) and given explicitly in the fourth subsection.

B.1.1 f_{13}

This function is cyclically invariant and lives entirely in PB_1. We find

$$\begin{aligned}
\delta_{22} f_{13} = \frac{1}{7}\Bigg(& \left\{\frac{\langle 1367\rangle\langle 2347\rangle}{\langle 1237\rangle\langle 3467\rangle}\right\}_2 \wedge \left\{\frac{\langle 1367\rangle\langle 2347\rangle\langle 4567\rangle}{\langle 1467\rangle\langle 2367\rangle\langle 3457\rangle}\right\}_2 \\
& - \left\{\frac{\langle 1247\rangle\langle 1256\rangle}{\langle 1245\rangle\langle 1267\rangle}\right\}_2 \wedge \left\{\frac{\langle 1245\rangle\langle 1567\rangle}{\langle 1257\rangle\langle 1456\rangle}\right\}_2 \\
& + \left\{\frac{\langle 1256\rangle\langle 2345\rangle}{\langle 1235\rangle\langle 2456\rangle}\right\}_2 \wedge \left(\left\{\frac{\langle 1236\rangle\langle 1245\rangle}{\langle 1234\rangle\langle 1256\rangle}\right\}_2 - \left\{\frac{\langle 1235\rangle\langle 1567\rangle\langle 2456\rangle}{\langle 1257\rangle\langle 1456\rangle\langle 2356\rangle}\right\}_2\right) \\
& + \left\{\frac{\langle 1247\rangle\langle 1345\rangle}{\langle 1234\rangle\langle 1457\rangle}\right\}_2 \wedge \left(\left\{\frac{\langle 1345\rangle\langle 1467\rangle}{\langle 1347\rangle\langle 1456\rangle}\right\}_2 - \left\{\frac{\langle 1245\rangle\langle 1467\rangle}{\langle 1247\rangle\langle 1456\rangle}\right\}_2\right) \\
& + \left(\left\{\frac{\langle 1247\rangle\langle 1345\rangle\langle 1567\rangle}{\langle 1257\rangle\langle 1347\rangle\langle 1456\rangle}\right\}_2 - \left\{\frac{\langle 1247\rangle\langle 1256\rangle\langle 1345\rangle}{\langle 1234\rangle\langle 1257\rangle\langle 1456\rangle}\right\}_2\right) \wedge \left(\left\{-\frac{\langle 1267\rangle\langle 1345\rangle}{\langle 1(27)(34)(56)\rangle}\right\}_2\right. \\
& \qquad \left. + \left\{-\frac{\langle 1237\rangle\langle 1456\rangle}{\langle 1(27)(34)(56)\rangle}\right\}_2\right) \\
& + \left(\left\{\frac{\langle 1247\rangle\langle 1256\rangle\langle 1346\rangle}{\langle 1234\rangle\langle 1267\rangle\langle 1456\rangle}\right\}_2 - \left\{\frac{\langle 1237\rangle\langle 1345\rangle\langle 1567\rangle}{\langle 1257\rangle\langle 1347\rangle\langle 1356\rangle}\right\}_2\right) \wedge \left\{-\frac{\langle 1234\rangle\langle 1567\rangle}{\langle 1(27)(34)(56)\rangle}\right\}_2 \Bigg) \\
& \qquad + \text{cyclic.}
\end{aligned}$$

B.1.2 f_{12}

If we first define the quantity X_1 by

$$\begin{aligned}
X_1 = & \left\{\frac{\langle 1367\rangle\langle 2347\rangle}{\langle 1237\rangle\langle 3467\rangle}\right\}_2 \wedge \left\{\frac{\langle 1267\rangle\langle 3467\rangle}{\langle 1467\rangle\langle 2367\rangle}\right\}_2 + \left\{\frac{\langle 1467\rangle\langle 2347\rangle}{\langle 1247\rangle\langle 3467\rangle}\right\}_2 \wedge \left\{\frac{\langle 1347\rangle\langle 4567\rangle}{\langle 1467\rangle\langle 3457\rangle}\right\}_2 \\
& - \left\{\frac{\langle 1247\rangle\langle 1345\rangle}{\langle 1234\rangle\langle 1457\rangle}\right\}_2 \wedge \left\{\frac{\langle 1245\rangle\langle 3457\rangle}{\langle 1457\rangle\langle 2345\rangle}\right\}_2 - \left\{\frac{\langle 1457\rangle\langle 2347\rangle}{\langle 1247\rangle\langle 3457\rangle}\right\}_2 \wedge \left\{\frac{\langle 1347\rangle\langle 4567\rangle}{\langle 1467\rangle\langle 3457\rangle}\right\}_2 \\
& + \left\{\frac{\langle 1256\rangle\langle 2345\rangle}{\langle 1235\rangle\langle 2456\rangle}\right\}_2 \wedge \left\{\frac{\langle 1236\rangle\langle 1245\rangle\langle 2567\rangle}{\langle 1235\rangle\langle 1267\rangle\langle 2456\rangle}\right\}_2 - \left\{\frac{\langle 1267\rangle\langle 2356\rangle}{\langle 1236\rangle\langle 2567\rangle}\right\}_2 \wedge \left\{\frac{\langle 1236\rangle\langle 2345\rangle\langle 2567\rangle}{\langle 1235\rangle\langle 2367\rangle\langle 2456\rangle}\right\}_2 \\
& + \left(\left\{\frac{\langle 1234\rangle\langle 1467\rangle\langle 3457\rangle}{\langle 1247\rangle\langle 1345\rangle\langle 3467\rangle}\right\}_2 - \left\{\frac{\langle 1245\rangle\langle 1467\rangle\langle 3457\rangle}{\langle 1247\rangle\langle 1345\rangle\langle 4567\rangle}\right\}_2\right) \wedge \left\{-\frac{\langle 1467\rangle\langle 2345\rangle}{\langle 4(12)(35)(67)\rangle}\right\}_2 \\
& + \left\{\frac{\langle 1467\rangle\langle 2367\rangle\langle 2457\rangle}{\langle 1267\rangle\langle 2347\rangle\langle 4567\rangle}\right\}_2 \wedge \left\{-\frac{\langle 1237\rangle\langle 4567\rangle}{\langle 7(16)(23)(45)\rangle}\right\}_2 \\
& - \left\{\frac{\langle 1467\rangle\langle 2367\rangle\langle 3457\rangle}{\langle 1367\rangle\langle 2347\rangle\langle 4567\rangle}\right\}_2 \wedge \left\{-\frac{\langle 1267\rangle\langle 3457\rangle}{\langle 7(16)(23)(45)\rangle}\right\}_2 \\
& + 2\left\{\frac{\langle 1245\rangle\langle 2467\rangle\langle 3457\rangle}{\langle 1247\rangle\langle 2345\rangle\langle 4567\rangle}\right\}_2 \wedge \left\{-\frac{\langle 1234\rangle\langle 4567\rangle}{\langle 4(12)(35)(67)\rangle}\right\}_2
\end{aligned}$$

and $X_2, \ldots, X_7$ by taking $i \to i+1$, then we find

$$
\begin{aligned}
\delta_{22} f_{12} = \frac{1}{7}(3,-4,3,-4,3,-4,3) \cdot (X_1, X_2, X_3, X_4, X_5, X_6, X_7) \\
&+ \left\{ \frac{\langle 1237\rangle\langle 1246\rangle}{\langle 1234\rangle\langle 1267\rangle} \right\}_2 \wedge \left(\left\{ \frac{\langle 1246\rangle\langle 1345\rangle}{\langle 1234\rangle\langle 1456\rangle} \right\}_2 + \left\{ \frac{\langle 1234\rangle\langle 1467\rangle\langle 3456\rangle}{\langle 1246\rangle\langle 1345\rangle\langle 3467\rangle} \right\}_2 \right. \\
&\qquad \left. + \left\{ \frac{\langle 1467\rangle\langle 3456\rangle}{\langle 1346\rangle\langle 4567\rangle} \right\}_2 + \left\{ \frac{\langle 1246\rangle\langle 1345\rangle\langle 4567\rangle}{\langle 1245\rangle\langle 1467\rangle\langle 3456\rangle} \right\}_2 \right) \\
&+ \left\{ \frac{\langle 1457\rangle\langle 3456\rangle}{\langle 1345\rangle\langle 4567\rangle} \right\}_2 \wedge \left(\left\{ \frac{\langle 1234\rangle\langle 1457\rangle}{\langle 1247\rangle\langle 1345\rangle} \right\}_2 + \left\{ \frac{\langle 1234\rangle\langle 1267\rangle\langle 1457\rangle}{\langle 1237\rangle\langle 1245\rangle\langle 1467\rangle} \right\}_2 + \left\{ \frac{\langle 1237\rangle\langle 1467\rangle}{\langle 1267\rangle\langle 1347\rangle} \right\}_2 \right. \\
&\qquad \left. + \left\{ \frac{\langle 1237\rangle\langle 1345\rangle\langle 1467\rangle}{\langle 1234\rangle\langle 1367\rangle\langle 1457\rangle} \right\}_2 + \left\{ \frac{\langle 1257\rangle\langle 1456\rangle}{\langle 1245\rangle\langle 1567\rangle} \right\}_2 \right) \\
&+ \left\{ \frac{\langle 1267\rangle\langle 2356\rangle}{\langle 1236\rangle\langle 2567\rangle} \right\}_2 \wedge \left\{ \frac{\langle 1236\rangle\langle 2345\rangle\langle 3567\rangle}{\langle 1235\rangle\langle 2367\rangle\langle 3456\rangle} \right\}_2 - \left\{ \frac{\langle 1247\rangle\langle 1345\rangle}{\langle 1234\rangle\langle 1457\rangle} \right\}_2 \wedge \left\{ \frac{\langle 1247\rangle\langle 1567\rangle\langle 3457\rangle}{\langle 1257\rangle\langle 1347\rangle\langle 4567\rangle} \right\}_2 \\
&+ \left(\left\{ \frac{\langle 1247\rangle\langle 1256\rangle\langle 1345\rangle}{\langle 1234\rangle\langle 1257\rangle\langle 1456\rangle} \right\}_2 + \left\{ \frac{\langle 1257\rangle\langle 1347\rangle\langle 1456\rangle}{\langle 1247\rangle\langle 1345\rangle\langle 1567\rangle} \right\}_2 \right) \wedge \left\{ -\frac{\langle 1247\rangle\langle 1567\rangle\langle 3456\rangle}{\langle 4567\rangle\langle 1(27)(34)(56)\rangle} \right\}_2 \\
&+ \left(\left\{ \frac{\langle 1235\rangle\langle 2367\rangle\langle 2456\rangle}{\langle 1236\rangle\langle 2345\rangle\langle 2567\rangle} \right\}_2 - \left\{ \frac{\langle 1235\rangle\langle 1267\rangle\langle 2456\rangle}{\langle 1236\rangle\langle 1245\rangle\langle 2567\rangle} \right\}_2 \right) \wedge \left\{ -\frac{\langle 1236\rangle\langle 2345\rangle\langle 4567\rangle}{\langle 3456\rangle\langle 2(13)(45)(67)\rangle} \right\}_2 \\
&+ \left\{ \frac{\langle 1467\rangle\langle 3457\rangle}{\langle 1347\rangle\langle 4567\rangle} \right\}_2 \wedge \left(\left\{ \frac{\langle 1237\rangle\langle 1467\rangle}{\langle 1267\rangle\langle 1347\rangle} \right\}_2 - \left\{ \frac{\langle 1267\rangle\langle 1347\rangle\langle 4567\rangle}{\langle 1247\rangle\langle 1567\rangle\langle 3467\rangle} \right\}_2 \right) \\
&+ \left\{ \frac{\langle 2367\rangle\langle 3456\rangle}{\langle 2346\rangle\langle 3567\rangle} \right\}_2 \wedge \left(\left\{ \frac{\langle 1234\rangle\langle 2367\rangle}{\langle 1237\rangle\langle 2346\rangle} \right\}_2 + \left\{ \frac{\langle 1234\rangle\langle 2367\rangle\langle 3456\rangle}{\langle 1236\rangle\langle 2345\rangle\langle 3467\rangle} \right\}_2 \right) \\
&+ \frac{4}{7} \left(\left\{ \frac{\langle 1257\rangle\langle 1456\rangle\langle 2356\rangle}{\langle 1235\rangle\langle 1567\rangle\langle 2456\rangle} \right\}_2 \wedge \left\{ -\frac{\langle 1235\rangle\langle 4567\rangle}{\langle 5(17)(23)(46)\rangle} \right\}_2 \right. \\
&\qquad \left. + \left\{ \frac{\langle 1357\rangle\langle 1456\rangle\langle 2356\rangle}{\langle 1235\rangle\langle 1567\rangle\langle 3456\rangle} \right\}_2 \wedge \left\{ -\frac{\langle 1567\rangle\langle 2345\rangle}{\langle 5(17)(23)(46)\rangle} \right\}_2 \right) \\
&+ \frac{4}{7} \left(\left\{ \frac{\langle 1247\rangle\langle 1256\rangle\langle 1345\rangle}{\langle 1234\rangle\langle 1257\rangle\langle 1456\rangle} \right\}_2 \wedge \left\{ -\frac{\langle 1237\rangle\langle 1456\rangle}{\langle 1(27)(34)(56)\rangle} \right\}_2 \right. \\
&\qquad \left. - \left\{ \frac{\langle 1367\rangle\langle 2347\rangle\langle 3456\rangle}{\langle 1347\rangle\langle 2346\rangle\langle 3567\rangle} \right\}_2 \wedge \left\{ -\frac{\langle 1367\rangle\langle 2345\rangle}{\langle 3(17)(24)(56)\rangle} \right\}_2 \right) \\
&- \frac{3}{7} \left(\left\{ \frac{\langle 1367\rangle\langle 1457\rangle\langle 2347\rangle}{\langle 1237\rangle\langle 1467\rangle\langle 3457\rangle} \right\}_2 \wedge \left\{ -\frac{\langle 1267\rangle\langle 3457\rangle}{\langle 7(16)(23)(45)\rangle} \right\}_2 \right. \\
&\qquad \left. + \left\{ \frac{\langle 1236\rangle\langle 2567\rangle\langle 3467\rangle}{\langle 1267\rangle\langle 2346\rangle\langle 3567\rangle} \right\}_2 \wedge \left\{ -\frac{\langle 1567\rangle\langle 2346\rangle}{\langle 6(12)(34)(57)\rangle} \right\}_2 \right) \\
&- \frac{3}{7} \left(\left\{ \frac{\langle 1235\rangle\langle 2367\rangle\langle 2456\rangle}{\langle 1236\rangle\langle 2345\rangle\langle 2567\rangle} \right\}_2 \wedge \left\{ -\frac{\langle 1234\rangle\langle 2567\rangle}{\langle 2(13)(45)(67)\rangle} \right\}_2 \right. \\
&\qquad \left. + \left\{ \frac{\langle 1245\rangle\langle 1467\rangle\langle 3457\rangle}{\langle 1247\rangle\langle 1345\rangle\langle 4567\rangle} \right\}_2 \wedge \left\{ -\frac{\langle 1247\rangle\langle 3456\rangle}{\langle 4(12)(35)(67)\rangle} \right\}_2 \right) \\
&+ \left(\left\{ \frac{\langle 1235\rangle\langle 2367\rangle\langle 4567\rangle}{\langle 2567\rangle\langle 3(12)(45)(67)\rangle} \right\}_2 - \left\{ -\frac{\langle 1237\rangle\langle 2345\rangle\langle 4567\rangle}{\langle 3457\rangle\langle 2(13)(45)(67)\rangle} \right\}_2 \right. \\
&\qquad \left. + \frac{4}{7} \left\{ \frac{\langle 1235\rangle\langle 2367\rangle\langle 2457\rangle}{\langle 1237\rangle\langle 2345\rangle\langle 2567\rangle} \right\}_2 \right) \wedge \left\{ -\frac{\langle 1267\rangle\langle 2345\rangle}{\langle 2(13)(45)(67)\rangle} \right\}_2 \\
&- \left\{ \frac{\langle 1256\rangle\langle 2345\rangle}{\langle 1235\rangle\langle 2456\rangle} \right\}_2 \wedge \left\{ \frac{\langle 2567\rangle\langle 3456\rangle}{\langle 2356\rangle\langle 4567\rangle} \right\}_2
\end{aligned}
$$

$$
\begin{aligned}
&+\left(\left\{\frac{\langle 1237\rangle\langle 1345\rangle\langle 4567\rangle}{\langle 3457\rangle\langle 1(23)(45)(67)\rangle}\right\}_2-\left\{\frac{\langle 1236\rangle\langle 1345\rangle\langle 4567\rangle}{\langle 3456\rangle\langle 1(23)(45)(67)\rangle}\right\}_2\right.\\
&\qquad\left.-\left\{\frac{\langle 1237\rangle\langle 1456\rangle}{\langle 1(23)(45)(67)\rangle}\right\}_2\right)\wedge\left\{\frac{\langle 1267\rangle\langle 1345\rangle}{\langle 1(23)(45)(67)\rangle}\right\}_2\\
&+\left\{-\frac{\langle 1234\rangle\langle 1567\rangle}{\langle 1(27)(34)(56)\rangle}\right\}_2\wedge\left(\left\{-\frac{\langle 1237\rangle\langle 1567\rangle\langle 3456\rangle}{\langle 3567\rangle\langle 1(27)(34)(56)\rangle}\right\}_2-\left\{\frac{\langle 1257\rangle\langle 1347\rangle\langle 3456\rangle}{\langle 1345\rangle\langle 7(12)(34)(56)\rangle}\right\}_2\right.\\
&\qquad\left.+\frac{3}{7}\left\{\frac{\langle 1247\rangle\langle 1256\rangle\langle 1346\rangle}{\langle 1234\rangle\langle 1267\rangle\langle 1456\rangle}\right\}_2\right)\\
&+\left\{\frac{\langle 1237\rangle\langle 3456\rangle}{\langle 3(12)(45)(67)\rangle}\right\}_2\wedge\left(\left\{\frac{\langle 1267\rangle\langle 1345\rangle\langle 3467\rangle}{\langle 1467\rangle\langle 3(12)(45)(67)\rangle}\right\}_2+\left\{\frac{\langle 1234\rangle\langle 1367\rangle\langle 4567\rangle}{\langle 1467\rangle\langle 3(12)(45)(67)\rangle}\right\}_2\right.\\
&\qquad\left.-\left\{\frac{\langle 1234\rangle\langle 1267\rangle\langle 1345\rangle\langle 4567\rangle}{\langle 1245\rangle\langle 1467\rangle\langle 3(12)(45)(67)\rangle}\right\}_2\right)\\
&+\left(\left\{\frac{\langle 1234\rangle\langle 1267\rangle\langle 3457\rangle\langle 4567\rangle}{\langle 1247\rangle\langle 3467\rangle\langle 5(12)(34)(67)\rangle}\right\}_2+\left\{-\frac{\langle 1234\rangle\langle 1267\rangle\langle 3456\rangle}{\langle 1236\rangle\langle 4(12)(35)(67)\rangle}\right\}_2-\left\{-\frac{\langle 1247\rangle\langle 3456\rangle}{\langle 4(12)(35)(67)\rangle}\right\}_2\right.\\
&\qquad\left.-\left\{\frac{\langle 4567\rangle\langle 3(12)(45)(67)\rangle}{\langle 3467\rangle\langle 5(12)(34)(67)\rangle}\right\}_2-\frac{3}{7}\left\{\frac{\langle 1245\rangle\langle 2467\rangle\langle 3457\rangle}{\langle 1247\rangle\langle 2345\rangle\langle 4567\rangle}\right\}_2\right)\wedge\left\{-\frac{\langle 1234\rangle\langle 4567\rangle}{\langle 4(12)(35)(67)\rangle}\right\}_2\\
&+\left(\left\{\frac{\langle 1234\rangle\langle 1267\rangle\langle 3456\rangle\langle 3567\rangle}{\langle 1236\rangle\langle 3467\rangle\langle 5(12)(34)(67)\rangle}\right\}_2+\left\{-\frac{\langle 1234\rangle\langle 1267\rangle\langle 3567\rangle}{\langle 1237\rangle\langle 6(12)(34)(57)\rangle}\right\}_2\right.\\
&\qquad\left.+\left\{\frac{\langle 3467\rangle\langle 5(12)(34)(67)\rangle}{\langle 3456\rangle\langle 7(12)(34)(56)\rangle}\right\}_2-\frac{3}{7}\left\{\frac{\langle 1246\rangle\langle 2567\rangle\langle 3467\rangle}{\langle 1267\rangle\langle 2346\rangle\langle 4567\rangle}\right\}_2\right)\wedge\left\{-\frac{\langle 1267\rangle\langle 3456\rangle}{\langle 6(12)(34)(57)\rangle}\right\}_2\\
&+\left(\left\{-\frac{\langle 1267\rangle\langle 3457\rangle}{\langle 7(16)(23)(45)\rangle}\right\}_2+\frac{4}{7}\left\{\frac{\langle 1367\rangle\langle 1457\rangle\langle 2357\rangle}{\langle 1237\rangle\langle 1567\rangle\langle 3457\rangle}\right\}_2\right.\\
&\qquad\left.-\left\{\frac{\langle 1467\rangle\langle 2367\rangle\langle 3457\rangle}{\langle 1367\rangle\langle 2347\rangle\langle 4567\rangle}\right\}_2\right)\wedge\left\{-\frac{\langle 1237\rangle\langle 4567\rangle}{\langle 7(16)(23)(45)\rangle}\right\}_2\\
&+\left(\left\{-\frac{\langle 1234\rangle\langle 3567\rangle}{\langle 3(17)(24)(56)\rangle}\right\}_2-\frac{3}{7}\left\{\frac{\langle 1347\rangle\langle 1356\rangle\langle 2346\rangle}{\langle 1234\rangle\langle 1367\rangle\langle 3456\rangle}\right\}_2\right.\\
&\qquad\left.+\left\{\frac{\langle 1367\rangle\langle 2347\rangle\langle 3456\rangle}{\langle 1347\rangle\langle 2346\rangle\langle 3567\rangle}\right\}_2\right)\wedge\left\{-\frac{\langle 1237\rangle\langle 3456\rangle}{\langle 3(17)(24)(56)\rangle}\right\}_2.
\end{aligned}
$$

B.1.3 f_{14}

This function lives entirely in PB_1. If we first define the quantity

$$
\begin{aligned}
Y = &\left\{\frac{\langle 2347\rangle\langle 2356\rangle}{\langle 2345\rangle\langle 2367\rangle}\right\}_2 \wedge \left\{\frac{\langle 2346\rangle\langle 3567\rangle}{\langle 2367\rangle\langle 3456\rangle}\right\}_2 + \left\{\frac{\langle 1367\rangle\langle 2347\rangle}{\langle 1237\rangle\langle 3467\rangle}\right\}_2 \wedge \left\{\frac{\langle 2347\rangle\langle 3567\rangle}{\langle 2367\rangle\langle 3457\rangle}\right\}_2 \\
&+ \left\{\frac{\langle 1257\rangle\langle 1456\rangle}{\langle 1245\rangle\langle 1567\rangle}\right\}_2 \wedge \left\{\frac{\langle 1257\rangle\langle 1456\rangle\langle 2345\rangle}{\langle 1235\rangle\langle 1457\rangle\langle 2456\rangle}\right\}_2 - \left\{\frac{\langle 1367\rangle\langle 1457\rangle\langle 2347\rangle}{\langle 1237\rangle\langle 1467\rangle\langle 3457\rangle}\right\}_2 \wedge \left\{\frac{\langle 1347\rangle\langle 4567\rangle}{\langle 1467\rangle\langle 3457\rangle}\right\}_2 \\
&- \left\{\frac{\langle 1237\rangle\langle 2356\rangle}{\langle 1235\rangle\langle 2367\rangle}\right\}_2 \wedge \left\{\frac{\langle 1236\rangle\langle 2567\rangle}{\langle 1267\rangle\langle 2356\rangle}\right\}_2 - \left\{\frac{\langle 1256\rangle\langle 2345\rangle}{\langle 1235\rangle\langle 2456\rangle}\right\}_2 \wedge \left\{\frac{\langle 1235\rangle\langle 2567\rangle}{\langle 1257\rangle\langle 2356\rangle}\right\}_2 \\
&+ \left\{\frac{\langle 1257\rangle\langle 1456\rangle\langle 2345\rangle}{\langle 1235\rangle\langle 1457\rangle\langle 2456\rangle}\right\}_2 \wedge \left\{-\frac{\langle 1235\rangle\langle 4567\rangle}{\langle 5(17)(23)(46)\rangle}\right\}_2 \\
&- \left\{\frac{\langle 1257\rangle\langle 1456\rangle\langle 2356\rangle}{\langle 1235\rangle\langle 1567\rangle\langle 2456\rangle}\right\}_2 \wedge \left\{-\frac{\langle 1235\rangle\langle 4567\rangle}{\langle 5(17)(23)(46)\rangle}\right\}_2 \\
&+ \left\{\frac{\langle 1235\rangle\langle 2367\rangle\langle 2457\rangle}{\langle 1237\rangle\langle 2345\rangle\langle 2567\rangle}\right\}_2 \wedge \left\{-\frac{\langle 1267\rangle\langle 2345\rangle}{\langle 2(13)(45)(67)\rangle}\right\}_2 \\
&- \left\{\frac{\langle 1367\rangle\langle 1457\rangle\langle 2347\rangle}{\langle 1237\rangle\langle 1467\rangle\langle 3457\rangle}\right\}_2 \wedge \left\{-\frac{\langle 1567\rangle\langle 2347\rangle}{\langle 7(16)(23)(45)\rangle}\right\}_2 \\
&+ \left\{\frac{\langle 1357\rangle\langle 2347\rangle\langle 2356\rangle}{\langle 1237\rangle\langle 2345\rangle\langle 3567\rangle}\right\}_2 \wedge \left\{-\frac{\langle 1237\rangle\langle 3456\rangle}{\langle 3(17)(24)(56)\rangle}\right\}_2 \\
&- \left\{\frac{\langle 1467\rangle\langle 2367\rangle\langle 3457\rangle}{\langle 1367\rangle\langle 2347\rangle\langle 4567\rangle}\right\}_2 \wedge \left\{-\frac{\langle 1567\rangle\langle 2347\rangle}{\langle 7(16)(23)(45)\rangle}\right\}_2
\end{aligned}
$$

then we find

$$
\begin{aligned}
\delta_{22} f_{14} = \frac{2}{7}(Y + \text{cyclic}) - 2Y \\
&+ \left(\left\{ \frac{\langle 1257\rangle\langle 1456\rangle}{\langle 1245\rangle\langle 1567\rangle} \right\}_2 - \left\{ \frac{\langle 1267\rangle\langle 2356\rangle}{\langle 1236\rangle\langle 2567\rangle} \right\}_2 \right. \\
&\quad \left. - \left\{ \frac{\langle 1257\rangle\langle 2456\rangle}{\langle 1245\rangle\langle 2567\rangle} \right\}_2 + \left\{ \frac{\langle 1235\rangle\langle 1267\rangle\langle 2456\rangle}{\langle 1236\rangle\langle 1245\rangle\langle 2567\rangle} \right\}_2 \right) \wedge \left\{ \frac{\langle 1256\rangle\langle 2345\rangle}{\langle 1235\rangle\langle 2456\rangle} \right\}_2 \\
&+ \left\{ \frac{\langle 1235\rangle\langle 2367\rangle\langle 2456\rangle}{\langle 1236\rangle\langle 2345\rangle\langle 2567\rangle} \right\}_2 \wedge \left(\left\{ \frac{\langle 1267\rangle\langle 2356\rangle}{\langle 1236\rangle\langle 2567\rangle} \right\}_2 - \left\{ -\frac{\langle 1267\rangle\langle 2345\rangle}{\langle 2(13)(45)(67)\rangle} \right\}_2 \right) \\
&+ \left(\left\{ \frac{\langle 1235\rangle\langle 2367\rangle\langle 2456\rangle}{\langle 1236\rangle\langle 2345\rangle\langle 2567\rangle} \right\}_2 + \left\{ \frac{\langle 1236\rangle\langle 1245\rangle\langle 2567\rangle}{\langle 1235\rangle\langle 1267\rangle\langle 2456\rangle} \right\}_2 \right) \wedge \left\{ -\frac{\langle 1237\rangle\langle 2456\rangle}{\langle 2(13)(45)(67)\rangle} \right\}_2 \\
&- \left\{ \frac{\langle 1367\rangle\langle 1457\rangle\langle 2357\rangle}{\langle 1237\rangle\langle 1567\rangle\langle 3457\rangle} \right\}_2 \wedge \left\{ -\frac{\langle 1237\rangle\langle 4567\rangle}{\langle 7(16)(23)(45)\rangle} \right\}_2 \\
&- \left\{ \frac{\langle 1367\rangle\langle 2347\rangle\langle 3456\rangle}{\langle 1347\rangle\langle 2346\rangle\langle 3567\rangle} \right\}_2 \wedge \left\{ -\frac{\langle 1237\rangle\langle 3456\rangle}{\langle 3(17)(24)(56)\rangle} \right\}_2 \\
&+ \left(\left\{ \frac{\langle 1367\rangle\langle 2347\rangle\langle 2356\rangle}{\langle 1237\rangle\langle 2346\rangle\langle 3567\rangle} \right\}_2 + \left\{ \frac{\langle 1347\rangle\langle 2346\rangle\langle 3567\rangle}{\langle 1367\rangle\langle 2347\rangle\langle 3456\rangle} \right\}_2 \right) \wedge \left\{ -\frac{\langle 1367\rangle\langle 2345\rangle}{\langle 3(17)(24)(56)\rangle} \right\}_2 \\
&- \left\{ \frac{\langle 2346\rangle\langle 3567\rangle}{\langle 2367\rangle\langle 3456\rangle} \right\}_2 \wedge \left\{ \frac{\langle 1237\rangle\langle 2346\rangle\langle 3567\rangle}{\langle 1367\rangle\langle 2347\rangle\langle 2356\rangle} \right\}_2 \\
&+ \left(- \left\{ \frac{\langle 1457\rangle\langle 2456\rangle}{\langle 1245\rangle\langle 4567\rangle} \right\}_2 - \left\{ \frac{\langle 1567\rangle\langle 2456\rangle}{\langle 1256\rangle\langle 4567\rangle} \right\}_2 \right) \wedge \left\{ \frac{\langle 1257\rangle\langle 1456\rangle}{\langle 1245\rangle\langle 1567\rangle} \right\}_2 \\
&- \left\{ \frac{\langle 1457\rangle\langle 2357\rangle\langle 2456\rangle}{\langle 1257\rangle\langle 2345\rangle\langle 4567\rangle} \right\}_2 \wedge \left\{ -\frac{\langle 1567\rangle\langle 2345\rangle}{\langle 5(17)(23)(46)\rangle} \right\}_2 \\
&+ \left(- \left\{ \frac{\langle 1567\rangle\langle 2357\rangle\langle 2456\rangle}{\langle 1257\rangle\langle 2356\rangle\langle 4567\rangle} \right\}_2 - \left\{ \frac{\langle 1567\rangle\langle 2357\rangle\langle 3456\rangle}{\langle 1357\rangle\langle 2356\rangle\langle 4567\rangle} \right\}_2 \right) \wedge \left\{ -\frac{\langle 1567\rangle\langle 2345\rangle}{\langle 5(17)(23)(46)\rangle} \right\}_2 \\
&+ \left(\left\{ \frac{\langle 1347\rangle\langle 1567\rangle}{\langle 1367\rangle\langle 1457\rangle} \right\}_2 + \left\{ \frac{\langle 1567\rangle\langle 3467\rangle}{\langle 1367\rangle\langle 4567\rangle} \right\}_2 \right) \wedge \left\{ \frac{\langle 1467\rangle\langle 3457\rangle}{\langle 1347\rangle\langle 4567\rangle} \right\}_2 \\
&+ \left(- \left\{ \frac{\langle 1347\rangle\langle 2346\rangle\langle 3567\rangle}{\langle 1367\rangle\langle 2347\rangle\langle 3456\rangle} \right\}_2 + \left\{ \frac{\langle 2346\rangle\langle 3567\rangle}{\langle 2367\rangle\langle 3456\rangle} \right\}_2 \right. \\
&\quad \left. + \left\{ \frac{\langle 1347\rangle\langle 3567\rangle}{\langle 1367\rangle\langle 3457\rangle} \right\}_2 - \left\{ \frac{\langle 1347\rangle\langle 4567\rangle}{\langle 1467\rangle\langle 3457\rangle} \right\}_2 \right) \wedge \left\{ \frac{\langle 1237\rangle\langle 3467\rangle}{\langle 1367\rangle\langle 2347\rangle} \right\}_2 \\
&+ \left(\left\{ \frac{\langle 1237\rangle\langle 1467\rangle\langle 3457\rangle}{\langle 1367\rangle\langle 1457\rangle\langle 2347\rangle} \right\}_2 + \left\{ \frac{\langle 1567\rangle\langle 2367\rangle\langle 2457\rangle}{\langle 1267\rangle\langle 2357\rangle\langle 4567\rangle} \right\}_2 + \left\{ \frac{\langle 1567\rangle\langle 2367\rangle\langle 3457\rangle}{\langle 1367\rangle\langle 2357\rangle\langle 4567\rangle} \right\}_2 \right. \\
&\quad \left. + \left\{ \frac{\langle 1367\rangle\langle 2347\rangle\langle 4567\rangle}{\langle 1467\rangle\langle 2367\rangle\langle 3457\rangle} \right\}_2 \right) \wedge \left\{ -\frac{\langle 1237\rangle\langle 4567\rangle}{\langle 7(16)(23)(45)\rangle} \right\}_2 .
\end{aligned}
$$

B.1.4 B_1

Here we display the non-Stasheff local contributions to the $B_2 \wedge B_2$ coproduct component of the two-loop seven-point NMHV ratio function (5.3.6). Exceptionally in this formula we make use of

the cross-ratios a_{ij} defined in eq. (2.1) of [61]. We find that

$$\begin{aligned}
B_1 = {} & (a_{12} \wedge a_{16}) \wedge (a_{12} \wedge a_{61}) + (a_{12} \wedge a_{16}) \wedge (a_{17} \wedge a_{61}) - (a_{12} \wedge a_{23}) \wedge (a_{12} \wedge a_{61}) \\
& - (a_{12} \wedge a_{23}) \wedge (a_{17} \wedge a_{61}) - (a_{12} \wedge a_{32}) \wedge (a_{12} \wedge a_{61}) - (a_{12} \wedge a_{32}) \wedge (a_{17} \wedge a_{61}) \\
& - (a_{12} \wedge a_{61}) \wedge (a_{13} \wedge a_{16}) + (a_{12} \wedge a_{61}) \wedge (a_{13} \wedge a_{23}) + (a_{12} \wedge a_{61}) \wedge (a_{13} \wedge a_{32}) \\
& - (a_{12} \wedge a_{61}) \wedge (a_{16} \wedge a_{23}) - (a_{12} \wedge a_{61}) \wedge (a_{16} \wedge a_{32}) + (a_{13} \wedge a_{16}) \wedge (a_{17} \wedge a_{61}) \\
& - (a_{13} \wedge a_{23}) \wedge (a_{17} \wedge a_{61}) - (a_{13} \wedge a_{32}) \wedge (a_{17} \wedge a_{61}) \\
& + (a_{16} \wedge a_{23}) \wedge (a_{17} \wedge a_{61}) + (a_{16} \wedge a_{32}) \wedge (a_{17} \wedge a_{61})
\end{aligned}$$

where we follow the slight abuse of notation explained in [46] of writing B_1 not explicitly as an element of $B_2 \wedge B_2$, but rather by writing the result of the iterated coproduct acting on B_1 according to $\{a\}_2 \wedge \{b\}_2 \mapsto (a \wedge (1 + a)) \wedge (b \wedge (1 + b))$ and then expanding all multiplicative terms out using the usual symbol rules. In other words, the above formula represents the symbol of the function B_1 antisymmetrized according to $a \otimes b \otimes c \otimes d \mapsto (a \wedge b) \wedge (c \wedge d)$.

Bibliography

[1] M. E. Peskin and D. V. Schroeder, *An Introduction to quantum field theory*. 1995. [link].

[2] L. Brink, J. H. Schwarz, and J. Scherk, "Supersymmetric Yang-Mills Theories," *Nucl.Phys.* **B121** (1977) 77. [doi].

[3] Z. Bern, L. J. Dixon, D. C. Dunbar, and D. A. Kosower, "One loop n point gauge theory amplitudes, unitarity and collinear limits," *Nucl. Phys.* **B425** (1994) 217–260. arXiv:hep-ph/9403226 [hep-ph].

[4] Z. Bern, L. J. Dixon, D. C. Dunbar, and D. A. Kosower, "Fusing gauge theory tree amplitudes into loop amplitudes," *Nucl. Phys.* **B435** (1995) 59–101. arXiv:hep-ph/9409265 [hep-ph].

[5] S. Caron-Huot, L. J. Dixon, A. McLeod, and M. von Hippel, "Bootstrapping a Five-Loop Amplitude from Steinmann Relations,". arXiv:1609.00669 [hep-th].

[6] R. P. Feynman, "Space-Time Approach to Quantum Electrodynamics,"*Phys. Rev.* **76** (Sep, 1949) 769–789. [link].

[7] M. L. Mangano and S. J. Parke, "Multiparton amplitudes in gauge theories," *Phys. Rept.* **200** (1991) 301–367. arXiv:hep-th/0509223 [hep-th].

[8] S. J. Parke and T. R. Taylor, "An Amplitude for n Gluon Scattering," *Phys. Rev. Lett.* **56** (1986) 2459. [doi].

[9] M. Srednicki, *Quantum field theory*. Cambridge University Press, 2007.

[10] H. Elvang and Y.-t. Huang, "Scattering Amplitudes,". arXiv:1308.1697 [hep-th].

[11] E. Witten, "Perturbative gauge theory as a string theory in twistor space," *Commun. Math. Phys.* **252** (2004) 189–258. arXiv:hep-th/0312171 [hep-th].

[12] F. A. Berends and W. Giele, "The Six Gluon Process as an Example of Weyl-Van Der Waerden Spinor Calculus," *Nucl. Phys.* **B294** (1987) 700–732. [doi].

[13] J. M. Henn and J. C. Plefka, "Scattering Amplitudes in Gauge Theories," *Lect. Notes Phys.* **883** (2014) pp.1–195. [doi].

[14] J. M. Drummond, J. Henn, G. P. Korchemsky, and E. Sokatchev, "Dual superconformal symmetry of scattering amplitudes in N=4 super-Yang-Mills theory," *Nucl. Phys.* **B828** (2010) 317–374. arXiv:0807.1095 [hep-th].

[15] F. A. Berends and W. T. Giele, "Recursive Calculations for Processes with n Gluons," *Nucl. Phys.* **B306** (1988) 759–808. [doi].

[16] Z. Bern, V. Del Duca, L. J. Dixon, and D. A. Kosower, "All non-maximally-helicity-violating one-loop seven-gluon amplitudes in N=4 super-yang-Mills theory," *Phys. Rev.* **D71** (2005) 045006. arXiv:hep-th/0410224 [hep-th].

[17] Z. Bern, L. J. Dixon, and D. A. Kosower, "All Next-to-maximally-helicity-violating one-loop gluon amplitudes in N=4 super-Yang-Mills theory," *Phys. Rev.* **D72** (2005) 045014. arXiv:hep-th/0412210 [hep-th].

[18] R. Britto, F. Cachazo, and B. Feng, "Generalized unitarity and one-loop amplitudes in N=4 super-Yang-Mills," *Nucl. Phys.* **B725** (2005) 275–305. arXiv:hep-th/0412103 [hep-th].

[19] R. Britto, F. Cachazo, and B. Feng, "Coplanarity in twistor space of N=4 next-to-MHV one-loop amplitude coefficients," *Phys. Lett.* **B611** (2005) 167–172. arXiv:hep-th/0411107 [hep-th].

[20] V. P. Nair, "A Current Algebra for Some Gauge Theory Amplitudes," *Phys. Lett.* **B214** (1988) 215–218. [doi].

[21] J. M. Drummond, J. Henn, G. P. Korchemsky, and E. Sokatchev, "Generalized unitarity for N=4 super-amplitudes," *Nucl. Phys.* **B869** (2013) 452–492. arXiv:0808.0491 [hep-th].

[22] J. M. Drummond and J. M. Henn, "All tree-level amplitudes in N=4 SYM," *JHEP* **04** (2009) 018. arXiv:0808.2475 [hep-th].

[23] R. Penrose, "Twistor algebra," *J. Math. Phys.* **8** (1967) 345. [doi].

[24] A. Hodges, "Eliminating spurious poles from gauge-theoretic amplitudes," *JHEP* **05** (2013) 135. arXiv:0905.1473 [hep-th].

[25] M. B. Green, J. H. Schwarz, and L. Brink, "N=4 Yang-Mills and N=8 Supergravity as Limits of String Theories," *Nucl. Phys.* **B198** (1982) 474–492. [doi].

[26] R. Roiban, "Review of AdS/CFT Integrability, Chapter V.1: Scattering Amplitudes - a Brief Introduction," *Lett. Math. Phys.* **99** (2012) 455–479. arXiv:1012.4001 [hep-th].

[27] C. Anastasiou, Z. Bern, L. J. Dixon, and D. A. Kosower, "Planar amplitudes in maximally supersymmetric Yang-Mills theory," *Phys. Rev. Lett.* **91** (2003) 251602. arXiv:hep-th/0309040 [hep-th].

[28] Z. Bern, L. J. Dixon, and V. A. Smirnov, "Iteration of planar amplitudes in maximally supersymmetric Yang-Mills theory at three loops and beyond," *Phys. Rev.* **D72** (2005) 085001. arXiv:hep-th/0505205 [hep-th].

[29] Z. Bern, M. Czakon, D. A. Kosower, R. Roiban, and V. A. Smirnov, "Two-loop iteration of five-point N=4 super-Yang-Mills amplitudes," *Phys. Rev. Lett.* **97** (2006) 181601. arXiv:hep-th/0604074 [hep-th].

[30] F. Cachazo, M. Spradlin, and A. Volovich, "Iterative structure within the five-particle two-loop amplitude," *Phys. Rev.* **D74** (2006) 045020. arXiv:hep-th/0602228 [hep-th].

[31] A. B. Goncharov, "Multiple polylogarithms, cyclotomy and modular complexes," *Math. Res. Lett.* **5** (1998) 497–516. arXiv:1105.2076 [math.AG].

[32] J. Golden, A. B. Goncharov, M. Spradlin, C. Vergu, and A. Volovich, "Motivic Amplitudes and Cluster Coordinates," *JHEP* **01** (2014) 091. arXiv:1305.1617 [hep-th].

[33] V. Del Duca, C. Duhr, and V. A. Smirnov, "An Analytic Result for the Two-Loop Hexagon Wilson Loop in N = 4 SYM," *JHEP* **03** (2010) 099. arXiv:0911.5332 [hep-ph].

[34] V. Del Duca, C. Duhr, and V. A. Smirnov, "The Two-Loop Hexagon Wilson Loop in N = 4 SYM," *JHEP* **05** (2010) 084. arXiv:1003.1702 [hep-th].

[35] A. B. Goncharov, M. Spradlin, C. Vergu, and A. Volovich, "Classical Polylogarithms for Amplitudes and Wilson Loops," *Phys. Rev. Lett.* **105** (2010) 151605. arXiv:1006.5703 [hep-th].

[36] D. Gaiotto, J. Maldacena, A. Sever, and P. Vieira, "Pulling the straps of polygons," *JHEP* **12** (2011) 011. arXiv:1102.0062 [hep-th].

[37] J. M. Drummond, J. Henn, V. A. Smirnov, and E. Sokatchev, "Magic identities for conformal four-point integrals," *JHEP* **01** (2007) 064. arXiv:hep-th/0607160 [hep-th].

[38] Z. Bern, M. Czakon, L. J. Dixon, D. A. Kosower, and V. A. Smirnov, "The Four-Loop Planar Amplitude and Cusp Anomalous Dimension in Maximally Supersymmetric Yang-Mills Theory," *Phys. Rev.* **D75** (2007) 085010. arXiv:hep-th/0610248 [hep-th].

[39] L. F. Alday and J. M. Maldacena, "Gluon scattering amplitudes at strong coupling," *JHEP* **06** (2007) 064. arXiv:0705.0303 [hep-th].

[40] J. M. Drummond, G. P. Korchemsky, and E. Sokatchev, "Conformal properties of four-gluon planar amplitudes and Wilson loops," *Nucl. Phys.* **B795** (2008) 385–408. arXiv:0707.0243 [hep-th].

[41] J. M. Drummond, J. Henn, G. P. Korchemsky, and E. Sokatchev, "On planar gluon amplitudes/Wilson loops duality," *Nucl. Phys.* **B795** (2008) 52–68. arXiv:0709.2368 [hep-th].

[42] L. F. Alday and J. Maldacena, "Comments on gluon scattering amplitudes via AdS/CFT," *JHEP* **11** (2007) 068. arXiv:0710.1060 [hep-th].

[43] J. M. Drummond, J. Henn, G. P. Korchemsky, and E. Sokatchev, "Conformal Ward identities for Wilson loops and a test of the duality with gluon amplitudes," *Nucl. Phys.* **B826** (2010) 337–364. arXiv:0712.1223 [hep-th].

[44] S. Fomin and A. Zelevinsky, "Cluster algebras I: Foundations," *ArXiv Mathematics e-prints* (Apr., 2001) . math/0104151.

[45] S. Fomin and A. Zelevinsky, "Cluster algebras II: Finite type classification," *Inventiones Mathematicae* **154** (Oct., 2003) 63–121. math/0208229.

[46] J. Golden, M. F. Paulos, M. Spradlin, and A. Volovich, "Cluster Polylogarithms for Scattering Amplitudes," *J. Phys.* **A47** (2014) no. 47, 474005. arXiv:1401.6446 [hep-th].

[47] J. Golden and M. Spradlin, "A Cluster Bootstrap for Two-Loop MHV Amplitudes," *JHEP* **02** (2015) 002. arXiv:1411.3289 [hep-th].

[48] L. J. Dixon, J. M. Drummond, and J. M. Henn, "Analytic result for the two-loop six-point NMHV amplitude in N=4 super Yang-Mills theory," *JHEP* **01** (2012) 024. arXiv:1111.1704 [hep-th].

[49] L. J. Dixon, J. M. Drummond, and J. M. Henn, "Bootstrapping the three-loop hexagon," *JHEP* **11** (2011) 023. arXiv:1108.4461 [hep-th].

[50] L. J. Dixon, J. M. Drummond, M. von Hippel, and J. Pennington, "Hexagon functions and the three-loop remainder function," *JHEP* **12** (2013) 049. arXiv:1308.2276 [hep-th].

[51] L. J. Dixon, J. M. Drummond, C. Duhr, and J. Pennington, "The four-loop remainder function and multi-Regge behavior at NNLLA in planar N = 4 super-Yang-Mills theory," *JHEP* **06** (2014) 116. arXiv:1402.3300 [hep-th].

[52] R. J. Eden, P. V. Landshoff, D. I. Olive, and J. C. Polkinghorne, *The Analytic S-Matrix*. Cambridge University Press, 1966.

[53] Z. Bern, L. J. Dixon, and D. A. Kosower, "On-shell recurrence relations for one-loop QCD amplitudes," *Phys. Rev.* **D71** (2005) 105013. arXiv:hep-th/0501240 [hep-th].

[54] Z. Bern, L. J. Dixon, and D. A. Kosower, "Bootstrapping multi-parton loop amplitudes in QCD," *Phys. Rev.* **D73** (2006) 065013. arXiv:hep-ph/0507005 [hep-ph].

[55] C. F. Berger, Z. Bern, L. J. Dixon, D. Forde, and D. A. Kosower, "Bootstrapping One-Loop QCD Amplitudes with General Helicities," *Phys. Rev.* **D74** (2006) 036009. arXiv:hep-ph/0604195 [hep-ph].

[56] D. C. Dunbar and W. B. Perkins, "Two-loop five-point all plus helicity Yang-Mills amplitude," *Phys. Rev.* **D93** (2016) no. 8, 085029. arXiv:1603.07514 [hep-th].

[57] D. C. Dunbar, G. R. Jehu, and W. B. Perkins, "The two-loop n-point all-plus helicity amplitude," *Phys. Rev.* **D93** (2016) no. 12, 125006. arXiv:1604.06631 [hep-th].

[58] D. C. Dunbar, G. R. Jehu, and W. B. Perkins, "Two-loop six gluon all plus helicity amplitude," *Phys. Rev. Lett.* **117** (2016) no. 6, 061602. arXiv:1605.06351 [hep-th].

[59] F. Gliozzi, J. Scherk, and D. I. Olive, "Supersymmetry, Supergravity Theories and the Dual Spinor Model," *Nucl. Phys.* **B122** (1977) 253–290. [doi].

[60] L. J. Dixon and M. von Hippel, "Bootstrapping an NMHV amplitude through three loops," *JHEP* **10** (2014) 065. arXiv:1408.1505 [hep-th].

[61] J. M. Drummond, G. Papathanasiou, and M. Spradlin, "A Symbol of Uniqueness: The Cluster Bootstrap for the 3-Loop MHV Heptagon," *JHEP* **03** (2015) 072. arXiv:1412.3763 [hep-th].

[62] L. J. Dixon, J. M. Drummond, C. Duhr, M. von Hippel, and J. Pennington, "Bootstrapping six-gluon scattering in planar N=4 super-Yang-Mills theory," *PoS* **LL2014** (2014) 077. arXiv:1407.4724 [hep-th].

[63] Z. Bern, J. J. M. Carrasco, H. Johansson, and D. A. Kosower, "Maximally supersymmetric planar Yang-Mills amplitudes at five loops," *Phys. Rev.* **D76** (2007) 125020. arXiv:0705.1864 [hep-th].

[64] A. Brandhuber, P. Heslop, and G. Travaglini, "MHV amplitudes in N=4 super Yang-Mills and Wilson loops," *Nucl. Phys.* **B794** (2008) 231–243. arXiv:0707.1153 [hep-th].

[65] Z. Bern, L. J. Dixon, D. A. Kosower, R. Roiban, M. Spradlin, C. Vergu, and A. Volovich, "The Two-Loop Six-Gluon MHV Amplitude in Maximally Supersymmetric Yang-Mills Theory," *Phys. Rev.* **D78** (2008) 045007. arXiv:0803.1465 [hep-th].

[66] J. M. Drummond, J. Henn, G. P. Korchemsky, and E. Sokatchev, "Hexagon Wilson loop = six-gluon MHV amplitude," *Nucl. Phys.* **B815** (2009) 142–173. arXiv:0803.1466 [hep-th].

[67] J. Drummond, J. Henn, G. Korchemsky, and E. Sokatchev, "The hexagon Wilson loop and the BDS ansatz for the six-gluon amplitude," *Phys.Lett.* **B662** (2008) 456–460. arXiv:0712.4138 [hep-th].

[68] J. Bartels, L. Lipatov, and A. Sabio Vera, "BFKL Pomeron, Reggeized gluons and Bern-Dixon-Smirnov amplitudes," *Phys.Rev.* **D80** (2009) 045002. arXiv:0802.2065 [hep-th].

[69] D. A. Kosower, R. Roiban, and C. Vergu, "The Six-Point NMHV amplitude in Maximally Supersymmetric Yang-Mills Theory," *Phys. Rev.* **D83** (2011) 065018. arXiv:1009.1376 [hep-th].

[70] L. J. Dixon, M. von Hippel, and A. J. McLeod, "The four-loop six-gluon NMHV ratio function," *JHEP* **01** (2016) 053. arXiv:1509.08127 [hep-th].

[71] V. V. Fock and A. B. Goncharov, "Cluster ensembles, quantization and the dilogarithm," *Ann. Sci. Éc. Norm. Supér. (4)* **42** (2009) no. 6, 865–930. arXiv:math/0311245 [math.AG].

[72] M. Gekhtman, M. Shapiro, and A. Vainshtein, "Cluster algebras and Poisson geometry," *Mosc. Math* **J** (2003) no. 3, 899. arXiv:0208033 [math].

[73] N. Arkani-Hamed, J. L. Bourjaily, F. Cachazo, A. B. Goncharov, A. Postnikov, and J. Trnka, *Scattering Amplitudes and the Positive Grassmannian*. Cambridge University Press, 2012. arXiv:1212.5605 [hep-th].

[74] L. F. Alday, D. Gaiotto, J. Maldacena, A. Sever, and P. Vieira, "An Operator Product Expansion for Polygonal null Wilson Loops," *JHEP* **1104** (2011) 088. arXiv:1006.2788 [hep-th].

[75] A. Sever and P. Vieira, "Multichannel Conformal Blocks for Polygon Wilson Loops," *JHEP* **1201** (2012) 070. arXiv:1105.5748 [hep-th].

[76] B. Basso, A. Sever, and P. Vieira, "Spacetime and Flux Tube S-Matrices at Finite Coupling for $\mathcal{N} = 4$ Supersymmetric Yang-Mills Theory," *Phys.Rev.Lett.* **111** (2013) no. 9, 091602. arXiv:1303.1396 [hep-th].

[77] B. Basso, A. Sever, and P. Vieira, "Space-time S-matrix and Flux tube S-matrix II. Extracting and Matching Data," *JHEP* **1401** (2014) 008. arXiv:1306.2058 [hep-th].

[78] B. Basso, A. Sever, and P. Vieira, "Space-time S-matrix and Flux-tube S-matrix IV. Gluons and Fusion," *JHEP* **1409** (2014) 149. arXiv:1407.1736 [hep-th].

[79] A. V. Belitsky, "On factorization of multiparticle pentagons," *Nucl. Phys.* **B897** (2015) 346–373. arXiv:1501.06860 [hep-th].

[80] B. Basso, J. Caetano, L. Cordova, A. Sever, and P. Vieira, "OPE for all Helicity Amplitudes II. Form Factors and Data Analysis," *JHEP* **12** (2015) 088. arXiv:1508.02987 [hep-th].

[81] B. Basso, A. Sever, and P. Vieira, "Hexagonal Wilson loops in planar $\mathcal{N} = 4$ SYM theory at finite coupling," *J. Phys.* **A49** (2016) no. 41, 41LT01. arXiv:1508.03045 [hep-th].

[82] A. V. Belitsky, "Matrix pentagons,". arXiv:1607.06555 [hep-th].

[83] J. M. Drummond and G. Papathanasiou, "Hexagon OPE Resummation and Multi-Regge Kinematics," *JHEP* **02** (2016) 185. arXiv:1507.08982 [hep-th].

[84] L. Córdova, "Hexagon POPE: effective particles and tree level resummation," *JHEP* **01** (2017) 051. arXiv:1606.00423 [hep-th].

[85] H. T. Lam and M. von Hippel, "Resumming the POPE at One Loop," *JHEP* **12** (2016) 011. arXiv:1608.08116 [hep-th].

[86] N. Arkani-Hamed and J. Trnka, "The Amplituhedron," *JHEP* **1410** (2014) 30. arXiv:1312.2007 [hep-th].

[87] N. Arkani-Hamed and J. Trnka, "Into the Amplituhedron," *JHEP* **12** (2014) 182. arXiv:1312.7878 [hep-th].

[88] T. Dennen, I. Prlina, M. Spradlin, S. Stanojevic, and A. Volovich, "Landau Singularities from the Amplituhedron,". 1612.02708 [hep-th].

[89] S. Caron-Huot and S. He, "Jumpstarting the All-Loop S-Matrix of Planar N=4 Super Yang-Mills," *JHEP* **07** (2012) 174. arXiv:1112.1060 [hep-th].

[90] O. Steinnman, "Uber den Zusammenhang Zwischen Wightmanfunctionen und Retardierten Kommutatoren I," *Helv. Physica Acta* **33** (1960) 257–349.

[91] O. Steinmann, "Wightman-Funktionen und retardierten Kommutatoren. II," *Helv. Physica Acta* **33** (1960) 347.

[92] L. Dixon, J. Drummond, T. Harrington, A. McLeod, G. Papathanasiou, and M. Spradlin. To appear.

[93] J. Bartels, L. Lipatov, and A. Sabio Vera, "$\mathcal{N} = 4$ supersymmetric Yang Mills scattering amplitudes at high energies: The Regge cut contribution," *Eur.Phys.J.* **C65** (2010) 587–605. arXiv:0807.0894 [hep-th].

[94] L. Lipatov and A. Prygarin, "BFKL approach and six-particle MHV amplitude in $\mathcal{N} = 4$ super Yang-Mills," *Phys.Rev.* **D83** (2011) 125001. arXiv:1011.2673 [hep-th].

[95] J. Bartels, A. Kormilitzin, L. Lipatov, and A. Prygarin, "BFKL approach and $2 \to 5$ maximally helicity violating amplitude in $\mathcal{N} = 4$ super-Yang-Mills theory," *Phys.Rev.* **D86** (2012) 065026. arXiv:1112.6366 [hep-th].

[96] V. Fadin and L. Lipatov, "BFKL equation for the adjoint representation of the gauge group in the next-to-leading approximation at $\mathcal{N} = 4$ SUSY," *Phys.Lett.* **B706** (2012) 470–476. arXiv:1111.0782 [hep-th].

[97] L. Lipatov, A. Prygarin, and H. J. Schnitzer, "The Multi-Regge limit of NMHV Amplitudes in $\mathcal{N} = 4$ SYM Theory," *JHEP* **1301** (2013) 068. arXiv:1205.0186 [hep-th].

[98] L. J. Dixon, C. Duhr, and J. Pennington, "Single-valued harmonic polylogarithms and the multi-Regge limit," *JHEP* **10** (2012) 074. arXiv:1207.0186 [hep-th].

[99] J. Bartels, A. Kormilitzin, and L. Lipatov, "Analytic structure of the $n = 7$ scattering amplitude in $\mathcal{N} = 4$ SYM theory at multi-Regge kinematics: Conformal Regge pole contribution," *Phys.Rev.* **D89** (2014) 065002. arXiv:1311.2061 [hep-th].

[100] J. Bartels, A. Kormilitzin, and L. N. Lipatov, "Analytic structure of the $n = 7$ scattering amplitude in $\mathcal{N} = 4$ theory in multi-Regge kinematics: Conformal Regge cut contribution," *Phys. Rev.* **D91** (2015) no. 4, 045005. arXiv:1411.2294 [hep-th].

[101] T. Bargheer, "Systematics of the Multi-Regge Three-Loop Symbol,". arXiv:1606.07640 [hep-th].

[102] J. Broedel, M. Sprenger, and A. Torres Orjuela, "Towards single-valued polylogarithms in two variables for the seven-point remainder function in multi-Regge-kinematics," *Nucl. Phys.* **B915** (2017) 394–413. arXiv:1606.08411 [hep-th].

[103] V. Del Duca, S. Druc, J. Drummond, C. Duhr, F. Dulat, R. Marzucca, G. Papathanasiou, and B. Verbeek, "Multi-Regge kinematics and the moduli space of Riemann spheres with marked points," *JHEP* **08** (2016) 152. arXiv:1606.08807 [hep-th].

[104] G. Georgiou, "Null Wilson loops with a self-crossing and the Wilson loop/amplitude conjecture," *JHEP* **09** (2009) 021. arXiv:0904.4675 [hep-th].

[105] L. J. Dixon and I. Esterlis, "All orders results for self-crossing Wilson loops mimicking double parton scattering," *JHEP* **07** (2016) 116. arXiv:1602.02107 [hep-th]. [Erratum: JHEP08,131(2016)].

[106] https://goo.gl/vKCtoX.

[107] L. Magnea and G. F. Sterman, "Analytic continuation of the Sudakov form-factor in QCD," *Phys. Rev.* **D42** (1990) 4222–4227. [doi].

[108] S. Catani, "The Singular behavior of QCD amplitudes at two loop order," *Phys. Lett.* **B427** (1998) 161–171. arXiv:hep-ph/9802439 [hep-ph].

[109] G. F. Sterman and M. E. Tejeda-Yeomans, "Multiloop amplitudes and resummation," *Phys. Lett.* **B552** (2003) 48–56. arXiv:hep-ph/0210130 [hep-ph].

[110] S. Caron-Huot, "Superconformal symmetry and two-loop amplitudes in planar N=4 super Yang-Mills," *JHEP* **12** (2011) 066. arXiv:1105.5606 [hep-th].

[111] J. Golden and M. Spradlin, "The differential of all two-loop MHV amplitudes in $\mathcal{N} = 4$ Yang-Mills theory," *JHEP* **1309** (2013) 111. arXiv:1306.1833 [hep-th].

[112] J. Golden and M. Spradlin, "An analytic result for the two-loop seven-point MHV amplitude in $\mathcal{N} = 4$ SYM," *JHEP* **08** (2014) 154. arXiv:1406.2055 [hep-th].

[113] J. M. Drummond, "Review of AdS/CFT Integrability, Chapter V.2: Dual Superconformal Symmetry," *Lett. Math. Phys.* **99** (2012) 481–505. arXiv:1012.4002 [hep-th].

[114] L. Mason and D. Skinner, "Dual Superconformal Invariance, Momentum Twistors and Grassmannians," *JHEP* **0911** (2009) 045. arXiv:0909.0250 [hep-th].

[115] N. Arkani-Hamed, F. Cachazo, C. Cheung, and J. Kaplan, "A Duality For The S Matrix," *JHEP* **03** (2010) 020. arXiv:0907.5418 [hep-th].

[116] N. Arkani-Hamed, F. Cachazo, and C. Cheung, "The Grassmannian Origin Of Dual Superconformal Invariance," *JHEP* **03** (2010) 036. arXiv:0909.0483 [hep-th].

[117] J. Drummond and L. Ferro, "Yangians, Grassmannians and T-duality," *JHEP* **1007** (2010) 027. arXiv:1001.3348 [hep-th].

[118] N. Arkani-Hamed, J. L. Bourjaily, F. Cachazo, and J. Trnka, "Local Integrals for Planar Scattering Amplitudes," *JHEP* **06** (2012) 125. arXiv:1012.6032 [hep-th].

[119] L. F. Alday, D. Gaiotto, and J. Maldacena, "Thermodynamic Bubble Ansatz," *JHEP* **09** (2011) 032. arXiv:0911.4708 [hep-th].

[120] G. Yang, "A simple collinear limit of scattering amplitudes at strong coupling," *JHEP* **03** (2011) 087. arXiv:1006.3306 [hep-th].

[121] G. Yang, "Scattering amplitudes at strong coupling for 4K gluons," *JHEP* **12** (2010) 082. arXiv:1004.3983 [hep-th].

[122] A. Goncharov, "Multiple polylogarithms and mixed Tate motives,". arXiv:math/0103059 [math.AG].

[123] A. B. Goncharov, "Galois symmetries of fundamental groupoids and noncommutative geometry,"*Duke Math. J.* **128** (06, 2005) 209–284. arXiv:math/0208144 [math.AG].

[124] F. C. Brown, "Multiple zeta values and periods of moduli spaces $\overline{\mathfrak{M}}_{0,n}(\mathbb{R})$," *Annales Sci.Ecole Norm.Sup.* **42** (2009) 371. arXiv:math/0606419 [math.AG].

[125] A. B. Goncharov, "A simple construction of Grassmannian polylogarithms," *Adv. Math.* **241** (2013) 79–102. arXiv:0908.2238 [math.AG].

[126] C. Duhr, H. Gangl, and J. R. Rhodes, "From polygons and symbols to polylogarithmic functions," *JHEP* **10** (2012) 075. arXiv:1110.0458 [math-ph].

[127] A. Prygarin, M. Spradlin, C. Vergu, and A. Volovich, "All Two-Loop MHV Amplitudes in Multi-Regge Kinematics From Applied Symbology," *Phys. Rev.* **D85** (2012) 085019. arXiv:1112.6365 [hep-th].

[128] K. E. Cahill and H. P. Stapp, "OPTICAL THEOREMS AND STEINMANN RELATIONS," *Annals Phys.* **90** (1975) 438. [doi].

[129] R. C. Brower, H. Nastase, H. J. Schnitzer, and C.-I. Tan, "Analyticity for Multi-Regge Limits of the Bern-Dixon-Smirnov Amplitudes," *Nucl. Phys.* **B822** (2009) 301–347. arXiv:0809.1632 [hep-th].

[130] R. C. Brower, H. Nastase, H. J. Schnitzer, and C.-I. Tan, "Implications of multi-Regge limits for the Bern-Dixon-Smirnov conjecture," *Nucl. Phys.* **B814** (2009) 293–326. arXiv:0801.3891 [hep-th].

[131] S. Caron-Huot. Private communication.

[132] M. T. Grisaru, H. N. Pendleton, and P. van Nieuwenhuizen, "Supergravity and the S Matrix," *Phys. Rev.* **D15** (1977) 996. [doi].

[133] M. T. Grisaru and H. N. Pendleton, "Some Properties of Scattering Amplitudes in Supersymmetric Theories," *Nucl. Phys.* **B124** (1977) 81–92. [doi].

[134] B. Basso, A. Sever, and P. Vieira. Private communication.

[135] A. Sever. Talk at *amplitudes 2015*, http://amp15.itp.phys.ethz.ch/talks/Sever.pdf.

[136] B. Basso, S. Caron-Huot, and A. Sever, "Adjoint BFKL at finite coupling: a short-cut from the collinear limit," *JHEP* **01** (2015) 027. arXiv:1407.3766 [hep-th].

[137] T. Dennen, M. Spradlin, and A. Volovich, "Landau Singularities and Symbology: One- and Two-loop MHV Amplitudes in SYM Theory," *JHEP* **03** (2016) 069. arXiv:1512.07909 [hep-th].

[138] C. Vergu, "Unpublished,".

[139] J. S. Scott, "Grassmannians and Cluster Algebras," *Proc. Lond. Math. Soc. (3)* **92** (2006) no. 2, 345.

[140] D. Parker, A. Scherlis, M. Spradlin, and A. Volovich, "Hedgehog bases for A_n cluster polylogarithms and an application to six-point amplitudes," *JHEP* **11** (2015) 136. arXiv:1507.01950 [hep-th].

[141] S. Benvenuti, B. Feng, A. Hanany, and Y.-H. He, "Counting BPS Operators in Gauge Theories: Quivers, Syzygies and Plethystics," *JHEP* **11** (2007) 050. arXiv:hep-th/0608050 [hep-th].

[142] A. B. Goncharov, "Galois symmetries of fundamental groupoids and noncommutative geometry," *Duke Math. J.* **128** (2005) 209. arXiv:math/0208144 [math.AG].

[143] C. Anastasiou, A. Brandhuber, P. Heslop, V. V. Khoze, B. Spence, and G. Travaglini, "Two-Loop Polygon Wilson Loops in N=4 SYM," *JHEP* **05** (2009) 115. arXiv:0902.2245 [hep-th].

[144] M. F. Paulos and B. U. W. Schwab, "Cluster Algebras and the Positive Grassmannian," *JHEP* **10** (2014) 31. arXiv:1406.7273 [hep-th].

[145] W. Stein and D. Joyner, "SAGE: System for Algebra and Geometry Experimentation," *ACM SIGSAM Bulletin* **39** (2005) no. 2, 61–64. [link].

[146] Z. Chen and A. Storjohann, "A BLAS Based C Library for Exact Linear Algebra on Integer Matrices," in *Proceedings of the 2005 International Symposium on Symbolic and Algebraic Computation*, ISSAC '05, pp. 92–99. ACM, New York, NY, USA, 2005. [link].